UNIVERSITÁ DEGLI STUDI DI PADOVA

Dipartimento di Fisica e Astronomia "Galileo Galilei"

Corso di Laurea Magistrale in Fisica

Tesi di Laurea

Electromagnetic mode characterization in a Hall thruster used as hydrogen ion source

Laureando:
Stefano Milanese
Matricola:
1154533

Relatore:
Dott. Emilio Martines
Correlatore:
Dott. Matteo Zuin

Anno Accademico 2018-2019

Sommario

ATHENIS è un propulsore elettrico ad effetto Hall, creato per studiare l'utilizzo di tali propulsori nella produzione di ioni H^- grazie all'interazione con superfici cesiate. Il meccanismo di estrazione di ioni negativi è di fondamentale interesse nel riscaldamento di plasmi da fusione nucleare prodotti nel progetto ITER. I propulsori, che sfruttano un campo magnetico per confinare gli elettroni ed accelerare gli ioni, sono soggetti ad oscillazioni elettrostatiche che possono incidere sul rendimento a seconda della propagazione e della frequenza delle stesse.
Questo lavoro di tesi è dedicato allo studio delle condizioni di lavoro di ATHENIS. In particolare si è studiato i regimi operativi ottenibili con diverse alimentazioni, il ruolo dell'emissione termoionica di un filamento di tungsteno utilizzato come catodo e del flusso di propellente nell'accelerazione degli ioni prodotti e le caratteristiche dei plasmi generati con questo metodo. Oltre allo studio sulle caratteristiche generali lo scopo di questa tesi è di ottenere una caratterizzazione delle oscillazioni presenti. Il lavoro svolto copre una variegata attività sperimentale in quanto a costruzione e cablaggio delle sonde, costruzione del sistema di acquisizione, gestione del propulsore, acquisione ed analisi dati. I dati raccolti, analizzati in ambiente IDL tramite programmi scritti in itinere, coprono diverse condizioni di lavoro per Argon, Elio ed Idrogeno usati come propellenti, in modo da integrare i precedenti studi su ATHENIS, limitati ad Idrogeno ed Azoto.
I risultati ottenuti grazie ad una sonda di Mach, essenzialmente lavorando con Argon, mostrano la presenza di condizioni di pressione e corrente di filamento ottimali nell'accelerazione ionica, sebbene i parametri di plasma mostrino deboli dipendenze dalle condizioni di lavoro. Inoltre, l'osservazione delle fluttuazioni elettrostatiche, attuata tramite un array circolare di sonde elettrostatiche poste in sommità al propulsore, ha evidenziato la presenza di tre tipi di oscillazione in tre differenti bande di frequenze, la cui tipologia si è mostrata strettamente dipendente dal gas utilizzato e le relative frequenze e velocità di propagazione dipendenti dalle condizioni di pressione. In particolare si sono osservate oscillazioni note come *rotating spoke* e *transit-time*, ed un'ulteriore oscillazione di natura più misteriosa a frequenze prossime al MHz.

Abstract

ATHENIS is an electric Hall effect thruster, built to study the application of the said thrusters in H^- ions production thanks to the interaction with Cesium-planted surfaces. The negative ions extraction mechanism is of crucial interest in the heating of nuclear fusion plasmas, generated in the ITER project. Thrusters, that exploit a magnetic field to confine electrons and accelerate ions, are subject to electrostatic oscillations that can affect performances depending on their propagation and frequency.
This thesis task is addressed to study ATHENIS working conditions. In particular, I studied working regimes obtainable with different power supplies, the roles of thermoionic emission of a Tungsten filament used as cathode and the propellant flux in the acceleration of the produced ions, and the characteristics of the plasmas generated in this way. Besides the general properties study, the purpose of this thesis is to obtain a characterization of the present oscillations. The work done covers varied experimental activities including probes building and wiring, acquisition system building, thruster managing, data recording and analysis. Collected data, analyzed through expressly written software in IDL environment, cover different working condition for Argon, Helium and Hydrogen used as propellant, in order to integrate previous studies on ATHENIS, limited to Hydrogen and Nitrogen.
The results, obtained thanks to a Mach probe, mainly working with Argon, show the existence of optimal pressure and filament current conditions in ion acceleration, even if plasma parameters show weak bonds with working conditions. Moreover, the observation of electrostatic fluctuations, got by a circular electrostatic probes array set over the top of the thruster, showed the presence of three kinds of oscillation in three different frequency bands, strictly depending on the used gas. Their frequencies and propagation velocities rely on pressure conditions. In particular, oscillations known as *rotating spoke* and *transit-time* and one more curious oscillation near the MHz region have been observed.

Contents

1 Introduction

1.1 The physics of plasmas

A plasma is a particular kind of ionized gas [5] [3]. It is a strongly interacting N-body system since its degree of ionization is high enough to make Coulomb interactions that affect ions and electrons not negligible. About 99% of visibile matter in the Universe is in this state, consequently it is a topic of large interest that touches astrophysics, nuclear physics and medicine. Because plasmas exist over a large range of essential parameters, they are used for many human purpose: industry (arc cutting, film deposition, materials manipulation), medicine (surgery blades, wound sterilization, eye diseases treatment), aerospace industry (space propulsion), alternative energy sources (nuclear fusion reactors), and many others updating constantly. The particle density range covered by the many kinds of plasma is huge, from interstellar gas $n \sim 10^6 m^{-3}$ to over $10^{32} m^{-3}$ in stars core.

One fundamental feature of a proper plasma is its *quasi-neutrality*, which means that electron density n_e and ion density n_i are nearly the same and it involves almost the whole volume of a plasma. Even small charge imbalance would generate strong fields such that neutrality would be quickly restored. Hereon, λ_D is the so called *Debye length*, defined as the distance such that the electric potential $V(r) = V_0 e^{\frac{-r}{\lambda_D}}$ decreases to $\frac{V_0}{e}$. It can be written as:

$$\lambda_D = \sqrt{\frac{\epsilon_0 T_e}{n e^2}},$$

with T_e electron temperature (eV) and it is typically about $10 \div 100 \mu m$. In fact, only within a few Debye lengths a charge imbalance can persist when facing a conductor object. Due to the presence of almost free charged particles, plasmas behave as a conductor re-arranging its spatial charge distribution when exposed to a voltage drop. Then, whenever facing a different potential, Debye length is the length that characterizes the screening of the plasma with external matter.

Introducing a *'plasma parameter'*, g, the actual definition of plasma for a

ionized gas is ensured whenever

$$g = \frac{1}{n{\lambda_D}^3} \ll 1.$$

The smallness of g signifies a high number of particle interacting strongly, i.e. showing a collective behavior. Plasma examples are shown in figure 1.1 below.

Electrons and ions, once affected by external fields, would find a convenient collective behavior very hard to describe fully by a single model. However there are many models working well in different conditions, depending on thermodynamical properties and on the presence or absence of magnetic fields. Actually magnetic field plays a great role over many properties. In fact it cannot be just screened and the presence of field lines through particle trajectories makes them turn around, describing helices and more complex orbits. Therefore a single particle orbit, whenever is needed to be studied, is decomposed in the circular motion around the field lines, which averaged over one or more periods can be ignored, and the guiding center motion, which consists of the overall motion along and through the field lines.In this way collisions show a strong anisotropy as well as every other dynamical property. Magnetic fields therefore enrich plasmas behavior and have to be accurately considered in proper models. Their use over many kind of plasma is needed to confine, control, and manipulate them or even drive particular drifts as those concerning the sake of this work. The magnetic confinement is a very powerful tool: in this work it has a fundamental role to separate ion and electron motion but its greatest field of application is nuclear fusion experiments. For example, in toroidal magnetic confinement such as Tokamaks strong **B** fields make it possible to reach temperatures of tens of keV, necessary to start H-D reactions. Furthermore, Reversed Field Pinches as RFX (Reversed Field eXperiment) in Padua, make it possible to study complex phenomena in plasma self-arrangement of astrophysical interest [5].

Because of their wide parameters variability, it is mandatory to classify plasmas to fit the different applicability conditions of the various models. Plasmas can be classified by their degree of ionization and by useful parameters coming from their thermodynamical properties: density, temperature and pressure.

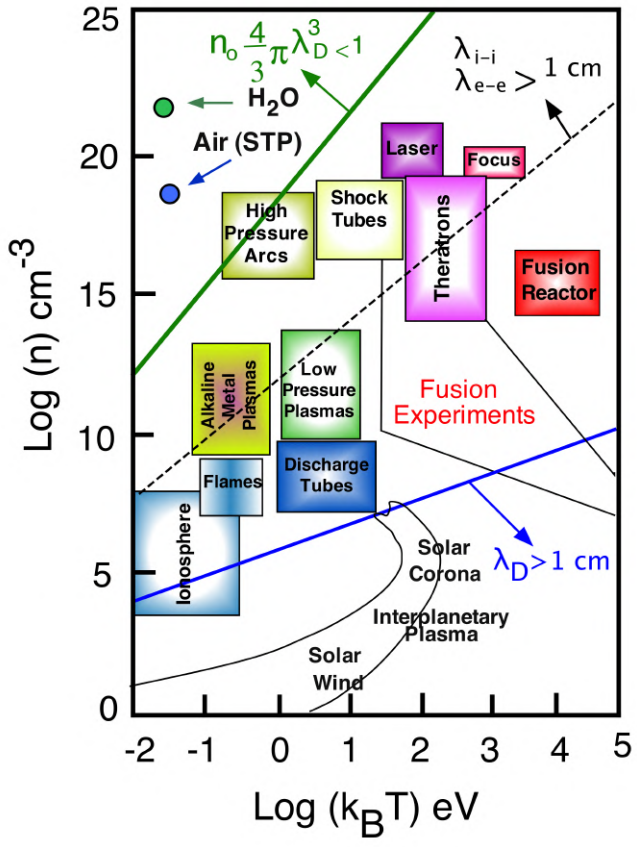

Figure 1.1: Various kind of plasma at different densities and temperatures.

Others parameters that will be found in this work will be collisional frequency, electron cyclotron frequency, plasma frequency and ion sound velocity. Collisional frequency ν_c can be representative to charged particle collisions or charged particle versus neutral particles collisions, depending on the degree of ionization. Except for very weakly ionized gases, Coulomb scattering dominates. Typically we consider electron-electron collisions more than others because of ions greater inertia that make them usually move slower. Electron cyclotron frequency is needed whenever a magnetic field exists and it works as a threshold value for different regimes, when compared to collisional frequency.

It can be easily found solving the usual equation of motion of a charge particle in a magnetic field and it is defined as

$$\omega_{ce} = \frac{eB}{m_e},$$

where m_e here is electron mass. Electron plasma frequency represents the nat-

ural frequency with which electrons oscillate around ions, usually considered at rest for their greater mass, and it is defined as

$$\omega_p = \sqrt{\frac{4\pi n_0 e^2}{m_e}}\,.$$

In a similar way, ion plasma frequency is defined by substituting ion mass to electron mass. Finally, ion sound speed, has its role in acoustic waves propagating in plasmas and also in interfacing plasmas with conductors. It is defined as

$$c_s = \sqrt{\frac{T_e}{m_i}}\,,$$

with m_i ion mass. The dimensionless quantity that can be used to estimate ion velocity, v_i, when any process occurs in accelerating ions, is the so called *Mach number*

$$M = v_i/c_s$$

and will be found in ATHENIS preliminary analysis in section 3. It is a convenient dimensionless parameter to understand shock wave propagation and also edge phenomena as will be seen in the next paragraph. Typical plasma parameters for a few kind of the most familiar are summarized in the table below [3] .

Plasma	**Density** $[m^{-3}]$	**Electron** ω_p $[Hz]$	T_{e^-} $[eV]$
Fusion reactor	10^{21}	$3 \cdot 10^{11}$	10^4
Flame	10^{14}	10^8	0.1
Solar wind	$5 \cdot 10^6$	10^4	10
Glow discharge	10^{15}	$3 \cdot 10^8$	2

1.1.1 Debye sheath

It is worth understanding the plasma interaction with conductors. The underlying dynamics depends on the fact that electrons are much lighter than ions and, moreover, ion temperature is typically lower than electron temperature in ordinary plasma experiments. Once facing the plasma, a conductor is immediately reached by the electron flux. Consequently it will bring its potential negatively with respect to plasma potential. In this way incoming

electrons will be reduced and ions will be easily accelerated, until a dynamic equilibrium is reached. This would happen when ion flux and electron flux is the same at the surface of the conductor. The conductor object will be then covered my a positive charged sheath, called *Debye Sheath*, thick from tens to hundreds λ_D.

Let's consider a simple 1D geometry, setting the conductor at $x = s$ from the position ($x = 0$) where the main plasma faces the sheath. Assuming static and stationary conditions, homogeneous temperature and no magnetic fields, we take the collisionless electron flux momentum equation, riduced to:

$$en_e \frac{d\Phi}{dx} = \frac{dp_e}{dx}.$$

Here, n_e is the electron density and $p_e = n_e T_e$ is the electron pressure. Substituting pressure expression and integrating the equation, the following density profile is obtained:

$$n_e = n_s exp\left(\frac{e\Phi}{T_e}\right),$$

where n_s is the density at the plasma-sheath interface. From a Maxwellian distribution, the flux at the surface of the conductor is

$$\Gamma_e = \frac{1}{4} n_e v_{te} = \frac{1}{4} n_s v_{te} exp\left(\frac{e\Phi_w}{T_e}\right),$$

where v_{te} is electron thermal velocity and Φ_w the potential of the conductor. Ion flux is conserved through the whole sheath and it can be demonstrated to be:

$$\Gamma_i = n_s c_s.$$

Equating the fluxes, the conductor wall potential is

$$\Phi_w - \frac{1}{2} T_e ln\left(\frac{m_i}{2\pi m_e}\right).$$

Since ions are accelerated, because of the so called Bohm's criterion, until they reach c_s ($M = 1$) at the edge of the sheath on the plasma side, the voltage drop between the plasma and the interface between plasma and sheath is deducible from

$$\frac{1}{2} m_i c_s^2 = e\Phi_p,$$

that is

$$\Phi_p = \frac{T_e}{2e}.$$

Then the relation between plasma and floating (conductor) potential is:

$$\Phi_p = \Phi_f + \delta \frac{T_e}{e},$$

with

$$\delta = \frac{1}{2}\left[ln\left(\frac{m_i}{2\pi m_e}\right) + 1\right],$$

which is 3.3 for Hydrogen, 4 for Helium and 5.2 for Argon.
How thick is a sheath? We can apply Child law to ions to estimate it:

$$j = \frac{4\epsilon_0 \Delta V^{3/2}}{9s^2}\sqrt{\frac{2e}{m_i}},$$

where s in the sheath thickness and ΔV is the total applied voltage. We are supposing here that all the voltage drop is through the sheath. Since ions enter the sheath at the speed of c_s,

$$j = e n_s c_s.$$

Therefore the sheath thickness, about even 100 λ_D, is

$$s = \frac{\sqrt{2}\lambda_D}{3}\left(\frac{2e\Delta V}{T_e}\right)^{3/4}.$$

1.2 Hall thrusters

Space research has been making strides since its dawn. A large effort has been made to apply electric propulsion to spacecrafts and substitute chemical propulsion. Electrostatic thrusters work accelerating and neutralizing a ionized propellant usually extracting it from a plasma thanks to potential grids, magnetohydrodynamical mechanisms or more. Already in years sixties hall effect based thrusting was studied and gave birth to Hall-effect thrusters, used for the first time in 1971 in Russia to launch METEOR-18 satellite . They have been studied, developed and equipped on spacecrafts all over the world nowadays, and they appear to be the most commonly used to stabilize satellite orbits.

1.2.1 Hall-effect thruster principles

A Hall Effect Thruster (HET) is a type of electrostatic thruster in which a propellant gas is ionized and accelerated by a few hundreds volts potential between an anode, which coincides with the bottom of the thruster, and an external cathode, which is usually a hot cathode electron source. Perpendicularly to the electric field, a radial magnetic field confines electrons inside a toroidal channel creating an $E \times B$ drift current (see par. 1.2.3). This mechanism enhances ionization and gives Hall thrusters their name. Ions, on the other hand, are not magnetized because of their larger mass and they are ejected at typically $10 \div 50$ km/s [2]. Once passed through the acceleration region just on the edge of the thruster, ions are neutralized by incoming electrons, so the plume is no more electrically affected and a neat high speed gas flow, that permits spacecrafts thrust, is obtained. A complete scheme of a typical device is shown in fig.1.2.
The injected gas comes from the bottom of the thruster. Typical propellant is a noble gas (xenon, argon, krypton), but the choice can include many other materials, even solid fuels. Thanks to the magnetic field and a relatively low neutral density, electron axial mobility is reduced at the top edge of the thruster, letting the electric field increase and extract ions. In this way it behaves as a gridless ion source.

1.2.2 Thruster efficiency

Thruster's efficiency is defined as

$$\eta = \frac{F^2}{2\dot{m}P}$$

where $F^2/2\dot{m}$ is the minimum power required, while $P = I_{acc}V_{acc}$ is the actual power [1]. It can be expressed as a combination of three terms:

$$\eta = \eta_a \eta_f \eta_E.$$

The term

$$\eta_a = \frac{I_B}{I_a}$$

represents the anode efficiency: I_a is the total current (or anode current), I_B

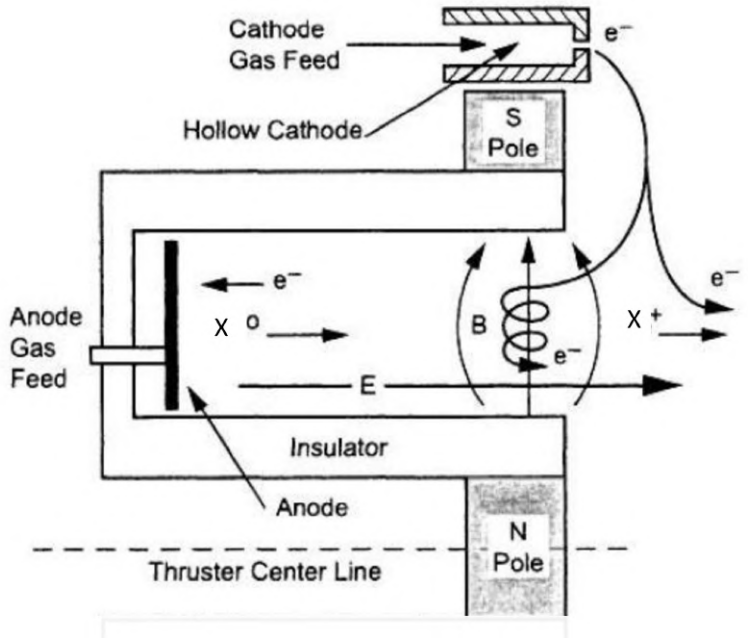

Figure 1.2: A typical Hall thruster scheme

is the fraction which neutralizes the ion beam, that is about 70% since about 20% of the current is given by electrons and it doesn't add any thrust. The term

$$\eta_f = \frac{\dot{m}_i}{\dot{m}}$$

is the utilization factor which regards how much of the neutral gas flow, $\dot{m}$ is ionized $\dot{m}_i$. It is a parameter quite hard to control because of its dependence with secondary electron emission that is affected by turbulence. Unfortunately, these topics are still hard to understand and nowadays researchers are often stressing the need of accurate models.

The last one is an energy related contribution

$$\eta_E = \left(\int_0^1 \sqrt{\frac{V}{V_a}} f\left(\frac{V}{V_a}\right) \frac{dV}{V_a} \right)^2$$

where V is the potential profile and V_a is the supply. It is strictly related to ionization for f is the ionization distribution. Experimental data show η_E between 0.6 and 0.9, which means ionization is mainly localized inside the channel. A good range is also found for η_f, from about 0.4 to 0.9. Hall thrusters usually operate with a working power of few kW, with a total

efficiency about $\eta \sim 60 \div 75\%$ that makes them tempting.

1.2.3 ExB drift

Charged particles, when moving across electric (**E**) and magnetic (**B**) fields, have to obey to Maxwell laws following complex trajectories. Magnetic field not only make particle rotate around, in fact whenever any force perpendicular to **B** appears also a drift appears. Plasmas affected by magnetic fields show many different dynamics and their study is far hardened from the simple ionized gas case. In the most general case the equation of motion is

$$m\frac{d\mathbf{v}}{dt} = \mathbf{F} + q\frac{\mathbf{v}\times\mathbf{B}}{c}$$

where **F** is a force perpendicular to **B** and **v** is the particle velocity. We can first ignore the velocity contribution parallel to **B** and we can break $\mathbf{v}_\perp$ in two components:

$$\mathbf{v}_c + \mathbf{v}_{gc}$$

where $\mathbf{v}_c$ is the velocity of the circular motion and $\mathbf{v}_{gc}$ is the velocity of the guiding center. Therefore the first part satisfies

$$m\frac{d\mathbf{v}_c}{dt} = q\frac{\mathbf{v}_c\times\mathbf{B}}{c}$$

and the second part

$$0 = \mathbf{F} + q\frac{\mathbf{v}_c\times\mathbf{B}}{c}.$$

The velocity of the guiding centre can be explicitly obtained performing a cross product with **B**:

$$\mathbf{F}\times\mathbf{B} = q\frac{\mathbf{B}\times(\mathbf{v}_{gc}\times\mathbf{B})}{c}$$

that means

$$\mathbf{v}_{gc} = \frac{c\mathbf{F}\times\mathbf{B}}{qB^2}.$$

Now, a general force would generate two different drifts for negatively and positively charged particles that would move in opposite directions. However, when the force is $q\mathbf{E}$ due to electric field, then positive and negative particles would drift in the same direction. Electrons in Hall thrusters are affected by this drift. We now have to consider that particles collide and this cause a

global viscous effect over the electron (and ion too) fluid. A rigorous way of proceeding will be found in the next section; to introduce the origin of Hall currents in plasmas and their effect we just consider the electron momentum equation:

$$\frac{e}{m}\left(\mathbf{E}+\mathbf{v}\times\mathbf{B}\right)+\nu_c\mathbf{v}=0, \tag{1}$$

where ν_c is the electron collision frequency and m the electron mass. A useful parameter is called *Hall parameter*, which is

$$h=\omega_{ce}/\nu_c,$$

where ω_{ce} is electron cyclotron frequency. It is easy to solve (1) and extract axial (E) and azimuthal ($E\times B$) velocities:

$$v_E=-\frac{eE}{m\nu\left(1+h^2\right)}, \tag{2}$$

$$v_{E\times B}=\frac{eEh}{m\nu\left(1+h^2\right)}. \tag{3}$$

Where, in the acceleration region, h is large, Hall parameter is given by the ratio of Hall current density and axial electron current density:

$$h=\frac{J_{E\times B}}{J_E},$$

since, by ω_{ce} definition,

$$v_E\simeq-\frac{E}{hB}, \tag{4}$$

$$v_{E\times B}\simeq\frac{E}{B}, \tag{5}$$

$$J_E=-env_E, \tag{6}$$

$$J_{E\times B}=-env_{E\times B}. \tag{7}$$

Then, in the acceleration region, electron mobility perpendicular to **B** field is strongly reduced and can be expressed ad $\mu_{e,E}=1/(Bh)$, while mobility parallel to **B** field is not affected and can be written with the unmagnetized case expression $\mu_{e,E\times B}=v_{E\times B}/E$. This shows how electrons are confined, even if collisions worsen the approximation.

1.3 Generalized Ohm's law

We consider now plasma phenomena developing over a long period such that collision frequency is greater than plasma frequency, $\nu_c \geq \nu_p$, and over a space much greater than Debye length, λ_D. Then we have to treat electron and ion fluid equations keeping a viscous term, to take into account collisions, as done before. We can also neglect charge separation, which happens within few λ_D. With these hypothesis, it is possible to step into a one-fluid model that simplifies the actual complex plasma behavior to the dynamics of only one fluid made of ions and electrons together. The start point is to consider electron fluid motion equation (and ion fluid similarly) which has this form:

$$m_e n \frac{\partial \mathbf{v}_e}{\partial t} = -\nabla p_e - ne\left(\mathbf{E} + \frac{\mathbf{v}_e}{c} \times \mathbf{B}\right) - m_e n \nu_c \left(\mathbf{v}_e - \mathbf{v}_i\right), \tag{8}$$

where the last term is a correction to collisionless fluid equation and must represent a viscous effect. It is useful, to introduce key quantities for the final equations, which clearly comes out from considering the relative motion of ion fluid and electron fluid and a few mean quantities:

$$\mathbf{j} = ne\left(\mathbf{v}_i - \mathbf{v}_e\right) \tag{9}$$

$$\rho = n\left(m_i + m_e\right) \tag{10}$$

$$\mathbf{v} = \frac{m_i \mathbf{v}_i + m_e \mathbf{v}_e}{m_i + m_e} \tag{11}$$

$$\eta = \frac{m_e \nu_c}{ne^2} \tag{12}$$

we call them, respectively, plasma current density, plasma mass density, plasma velocity and plasma resistivity. It is possible now to write down electron fluid motion equation multiplied by m_i and ion fluid motion equation multiplied by m_e:

$$m_i m_e n \frac{\partial \mathbf{v}_e}{\partial t} = m_i \left(-\nabla p_e - ne\left(\mathbf{E} + \frac{\mathbf{v}_e}{c} \times \mathbf{B}\right) + ne\eta j\right) \tag{13}$$

$$m_e m_i n \frac{\partial \mathbf{v}_e}{\partial t} = m_e \left(-\nabla p_i + ne\left(\mathbf{E} + \frac{\mathbf{v}_i}{c} \times \mathbf{B}\right) - ne\eta j\right) \tag{14}$$

then subtracting (13) from (14),

$$m_i m_e n \frac{\partial}{\partial t}\left(v_i - v_e\right) = ne\left(m_i + m_e\right)\mathbf{E} + \frac{ne}{c}\left(m_e\mathbf{v}_i + m_i\mathbf{v}_e\right)\times\mathbf{B} - m_e\nabla p_i + m_i\nabla p_e - \left(m_e + m_i\right)ne\eta\mathbf{j} \tag{15}$$

and substituting (9),(10),(11) it is obtained:

$$\mathbf{E} + \frac{\mathbf{v}}{c}\times\mathbf{B} = \frac{1}{\rho e}\left[\frac{m_e m_i n}{e}\frac{\partial}{\partial t}\left(\frac{\mathbf{j}}{n}\right) - \left(m_e - m_i\right)\frac{\mathbf{j}\times\mathbf{B}}{c} + m_e\nabla p_i - m_i\nabla p_e\right]. \tag{16}$$

Furthermore we can remove small terms: first of all linear terms in m_e, since $m_e \ll m_i$. It is also easy to see that

$$\left|\frac{m_e n}{e}\frac{\partial}{\partial t}\left(\frac{\mathbf{j}}{n}\right)\right| \Big/ \left|\frac{\mathbf{j}\times\mathbf{B}}{c}\right| \simeq \frac{m_e}{ec\mathbf{B}\tau} = \frac{1}{\omega_{ce}\tau},$$

where ω_{ce} is electron cyclotron frequency and τ the typical time scale, which we can assume to be much greater than the cyclotron period and therefore we come to the *Generalized Ohm's Law*:

$$\mathbf{E} + \frac{\mathbf{v}}{c}\times\mathbf{B} - \eta\mathbf{j} = \frac{1}{ne}\left(\frac{\mathbf{j}\times\mathbf{B}}{c} - \nabla p_e\right). \tag{17}$$

It is clear here why η is called resistivity. It is also worth noting that the $\mathbf{j}\times\mathbf{B}$ represents Hall effects. That means that also Hall current contribute to the total current in Ohm's law for plasmas. It is usually small and negligible, but for special cases as HET as well.

1.4 Hall thruster scaling

Hall thrusters typical dimensions and parameters are listed in the table below [2]. It is notable that their thrust might be quite low, but their specific impulse is high compared to thrusting not based on electric propulsion (specific impulse can be defined as thrust divided by mass flow rate or equivalently as impulse divided by propellant mass consumption).They are advantageous even respect to gridded ion thrusters because they do not have a space charge current limit (Child-Langmuir saturation). Although scaling thrusters is still empirical, they can be optimized quite easily, even to hundreds of kW in discharge power, or several N in thrust. The simplest scaling is to increase radial dimensions (homotetically) with $\sqrt{P}$ and the mass flow rate

proportionally to P. Note that density should be kept, in this way, around $10^{19}m^{-3}$. Great difficulties appear when scaling axially since there must be kept the same axial magnetic field distribution.

Power [W]	**Discharge voltage [V]**	**Current [A]**
1350	300	4.5
Thrust [mN]	**Flow [mg/s]**	**Channel area [cm^2]**
90.2	5.3	40

1.5 Adopted theoretical models

In this section I show which theoretical models stand behind the ignition of the HET and the measures that have been done on its plasma.

1.5.1 Cathode thermoionic emission

ATHENIS cathode was designed to be a Tungsten filament and, eventually, a hollow cathode which would guarantee better performances and longer life. Filaments help pre-ionization by emitting electrons through thermoionic emission. Emitted current density depends on the filament temperature, which depends on filament current. Thermoionic emission can be described by the Richardson's Law:

$$J_e = AT_{fil}^2 exp\left(-\frac{eW}{T_{fil}}\right) \tag{18}$$

where eW is the work function of the Tungsten ($4.55eV$), T_{fil} the filament temperature expressed in eV, and A a constant which depends on the material too, and for Tungsten is $7 \cdot 10^5 A/m^2K^2$.
Tungsten resistivity depends on temperature as

$$\rho(T) = \rho_0 T_{fil}^{1.2} Am \tag{19}$$

Comparing Ohm's law (20a) and black body radiation power (20b) it is possible to express filament voltage drop V_{fil} in terms of filament current I_{fil} (20c).

$$V_{fil} = \rho(T_{fil})\frac{L}{\pi r^2} I_{fil} \tag{20a}$$

$$V_{fil} I_{fil} = \epsilon \alpha_{SB} T_{fil}^4 2\pi r L \tag{20b}$$

$$V_{fil} = \tau I_{fil}^{13/7} \tag{20c}$$

where ϵ is a correction factor of 0.3, $\alpha_{SB} = 5.67 \cdot 10^{-8} J/m^2 K^4$ is Stefan-Boltzmann constant, r and L are respectively radius and length of the filament. Then, by a linear fit of (20c), ρ_0 can be estimated as:

$$\rho_0 = \tau^{0.7} \frac{\pi r^2}{L} \left(\epsilon \alpha_{SB} 2\pi r L\right)^{0.3}. \tag{21}$$

Finally by reversing (20a) and using (21) with (19), filament temperature is found:

$$T_{fil} = \left(\frac{V_{fil}}{I_{fil}} \frac{\pi r^2}{L \rho_0}\right)^{5/6}.$$

Every filament has been characterized to understand the role of filament current, that is the main parameter, along with pressure, on which we are interested in.

1.5.2 Langmuir characteristic

When an electrostatic probe, that is typically a small bare conductor, is polarized facing a plasma, the total current collected by the probe is just due to the difference between ion and electron contributes:

$$I = eA\left(\Gamma_e - \Gamma_i\right),$$

where A is the collecting area, e the elementary charge and Γ_e, Γ_i refer to electron particle flux and ion particle flux respectively. From the Debye sheath theory (sec. 1.1.1), these flux can be written as

$$\Gamma_e = \frac{1}{8} n_0 v_{te} exp\left(\frac{eV}{T_e}\right)$$

and

$$\Gamma_i = \frac{n_0 c_s}{2},$$

where T_e is the electron temperature and v_{te} is the thermal electron velocity. Therefore the electronic and ionic contributes, respectively, are:

$$I_e = eA\frac{1}{8}n_0 v_{te} exp\left(\frac{eV}{T_e}\right)$$

$$I_i = eA\frac{n_0 c_s}{2}$$

The floating potential,

$$V_f = -\frac{1}{2}T_e ln\left(\frac{m_i}{2\pi m_e}\right),$$

can be used as a reference and put into the merged expression by adding and subtracting it.
Then a characteristic obtained has the resulting form:

$$I = I_{is}\left[exp\left(\frac{e\left(V - V_f\right)}{T_e}\right) - 1\right],$$

where $I_{is} = 0.5eAn_0c_s$ is the ion saturation current, with n_0 the bulk plasma density and c_s the ion sound speed. From a fit of the characteristic it is possible to estimate saturation currents, plasma density, temperature, plasma and floating potential. It is also easy to recognize anomalous behaviors and to attach them to ions or electrons.

1.5.3 Mach probe

Mach number, as introduced previously, carries important information about ion velocity. To determine Mach numbers it is possible to use an appropriate probe made of two or more electrostatic probes. The probes have to be independent to each other and to collect current in the ion saturation region of the Langmuir curve. By comparing an upstream and a downstream measure in the simplest case of only two electrodes the thermal contribute is automatically removed from the upstream current and ion velocity is deduced from a proper model. Mach number relation with measured currents is the following:

$$\frac{J_N}{J_S} = e^{KM}, \tag{22}$$

where K is a calibration factor different from one model to another and depending on plasma peculiarities such as magnetization. For our purpose K is chosen as the best found in literature fitting our case [20]:

$$K = \sqrt{2\pi \frac{T_e}{T_i}}.$$

When showing results in sec. 3, upstream (downstream) current density, are substituted with the corresponding North (South) current densities, $J_N(J_S)$, and expressed in terms of collected currents thanks to the probe normalization factor:

$$\frac{I_N}{\alpha I_S} = e^{KM}. \tag{23}$$

Then, by definition, ion velocity will be estimate as

$$v_i = Mc_s. \tag{24}$$

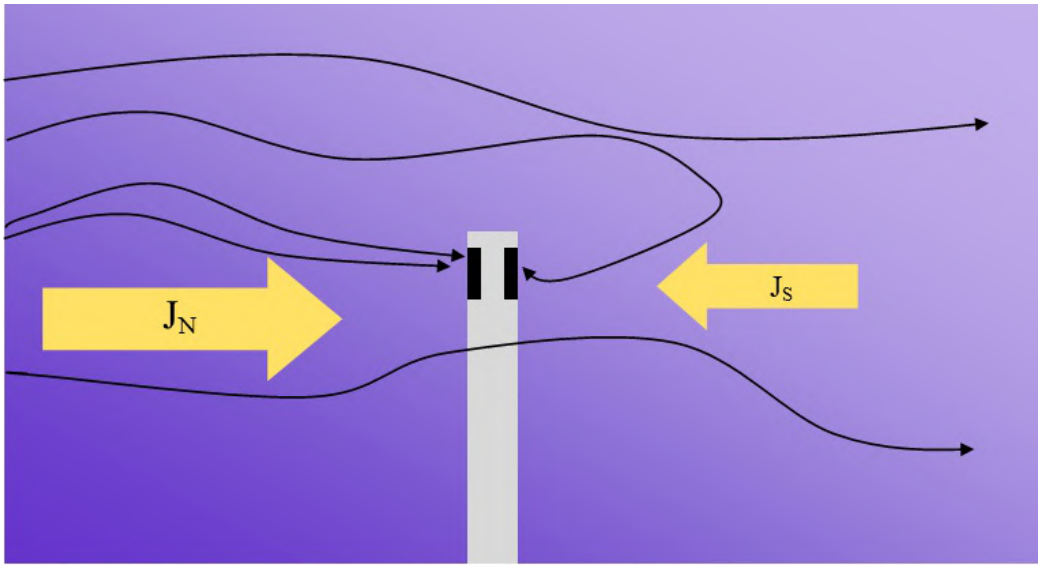

Figure 1.3: Mach functioning principle: the comparison between upstream current (J_N) and downstream current (J_S) permits to remove thermal contribute and estimate ion velocities.

1.6 Instabilities and oscillations in Hall thrusters

Hall thrusters show many kind of oscillations over a wide frequency band which affect thruster performance. They can affect ion beam divergence, efficiency and even be disruptive. They take place when the plasma adjusts particle ionization and diffusion to fit the imposed working conditions and, according to their characteristics, oscillations can be either coherent modes or turbulent. The study of instable modes is essential to understand turbulent electron mobility. We can see, roughly, what are the most common oscillations and instabilities known, classifying them by their frequency range. It will be clear that they actually cover a broad band and a rich variety of conditions.
Oscillations studies are based on some basic tools. Firstly, physical quantities (let's say $A(\mathbf{x}, t)$) can be broken up in two pieces:

$$A(x,t) = A_0 + A_1(\mathbf{x}, t)$$

a mean value, A_0, which is stationary and a perturbation, $A_1(x,t)$. Perturbations are considered to be small compared to their unperturbed values. This implies that quadratic terms in perturbed quantities are always negligible and therefore equations give a linear system to solve. This also implies that the *Principle of Superposition* holds and perturbations can be written as superposition of Fourier components. These components are waves typically writable as

$$A_1(x,t) = A_{1,0} exp\left(i\mathbf{kx} - i\omega t\right).$$

But actual oscillations can be made up of many independent sources or even consist of complex group structures, so when decomposing a signal, which typically differs from a sin-like wave, many harmonics can be found even though they don't have a physical relevance. Then triangular or step propagating perturbations show rich complex spectra once transformed. Here on, in formulas, n refers to density, E to electric field, B to magnetic field, ω to wave angular frequency and k to wave number.

1.6.1 Low frequency modes

A first kind of instability appear at frequencies between 15 and 22 kHz, often referred as '*Breathing mode*' [6]. It is a well known phenomena due to an

increasing of ionization in the near exit region, thanks to magnetic field lowering electron conductivity and therefore enhancing **E** field. In this way neutral density is depleted and the front of the flow is brought away. This leads to lowering ionization rate back and consequently restart the cycle. It can be better understood by writing ions and neutrals continuity equations, added a source term to include ionization [9] [12].

$$\frac{\partial n_i}{\partial t} = k n_i n_n - n_i \frac{v_i}{L}$$

$$\frac{\partial n_n}{\partial t} = -k n_i n_n + n_n \frac{v_n}{L}$$

where k is the ionization rate, the L the ionization region length, v_i and v_n respectively ion and neutrals velocities, and obviously n_i, n_n their densities. Once linearized and combined the two expressions, it is found

$$\omega = \frac{\sqrt{v_i v_n}}{L}$$

which fits observations on axial perturbations in many experiments.

A second sort of oscillations lies in the region of 5-25 kHz. It is an azimuthal perturbations often referred as *'rotating spoke'* and is also due to ionizations variations. Spokes nature is not very clear even though it is clear that the develop of an azimuthal local electric field E_θ creates an $E_\theta \times B$ drift that may increase electron transport. Depending on the phase shift ϕ between E_θ and density n, there grows an average axial electron current given by

$$\bar{J_x} = e \int n \frac{E_\theta}{B} \frac{dA}{A}$$

where the average is over θ. Writing

$$E_\theta = E_{\theta,1} sin\theta$$

$$n = n_0 + n_1 sin(\theta + \phi),$$

where n_1 is the amplitude of density perturbation, while $E_{\theta,1}$ is the amplitude of E field, this leads to an average axial current related to the phase shift by $\bar{J_x} = e n_1 \frac{E_{\theta,1}}{B} cos\phi$. This is possible because $\int_0^{2\pi} n E_\theta d\theta$ is not zero when both perturbations exist and are correlated. In this way the neat current gives an

anomalous diffusion of which the effective mobility is the ratio of $\bar{J}_x$ and the hall current J_θ. It is therefore:

$$\frac{1}{\omega_{ce}\tau_c} = \frac{1}{2}\frac{n_1 E_{\theta,1}}{n_0 E_x},$$

where τ_c denotes the average time between two collisions. It has been invoked to explain the mechanism the concept of Critical Ionization Velocity (CIV). It means that a charge separation interface rotates with a velocity $V_C = \sqrt{\frac{2e\epsilon_i}{M}}$, where ϵ_i is the ionization energy of the propellant. The formation of the spoke can be qualitatively seen as an alteration of ionization process due to density uniformities and ionization waves, which cause a loss in just born ions. The axial tilt to which is subject a spoke is determined by how far ionization waves propagate along the anode while ions accelerate through the channel. Experiments with homopolar discharges devices and magnetrons match this velocity, and Particle In Cell simulations (PIC) provides a good explanation of the dynamics. Simulations also point out that this regime could be avoided when cathode is far enough and B is enough strong outside the HET. It is notable that these oscillations should not affect significantly the performance since it is said they are localized near the anode where the power dissipated by electron is smaller then at the edge. Increasing discharge power, ionization gets azimuthally uniform and becomes more efficient, dumping then the oscillation.

The most interesting low-frequency oscillation, in the $10 \div 20kHz$ range, is due to $E \times B$ drift and it seems to be quite hard to describe because of the subtle role of secondary electron emission. It consists of large fluctuations, even comparable to stationary values. To understand electron interaction with walls it is mandatory to simulate the dynamics with a PIC Montecarlo. For this sake ion fluid is treated as a super-particle embedded into electronic fluid. An approach like this has been used in 1-D and 2-D simulations and gives good self-consistent results, making no assumptions on electron cross-field transport. The nature of this instability can be made clear considering the case of shockwave propagating across B field. Linearizing electron Vlasov equation, cold ion fluid equation and Poisson's equation, a quite complicated

dispersion relation can be obtained:

$$1 + k^2\lambda_{De}^2 + g\left(\frac{\omega - k_z V_d}{\omega_{ce}}, \left(k_x^2 + k_y^2\right), k_y^2\rho\right) - \frac{k^2\lambda_{De}^2\omega_{pi}^2}{\left(\omega - k_x V_{i,b}\right)^2} = 0$$

where g is the Gordeev function, V_d is the electron azimuthal drift velocity, ω_{pi} is the ion plasma frequency, ρ the electron Larmor radius, $V_{i,b}$ the ion beam velocity[1]. This oscillation becomes unstable when $\omega - k_z V_d = n\omega_{ce}$ that is, empirically, $k_z V_d \simeq n\omega_{ce}$. These results can be interpreted as electron Bernstein modes doppler shifted to ion acoustic modes while the oscillations grow along the channel toward the exhaust region. Frequencies are just smaller than $\omega_p i$ and not affected by electron drift velocity as long as $V_d \leq V_{Te}$, where

$$V_{Te} = \sqrt{\frac{8T_e}{\pi m_e}}.$$

Wave vectors are in the mm range.
This instability, which develops where modes merge in a relatively short time, is responsible of increasing in electron cross-field mobility of about an order of magnitude out of the channel. The hall parameter is also affected and researches show that hall parameter at the exhaust region drop down to a few orders of magnitude, meaning that effective collision frequency grows there up to a factor 10. From the simulations, many interesting aspects have been dug out. After a brief growing ($\sim \mu s$) the mode tends to become turbulent smearing the resonant modes, and this is consistent with the shifting toward an acoustic ion instability, also verified by experimental data. Furthermore, density and field fluctuations amplitude increase with plasma density. The weak point of the study of this kind of instability is the lack of a precise expression of cross-field mobility to be used in two-fluid models. This kind of instability is found also in magnetron discharges [14] [13].

1.6.2 High frequency modes

Many recent papers have suggested that two-fluid ideal MHD oscillations typically appear in the range of $20 \div 60 kHz$ [6] [19] [7]. The basics assumptions to foresee them involve a collisionless plasma with un-magnetized ion fluid,

[1] In local coordinates, x and y refer respectively to axial and azimuthal direction, while z radial direction.

in the non-resonant limit. They can become unstable and their instability can be driven by B gradients, n gradients and even T gradients. The dispersion relation has the same structure, but slightly different numerical coefficients, both in the case of relevant or non-relevant electron diamagnetic drift. In the most general case the main parameter that controls stability is n_0/B_0^2 (unperturbed density and magnetic field values) and for strong electric field instability starts if [2]

$$\frac{\partial}{\partial x} ln\left(\frac{n_0}{B_0^2}\right) > \frac{k_\perp^2}{k_y^2 \rho_s^2}\left(e\frac{E_{0x}}{T_e} + \frac{\partial}{\partial x} ln\left(B_0^2\right)\right),$$

while for weak electric fields

$$\frac{\partial}{\partial x} ln\left(\frac{n_0}{B_0^2}\right) ln\left(B_0^2\right) > \frac{k_\perp^2}{4k_y^2 \rho_s^2}.$$

Coordinate system is the same as in footnote 1. It can be seen as a Rayleigh-Taylor instability for which temperature gradient has been neglected. Once included, the dispersion relation becomes a three roots equation. It is worth noting that a few assumptions made in the simplest models, such as overall homogeneity and homogeneous temperature, are not consistent with observations. On the other hand strengthening conditions give very good results. It is not very clear, nowadays, the role of radial electron mobility and resonant modes for this kind of instability.

Other oscillations cover a large band up to 500 kHz. A first group of oscillations that cover the $20 \div 100kHz$ band is due either to inhomogeneities in weakly ionized plasmas or to ionization variations. These mechanism in fact alter interactions of electrons and ions with neutrals and, therefore, show consequences between ion collision and electron collision frequencies. When due to inhomogeneities, instability can grow if[3]

$$L_{\nabla n_e} \leq \frac{T_e}{\omega_{ce} m_e}\sqrt{\frac{M_i}{T_e}}$$

with a grow rate of

$$\gamma \simeq k\sqrt{\frac{T_e}{M_i}}.$$

[2] $\rho_s^2 = T_e m_i c^2/e^2 B_0^2$ is the ion-sound Larmor radius.
[3] $L_{\nabla n_e}$ denotes the typical length of density gradients.

When due to ionization-driven electron density increasing [18], instabilities are driven if

$$\sqrt{2T_e/\epsilon_i} \leq \Omega_e.$$

A well understood oscillation covers the $70 \div 500kHz$ range and in the Russian literature on topic it's often referred as '$transit - time\ oscillation$ ', since their frequency are about v_{di}/L. These oscillations are nearly axial and can be easily found as magneto-sonic waves. Their amplitude, strongly related to electron mobility, grows with B until an optimum is reached; for higher fields they are quenched. Their dispersion relation can be obtained as

$$\omega \simeq k_x v_{di} \frac{b}{b+1},$$

where $b = v_B / \| v_{de_y} \|$ and with a grow rate, in the instability region:

$$\gamma \simeq k_x v_{di} \frac{\sqrt{b}}{b+1}.$$

They are also believed to play an important role in plasma transport phenomena and behave as turbulent oscillations easily detectable and predictable, analytically and numerically. It is also noteworthy that the grow rate can be shown to vary proportional to electron mobility $\mu_e^{-1/2}$.

1.6.3 MHz band

Higher frequency modes also exist, even over MHz. Like transit-time oscillations, higher oscillations arise with increasing **B**. Waves in this band propagate mostly azimuthally. Theories about flute modes ($k_z = 0$) are well defined and reach their conclusions either by starting from two fluid collisionless plasma equations, keeping unmagnetized ions and small inhomogeneities [7], or by the use of a more suited collisional weakly ionized plasma in $\mathbf{E} \times \mathbf{B}$ coupled fields [17]. Assuming the most relevant gradient is that of the charged particle density, its analysis starts from electrons and ions

momentum equation:

$$\Gamma_x^{\pm} = \left(-D_{\perp}^{\pm}\frac{\partial n}{\partial x} \pm \mu_{\perp}^{\pm} n E_x\right) \pm h_{\pm}\left(-D_{\perp}^{\pm}\frac{\partial n}{\partial y} \pm \mu_{\perp}^{\pm} n E_y\right) \tag{25}$$

$$\Gamma_y^{\pm} = -\left(-D_{\perp}^{\pm}\frac{\partial n}{\partial y} \pm \mu_{\perp}^{\pm} n E_y\right) \mp h_{\pm}\left(-D_{\perp}^{\pm}\frac{\partial n}{\partial x} \pm \mu_{\perp}^{\pm} n E_x\right) \tag{26}$$

$$\Gamma_z^{\pm} = \left(-D_{\parallel}^{\pm}\frac{\partial n}{\partial x} \pm \mu_{\parallel}^{\pm} n E_x\right). \tag{27}$$

D denotes the usual diffusivity, μ mobility, $\pm$ ions and electrons by their charge and the pedices $\perp$ and $\parallel$ their action with respect to magnetic field. The expression must be solved into continuity equation

$$\frac{\partial n}{\partial t} + \nabla \cdot \Gamma_{\pm} = 0.$$

So first solution has to be broken into a stationary piece and a perturbed piece, such as $n = n_0 + n_i e^{ik_x x + ik_y y - i\omega t}$ for what concerns density and $V = V_0 + V_i e^{ik_x x + ik_y y - i\omega t}$ for potential. It can be solved using the method of Kadmotsev-Nedospasov, which requires a trial solution. Once linearized, Simon assumes sin-like trial solutions for density and potential perturbations, and a few boundary conditions in a axially finite slab of thickness l:

$$V_i(0) = V_i(l) = 0 \tag{28}$$

$$n_i(0) = n_i(l) = 0 \tag{29}$$

Also total electric current (Γ) boundary condition has to be set such that $\Gamma_i(0) = \Gamma_i(l) = 0$. Axial oscillations seems to be not much considered anywhere in literature, because non-flute solutions, that consist of axial oscillations are ignored as Choueiri does. Then, keeping only azimuthal modes, the expression for the frequency becomes:

$$\omega = \frac{\Psi k_y \frac{dn_0}{dx}\left[\omega_{c+}\mu_{\perp+} - \omega_{c-}\mu_{\perp-}\right] - n_i\left(Y_+ - Y_-\right)k_y\Theta}{n_i^2\left(Y_+ + Y_-\right)^2 + k_y^2\left(\frac{dn_0}{dx}\right)^2\left[\omega_{c+}\mu_{\perp+} - \omega_{c-}\mu_{\perp-}\right]}, \tag{30}$$

where

$$\Psi = -n_i\Lambda^4\left(\mu_{\perp-}D_{\perp+} + \mu_{\perp+}D_{\perp-}\right)$$

with $\Lambda^2 = k_y^2 + (\pi/l)^2$ and, denoting ion and electron cyclotron frequency with $\omega_{c\pm}$,

$$\Theta = -E_{0x} n_i \left[\omega_{c+}\Lambda^2 \mu_{\perp-} - \omega_{c-}\Lambda^2 \mu_{\perp+}\right] + \frac{dn_0}{dx}\left[\omega_{c-}\Lambda^2 D_{\perp+} - \omega_{c+}\Lambda^2 D_{\perp-} + \frac{1}{2}\mu_{\perp-}\mu_{\perp+}\left(\omega_{c+} + \omega_{c-}\right)\frac{dE_i}{dx}\right]. \tag{31}$$

Instability grow rate corresponds to the imaginary part of the solution and results:

$$\gamma = \frac{k_y^2 \Theta \frac{dn_0}{dx}\left[\omega_{c+}\mu_{\perp+} - \omega_{c-}\mu_{\perp-}\right] + \Psi n_i \left(Y_+ + Y_-\right)^2}{n_i^2 \left(Y_+ + Y_-\right)^2 + k_y^2 \left(\frac{dn_0}{dx}\right)^2 \left[\omega_{c+}\mu_{\perp+} - \omega_{c-}\mu_{\perp-}\right]}. \tag{32}$$

The solutions found by Simon seems to be different from the ones found by Esipchuck and Tilinin, done thanks to the same method used to find other oscillations [7] but trigger by the magnetic field gradient when $\partial B_r \partial x > 0$.

2 Experimental setup

2.1 ATHENIS thruster

ATHENIS (Alternative Thruster Hall Effect Negative Ion Source) was developed to study H^- ions production by H^+ interactions with cesium-coated surfaces. The generation of negative Hydrogen ion beams is a powerful technique to heat tokamak plasmas in order to help them to reach fusion conditions. Tokamaks work with a hot plasma confined through a screwed toroidal magnetic field of about a few tesla. Particles injected into tokamaks cannot ever be charged otherwise they would be quickly lost as they find on their way the magnetic field, so it is mandatory to produce neutral particle beams and this is obtained typically by charge exchange interactions of a electrically charged beam with a neutralizing gas at rest. Unfortunately H^+ ions, at the required beam energy of $\sim 100keV$ needed to reach plasma core, tend to ionize again once neutralized so that the neutral beam produced is too soft. On the other hand, H^- ions are not affected by this problem and, further on, since the neutral particle production display a maximum depending on beam energy and bulk plasma density, neutral beam density can be tuned properly. Neutral beam production is one of the key research activities at Consorzio RFX in Padua, as part of ITER international research program. To generate negative Hydrogen ions the mechanism under study is a sputtering reaction between H^+ and Tungsten Cesium-coated surface. Sputtering over Tungsten surfaces frees Hydrogen ions, possibly negatively charged. The cover lowers work function from $4.55eV$ to $\sim 1.8eV$ maximizing the probability of having negative sputtered ions while positive ions are preferably kept at the surface.

ATHENIS thruster is not a thruster optimized for satellite propulsion: its design and dimensions have not such a sake. Even if built with not an optimal design for thrusting and cooling, it was found having an incredibly good functioning as it is actually optimized to furnish a positive H ion beams that is accelerated toward a cesiated surface. Its concept can offer several advantages: a limited amount of co-extracted electrons from surfaces, a more uniform generation of negative ions and a lower rate of destruction of negative ions than other techniques. Numerical data about its efficiency and working condition can be found in section 3 and in previous studies [8].

The main body consist of a steel block with a cylindrical 25.2 mm diameter slot, 58.5 mm long. In this block are inserted 15 arrays of permanent magnets that provide a magnetic field of about 20 mT at its maximum. A central magnetic rod (12 mm diameter) provides to close magnetic lines and, being insulated from the main body, its potential can be set independently. To ensure insulation, it is enveloped with a quartz crystal glass tube as well as the slot walls. The top of the thruster is also covered with a thick crystal slab, since the whole body is at the same potential and letting it exposed to the chamber would create a plasma outside the channel. If this happens the current would be closed also outside the channel, impeding the switching on of the anode. A boron nitride cap protects the top of the central rod from the plasma. It is mandatory to protect it from overheating since it is magnetized and if it is brought to high temperatures **B** field is strongly affected. From the bottom of the thruster the propellant gas flows in.
ATHENIS did not have an active cooling system during this thesis work, so measures done on it were developed over short time lapses to permit the switching off of the thruster and avoid overheating.The whole structure is shown in fig.s 2.4 and 2.5 while ATHENIS thruster in fig. 2.6.

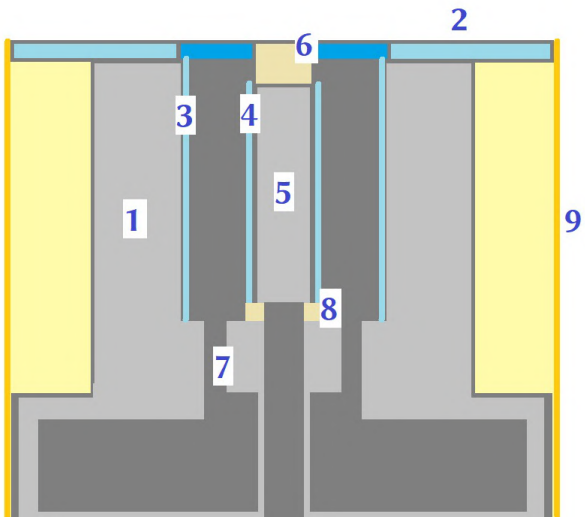

Figure 2.4: Thruster structure (not in scale): 1. Main body, 2. quartz slab, 3. inner large quartz, 4. inner tight quartz, 5. magnetic rod, 6. rod BNO top, 7. gas holes, 8. insulator washer, 9. external kapton and mylar insulation

Previous studies on ATHENIS have determined its magnetic field profile, plasma densities and electron temperatures operating in Nitrogen and Hydrogen in a High Impedence working regime [8]. For both gases, densities

are about $10^{17}m^{-3}$ and electron temperatures between 2 and $4eV$. Magnetic profile is shown in figure 2.7.

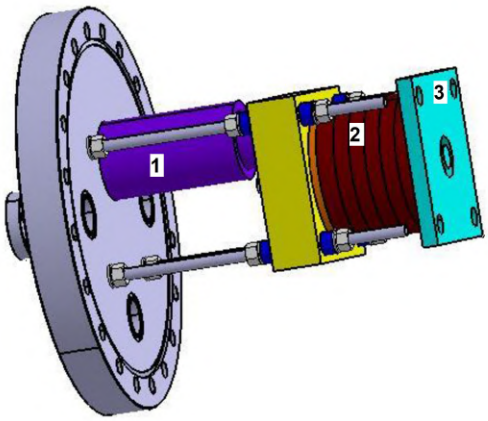

Figure 2.5: Thruster structure: 1. Peek gas channel, 2. main body, 3. protecting quartz slab.

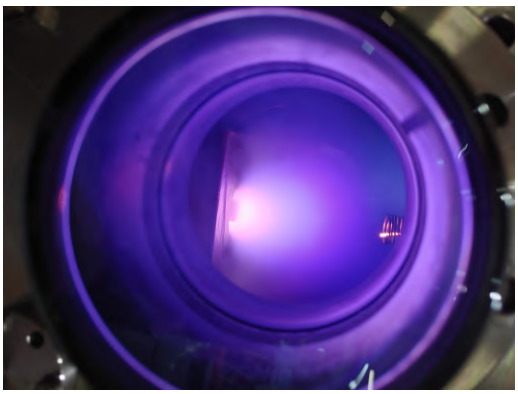

(a) *ATHENIS thruster operating with Ar propellant.*

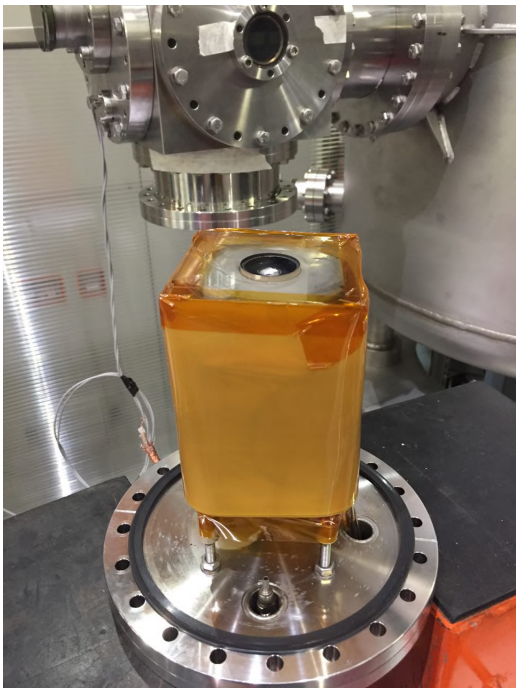

(b) *ATHENIS thruster outside its vacuum chamber.*

Figure 2.6: AHTENIS Thruster photos

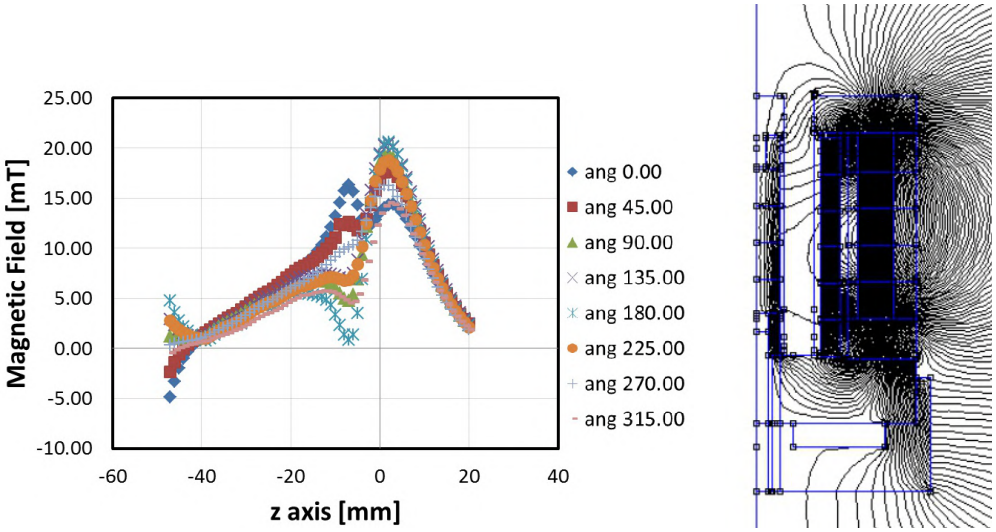

(a) *ATHENIS magnetic axial profile at different angles.*

(b) *ATHENIS magnetic profile.*

Figure 2.7: ATHENIS magnetic profile according to previous studies [8].

2.2 Vacuum and power setup

Hall thrusters have to be tested at low pressures, like usual experiments involving plasmas. To reach good vacuum conditions the whole system was set into a vacuum chamber as shown in fig.2.8. A rotary pump ($60m^3/s$) sets up the pre-vacuum with a limit pressure of $10^{-3}mbar$, in series with a turbopump ($1000l/s$) that can bring pressure down to $10^{-7}mbar$. The thruster is placed in a smaller chamber on a main chamber side. In this way it is easy to fix problems and to add or remove probes.

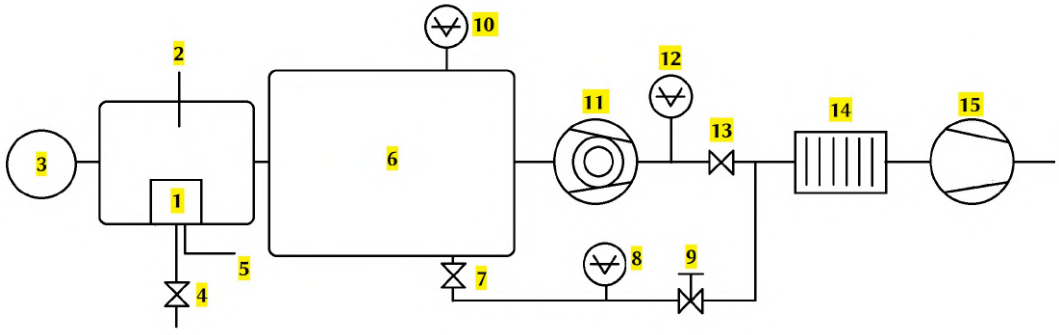

Figure 2.8: Vacuum setup: 1. Hall Effect Thruster, 2. Tungsten pre-ionization filament or cathode, 3. Probes, 4. Propellant inlet, 5. Anode, 6. Main vacuum chamber, 7. Rotary pump line valve (VGP), 8. and 12. Pre-vacuum pirani gauges, 9. Vent valve, 10. Full range pressure gauge, 11. Turbomolecular pump, 13. Turbo line valve (VGT), 14. Sieve trap, 15. Rotary pump

(a) *KEPCO anode power supply.*

(b) *Cathode polarization TENMA power supply.*

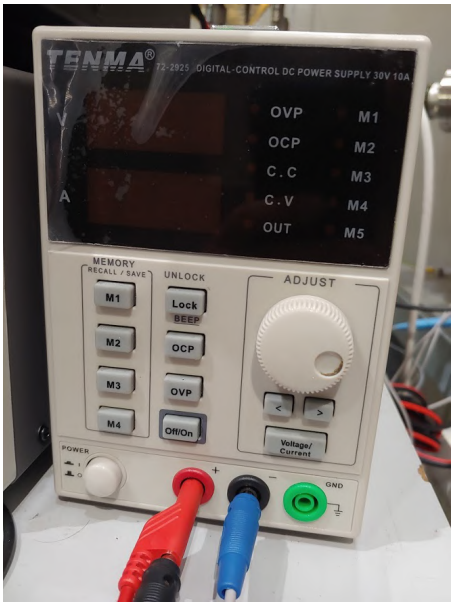

(c) *Cathode filament power supply.*

(d) *MKS flow controller.*

(e) *MKS flow controller module.*

Figure 2.9: Experimental instrumentation used to run ATHENIS.

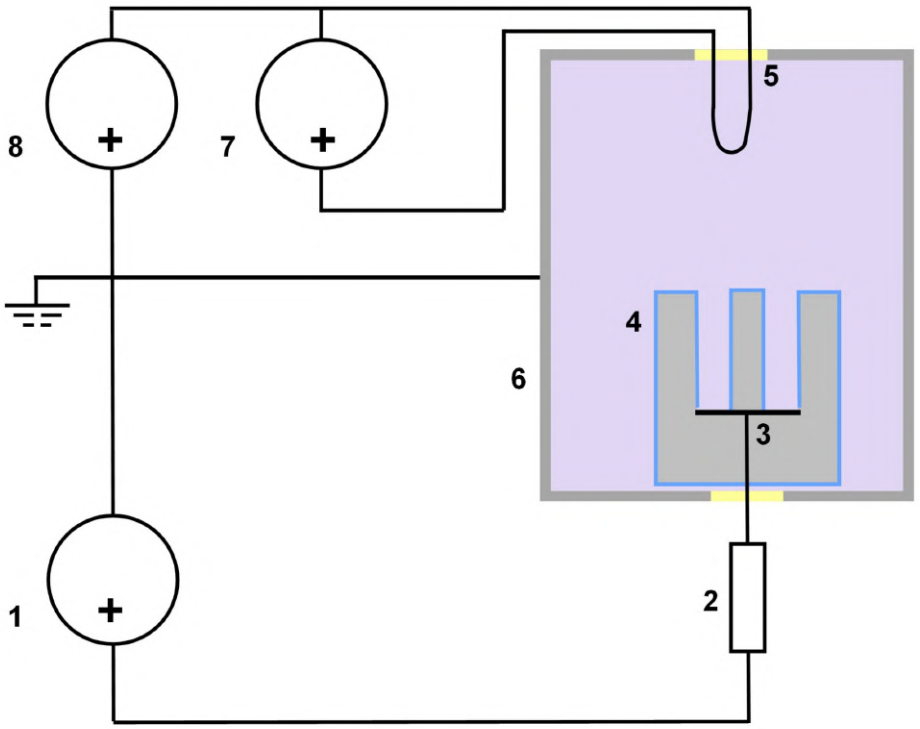

Figure 2.10: ATHENIS electric circuit: 1. Anode power supply, 2. Shunt resistance, 3. Anode, 4. HET, 5. Cathode (Tungsten filament), 6. Vacuum chamber set to ground, 7. Filament supply, 8. Filament polarization supply.

Flow [SCCM]	100	90	80	70	60	50	40	30	20	10
Pressure [$10^{-3}mbar$]	4	3.5	3.1	2.5	2.2	1.8	1.5	1.2	0.79	0.37
Ar flow [mg/s]	2.98	2.68	2.38	2.10	1.79	1.49	1.19	0.89	0.60	0.30
He flow [ug/s]	300	270	240	210	180	150	120	90	60	30
H flow [ug/s]	75	68	60	52	45	37	30	22	15	7.5

Anode was controlled with two different settings. One of these is a series of two or three Kepco power supplies that can work up to 300 V, 4A. Alternatively a single TDK power supply, working with 0-600V, 1.3 A. A Tungsten wire was often use as a cathode at least in a pre-ionization step, especially when driving anode potential with only two Kepco, since the lower the potential drop between anode and ground (or cathode) the harder is to switch on the thruster. Once it was ignited, the filament was brought to ground potential, for its scope was only to keep a good spatial ionization and facing the plasma quickly damages it. Tungsten filaments operated with a current range of 5-7 A, that is with an emitting power of $\sim 40W$. To set its current input a

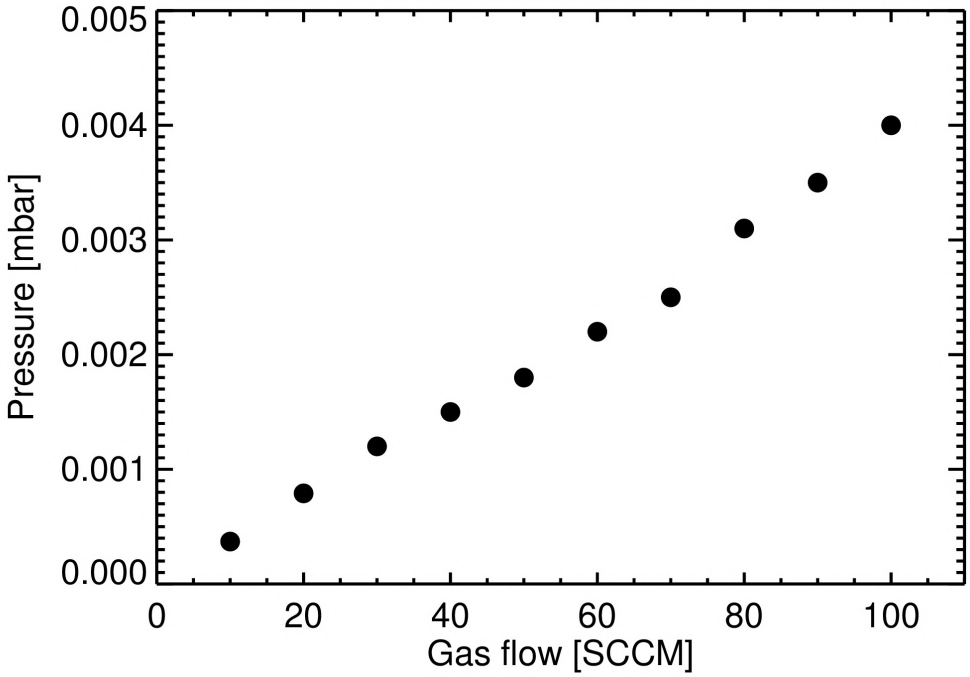

Figure 2.11: Pressure (mbar) and flow (SCCM) linearity.

TENMA DC power supply (30 V, 10 A) was used, while for its polarization a TENMA DC double power supply (32 V, 3 A) was used, coupling the two channels in series so that a total 64V bias could be reached. The circuit scheme is shown in fig. 2.10; all the instrumentations can be seen in fig. 2.9.

A ICOM IC-7300 50MHz transmitter has been also tested as electron source to keep alive the thruster, sometimes together with the filament. The gas flow (H, He, Ar, N_2) was controlled by a MKS flow controller which gives also numerically the flow in SCCM (Standard Cubic Centimeter per Minute). Pressure shows to be linearly proportional to the flow so that missing points can be extrapolated (the relation between pressure and flow is shown in fig. 2.11). Note that at fixed SCCM, the mass flow depends on mass as shown in the table. Helium and Hydrogen flows are too little to ignite the thruster; that is why, as will be explained in sec. 3, a greater pressure were needed so that it could no longer be controlled directly with the MKS but setting the gas cylinder valve.

To record probe signals, three yokogawa measurement stations were used: a DL716 for the Mach probe data and two WE800 for the fluctuation data.

2.3 Diagnostic system

All the main useful quantities for general purpose are obtained thanks to a Mach probe, which is a double electrostatic probe (fig. 2.12). The probe electrodes were two 1.5 mm thick Tungsten sticks inserted into a MACOR (ceramic) arm, axially perforated and open on the opposite sides. The probe was clamped to a mounting bracket able to rotate around its axis.
The exact collecting area values are not necessary to know Mach numbers as will be explained in sec.3.3. It was set about 2 cm above the center of the thruster, to measure plume properties (fig. 2.13). Electrodes had to be small and with a good shunt resistance to collect a small portion of the total current otherwise the probe would have affected the plasma.

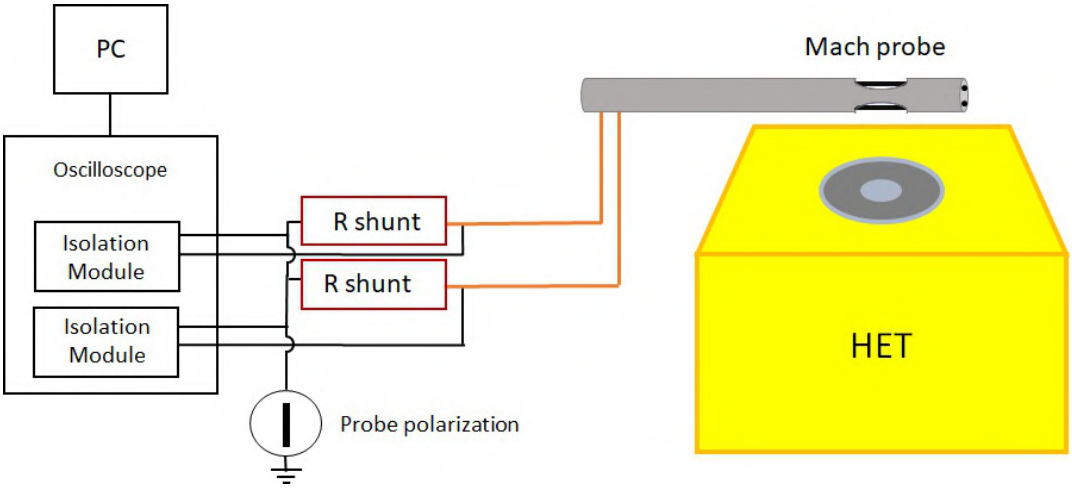

Figure 2.12: Scheme of functioning of the mach probe (not in scale). Electrodes are polarized, the current forced through shunt resistances and their voltage drop read by the oscilloscope.

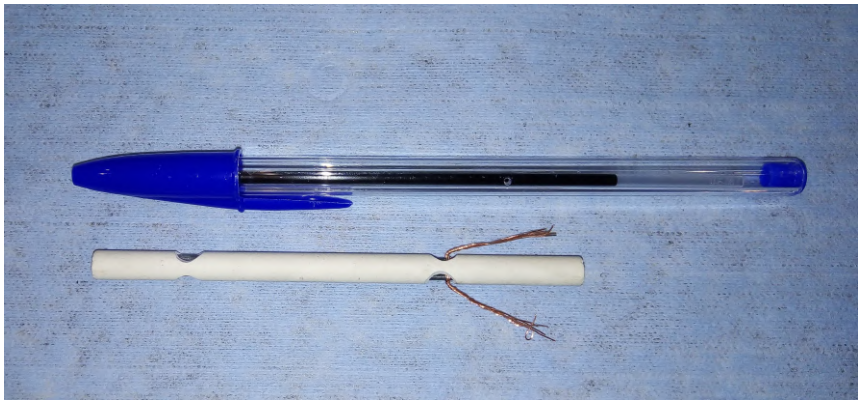

(a) *Mach probe body compared to a biro pen.*

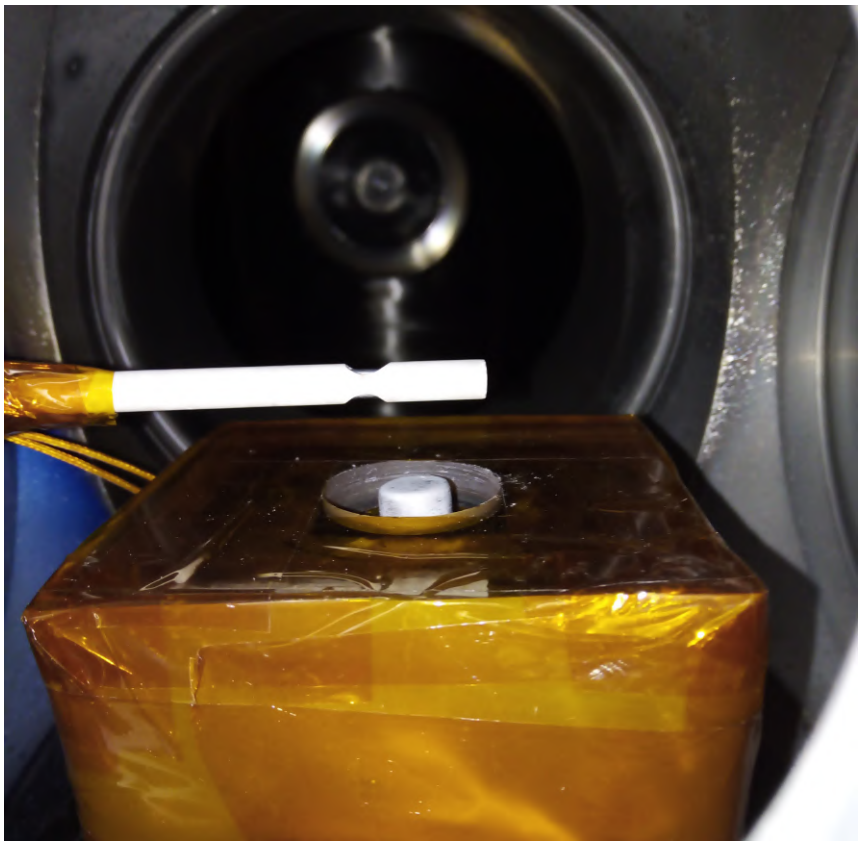

(b) *Ready setting for the probe, just above the hall thruster.*

Figure 2.13

2.4 Instabilities study probe

To measure electrostatic fluctuations, a specific probe has been built. It consists of an array of 24 electrodes clamped between two PEEK (PolyEther Ether Ketone) rings. A preliminary setting has been tried, with the probes inserted into an aluminum ring, which does not affect significantly magnetic fields for

it is paramagnetic, but it couples capacitively the probes. The angle between every probe was about 15°. The probe can be seen in fig. 2.15.
Every probe was a shielded cable, their metal braid was cut a few cm before the end, to be surely covered inside the PEEK rings, and forced to ground on the two electronic boards (fig. 2.16). At their end, the cable kernel was opened so that the surface exposed to the plasma was about 3 mm long and 1 mm of diameter. They were aligned thanks to rails printed expressly for that on the PEEK rings, and they were inserted with their point at 1.9 cm from the center. Once ready, the probes were fixed over the HET top, ready to measure electrostatic fluctuations at about $5mm$ from the thruster exit. To prevent damages due to direct exposition and to cover completely the metal braids, the inside was brushed with Boron Nitride, which is a good cheap insulator, suitable for vacuum, that can stand direct plasma.
Signals were read through a voltage divider expressly made for our case: quenched by a $680k\Omega$ resistor and shunt on a $4.7k\Omega$ resistor. Both resistors has been chosen to stand $1W$. A complete scheme of fluctuation probes working is reported in fig. 2.14

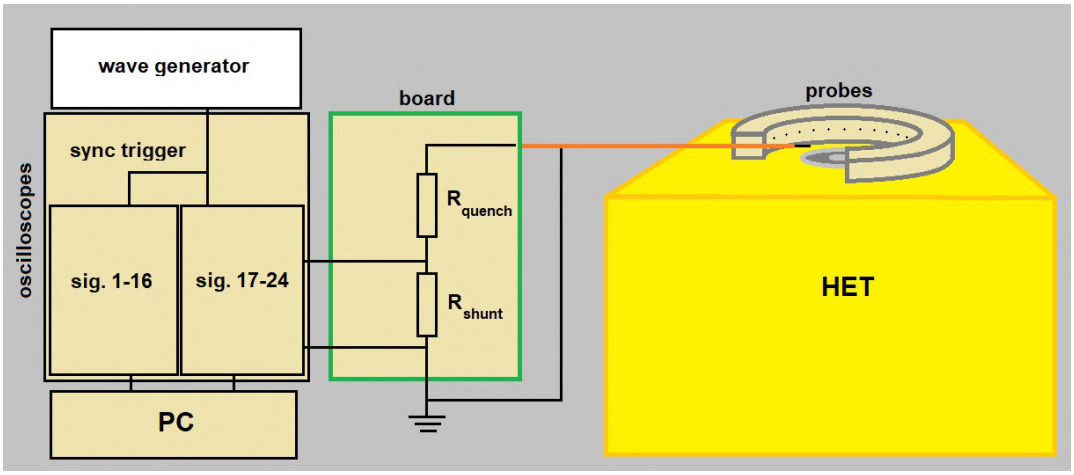

Figure 2.14: Scheme of functioning of the fluctuation probe system (not in scale): every probe has its own voltage divider, from which signals are recorded by the modules. Two measuring stations start acquisition simultaneously, triggered by an external pulse.

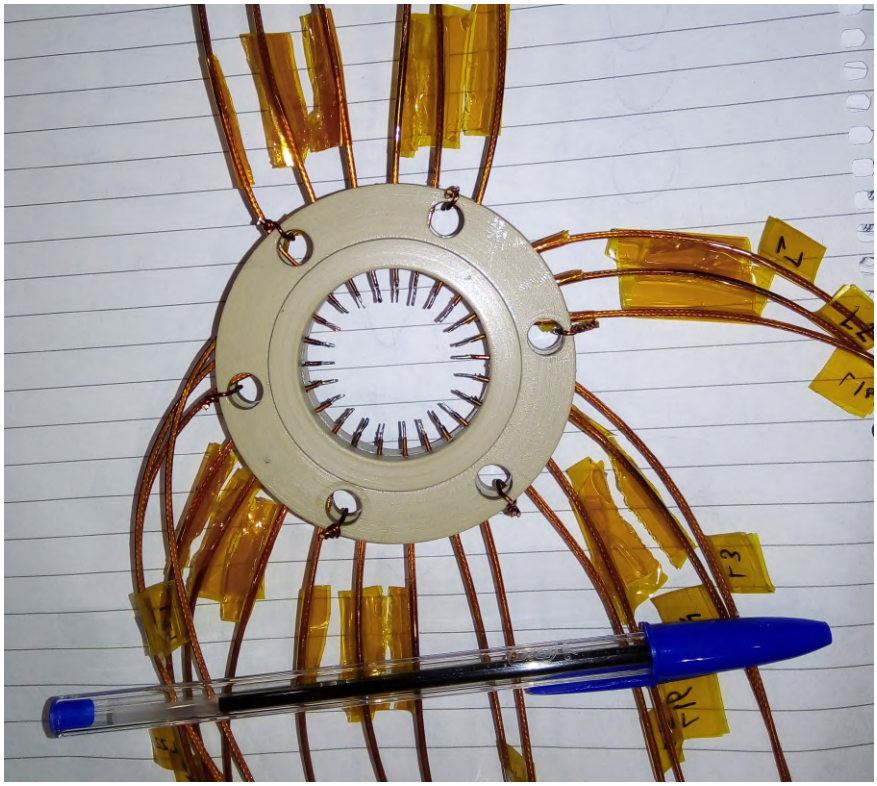

(a) *Probe body compared to a biro pen.*

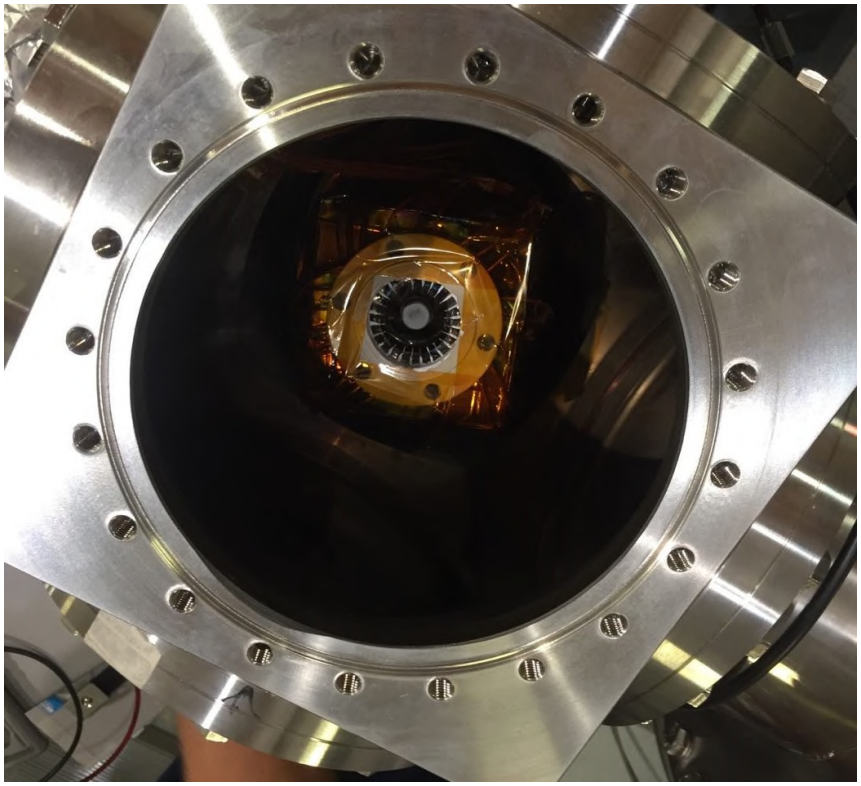

(b) *Ready setting for the prove, just above the hall thruster.*

Figure 2.15

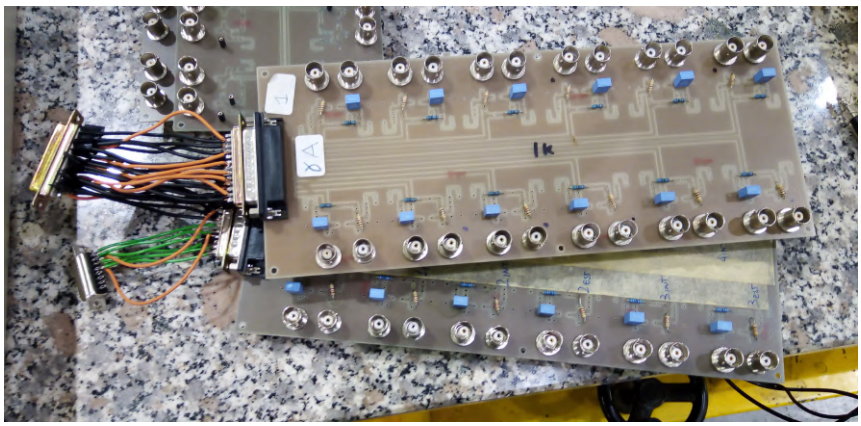

(a) *Electronic boards expressly made for the probe system. .*

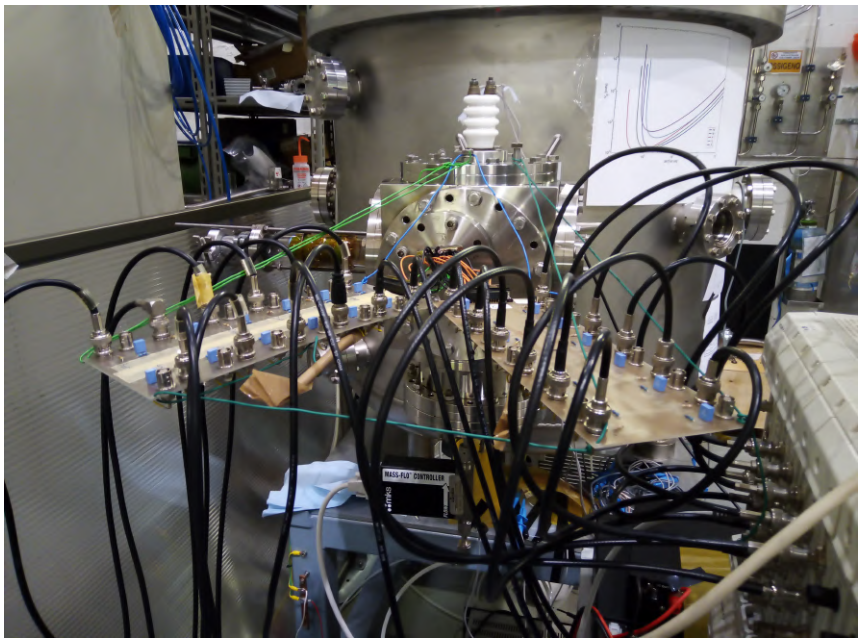

(b) *Boards ready for acquisition.*

Figure 2.16

3 Experimental analysis and results

3.1 Main schedule

First thing to study ATHENIS HET is to switch it on. To set the chamber ready both pumps were needed working with Argon and Helium, while Hydrogen and Nitrogen plasma needed higher pressure as learned from their Paschen curves.The rotary pump was the first to be switched on, to bring pressure down to $\sim 10^{-1} mbar$, then the turbo-molecular one could be switched on if a safety threshold was reached. A full range pressure gauge added an automatic binary condition whether a preset threshold was reached or not. When only the rotary pump was running, both the lines were left open to gain conductance while, when using the turbo-molecular pump, a valve (VGP in 2.8) was close to make them work in series. Meanwhile the Tungsten filament could be slowly heated up.
It couldn't be simply brought quickly to $\sim 5 \div 6A$ for in this way it would be easily eroded. Gases cylinders were opened and, by setting properly an MKS controller, the gas inlet was open. Flows between 0 and 100 SCCM were directly controlled by the MKS while greater flows were adjusted manually by changing it directly on the cylinders. Since pressure is linearly proportional to flow (fig.2.11) it could be checked just by measuring vacuum chamber pressure. Experimental results, hereon, will be presented depending on pressure (mbar), instead of gas flow (SCCM). Then by bringing the filament potential about 64V lower than ground (vacuum chamber) a soft plasma was created near the cathode. This step which could appear unneeded, was actually necessary to ignite the HET by switching on its power supply and setting it to, often, its maximum voltage. Whenever the thruster started, cathode polarization was brought back to zero. Sometimes it was difficult to start it anyway, so cathode polarization could be kept on or pressure could be changed and eventually brought back to needed working conditions.
Two working regimes have been studied: a High Impendence regime (HI), thanks to TDK power supply characterized by low current ($I_{limit} \sim 1.3A$); and a Low Impedence regime (LI) with Kepco supplies ($I_{limit} \sim 4A$). Argon HI data points are black and blue, while Argon LI points are yellow and red. The cyan triangles, instead, are Helium data. A better understanding of their relation with power and pressure is shown in figure 3.17.

Floating potential reaches 66% of the discharge voltage, and it keeps between $40 \div 60\%$ for LI (fig. 3.18), while it is between $20 \div 30\%$ for HI. This results confirm partially what is said by other experiments that V_f can reach about 90% of the discharge voltage. Filament current significantly affects floating potential that is lower for higher currents for both LI and HI data points. Previous measures on ATHENIS [8] on Hydrogen and Nitrogen were performed with the same HI regime, resulting in a systematically lower electron density.

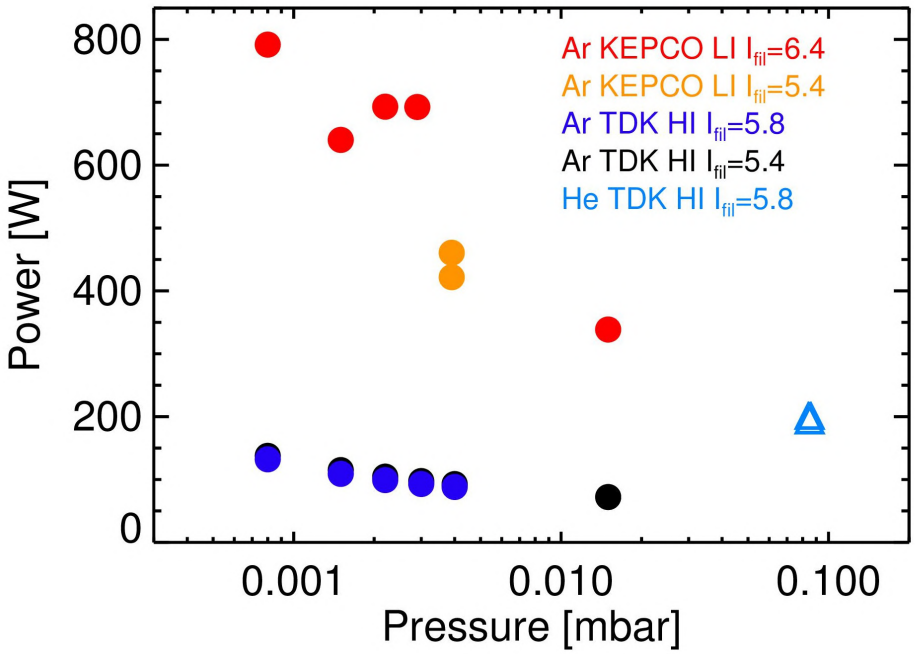

Figure 3.17: Working regimes plotted in relation to relevant parameters: pressure, filament current and working power. Argon data are represented by the dots, while Helium data by the triangles.

3.2 Cathode behaviour

Many cathode configurations have been explored to ensure a stable working of the HET. Mostly 0.025 cm diameter Tungsten filaments have been used, with different length and shapes. The filaments were from 7.2 to 20.5 cm long and could be either curly or 'U-folded'. The longer the filament, the higher its voltage drop is needed to heat it up enough. The configuration which ensured a longer life was found to be a 8 cm long U-folded filament clamped on the higher voltage side to a 1 mm thick Tungsten grid. While the thin filament provides spatial charge by thermoionic emission, the grid collects most of

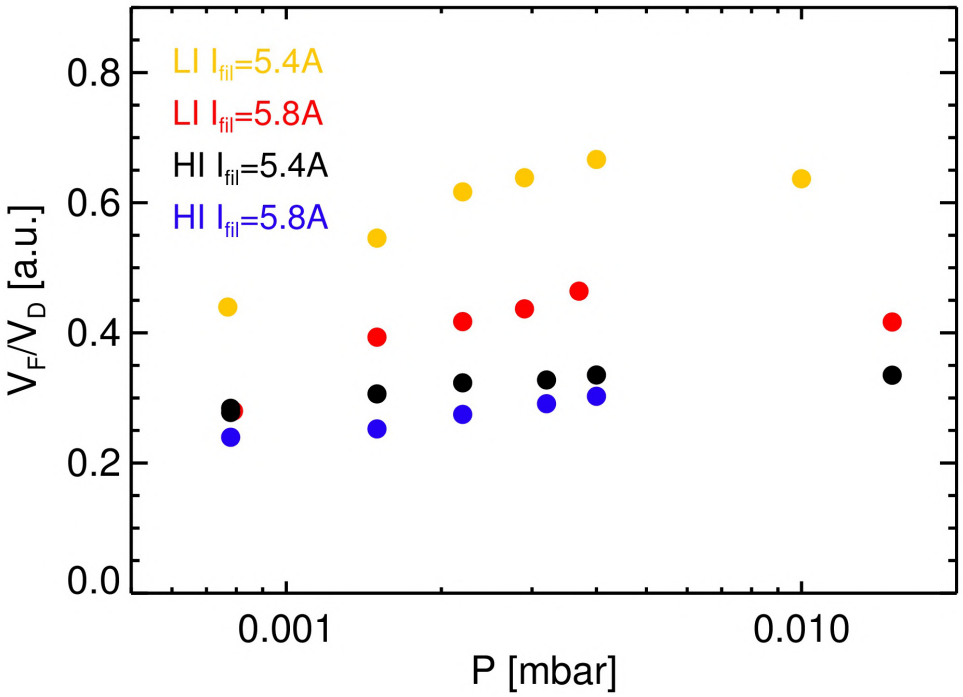

Figure 3.18: Floating potential normalized over discharge voltage. Orange and red dots are about Low Impedence regime and black and blue dots are about High Impedence regime. Filament current significantly affects floating potential that is lower for higher currents.

the total current, avoiding filament overheating. Nevertheless, propellant ions coming from the anode end sputtering over the filament and so act as the main erosion cause and the grid has a marginal effect over filament life. Every filament used has been characterized. A few V_{fil} vs I_{fil} curves have been reported in fig. 3.19. Temperature curves and emitted current curves for different filaments can be found in fig.3.20, fig.3.21. Note that the until 2A, data do not display a perfect behavior, but this is only due to a difficulty to reach thermal equilibrium at low voltage.

Also a Radio Frequency source was added to explore cathodes behavior. Mainly it was needed to help pre-ionization when pressure or filament conditions were not enough to provide a good electron density. Typically, the RF source were necessary with pressures lower than $1.2 \cdot 10^{-3} mbar$. The RF source was switched on and frequency tuned to one of the resonances proper of the vacuum chamber. Many of them were found, mostly used were at 14, 26, 35 and 47 MHz. The RF antenna consists of a glass tube closed on one side and opened to the chamber on the other one. A primary coil of two turns and a secondary of about 50 turns were wrapped around the cylinder.

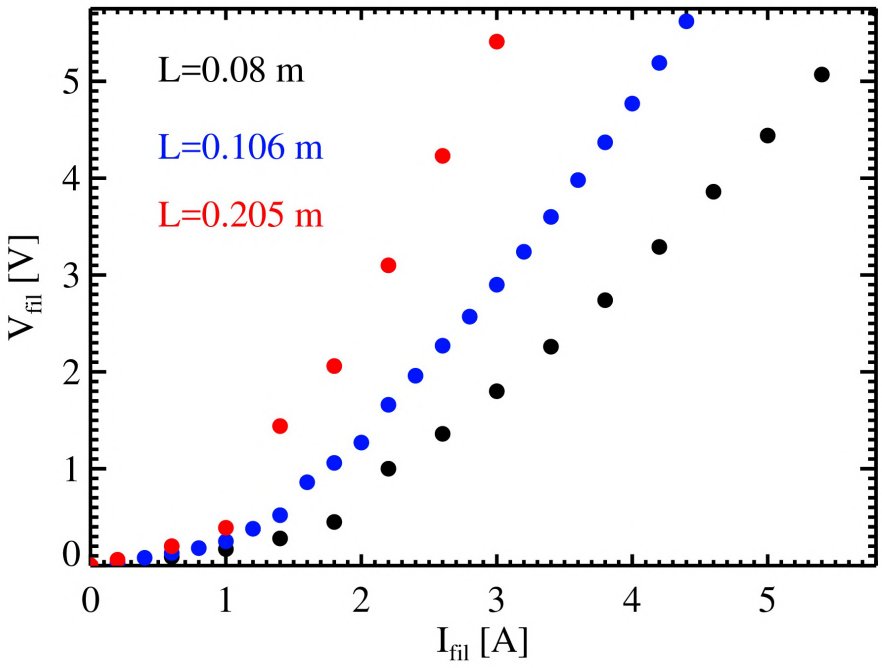

Figure 3.19: Filament V-I curves for different lengths

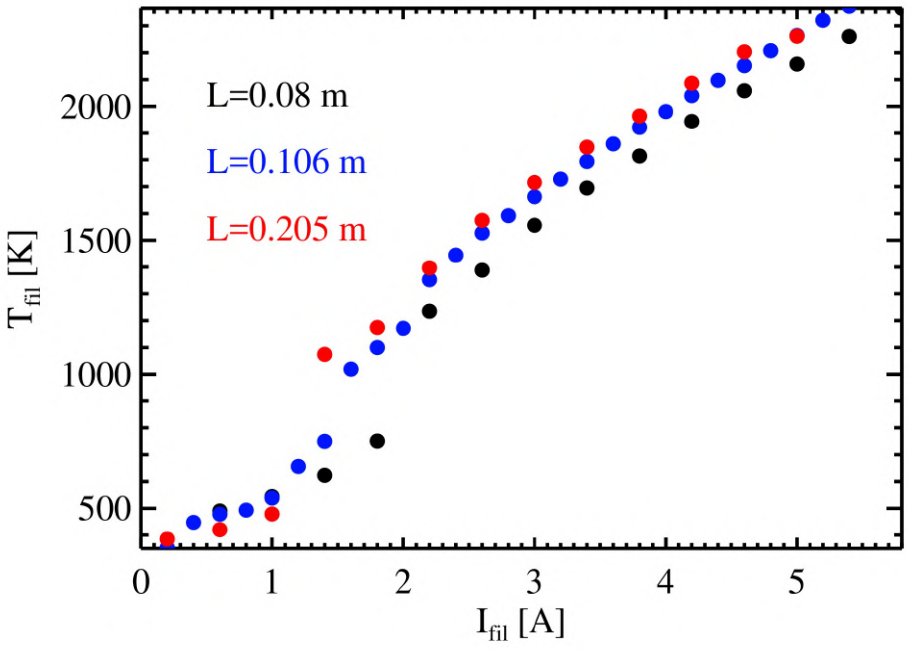

Figure 3.20: Filament temperature for different lengths

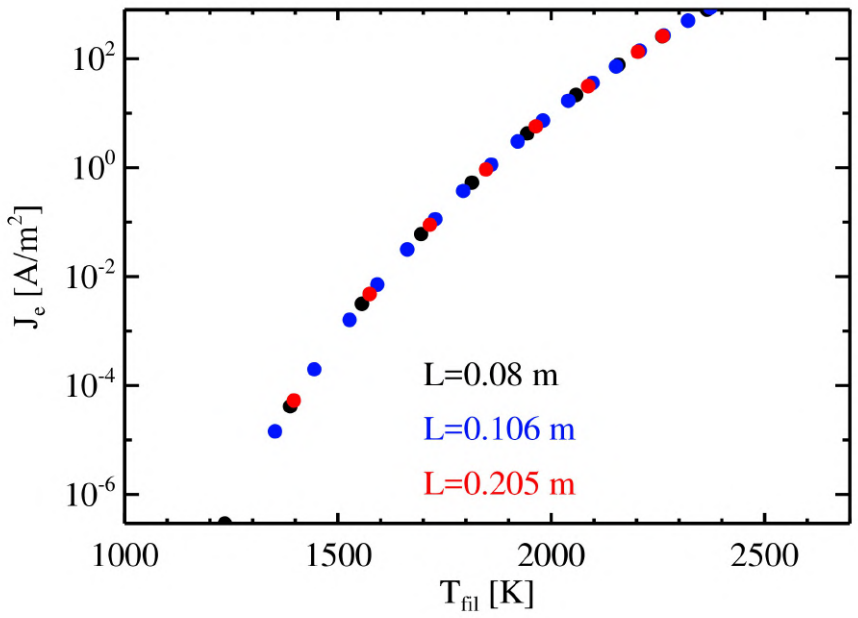

(a)

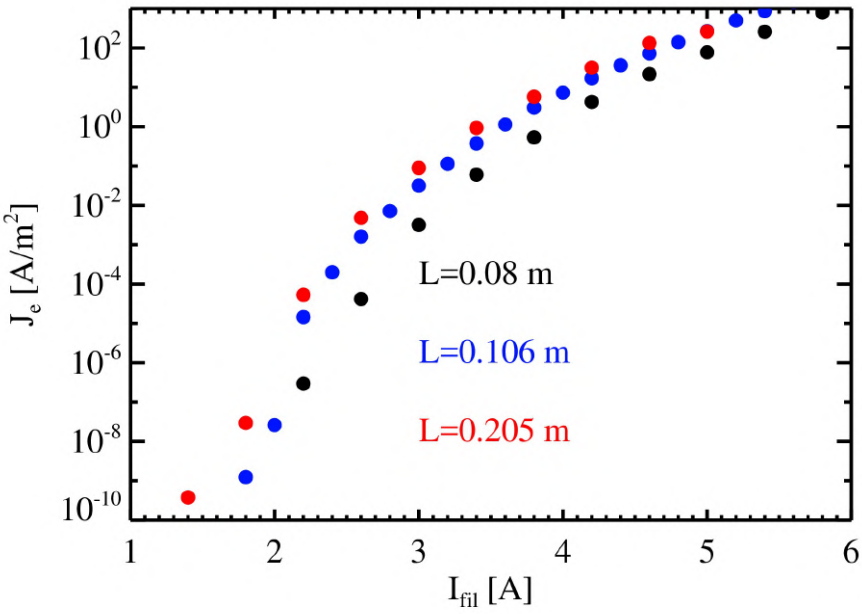

(b)

Figure 3.21: Emitted current density J_e depending on temperature (a). Clearly there is no difference between different lengths. Also J_e depending on filament current (b)

Rarely RF usage was found to be enough to keep on a soft Argon plasma inside the thruster, at $4 \cdot 10^{-3} mbar$. Unfortunately it was not strong enough to be measured and characterized properly. Also, when Argon pressure was higher then $8 \cdot 10^{-2} mbar$ the antenna, totally disconnected, switched on by herself.

This case is worth to be investigated since it's related to an intrinsic resonance of the system. RF were used only with Mach measures of the plume.

Finally, the presence of arcs suggested further studies to be made on cathode properties. They both acted as trigger of instability, when happening at high pressure, or as source of ions. Arcs developed, in fact, also between the filament support and the chamber in certain conditions, since at low pressure they are easily generated. Then the HET got an incredibly strong plasma. This suggested that arc ignition should be under study as well as carbon-fiber field-effect cathodes.

3.3 Mach probe measuring method

Once switched on ATHENIS, three kinds of measures were performed. The first kind of them was a floating measure, that means letting probes measure floating potential, by keeping off their power supply. Floating potential is the potential a conductor reaches by facing a plasma and it is completely determined by plasma conditions. This kind of measure was useful also to provide an anode current, I_{anode}, scan by varying anode potential. For both the other kind of measure, a polarization was needed.

The second type was needed to renormalize probe area to correctly estimate Mach number. In fact the effective areas are not perfectly equal and are subject to changes due to probe erosion by sputtering, and deposition of Tungsten on the edges. The Tungsten deposition causes a resistive coupling between the two probes, so probes had to be cleaned whenever a too thick film between the two was found, that is when they were not completely isolated from each other. To renormalize areas, a few complete rotations of the probe were performed clockwise and counterclockwise. In this way, switching 'North' and 'South' electrodes, we could estimate areas ratio by the minimum and maximum value read by electrodes when facing upstream or downstream. Since North was by default set upstream, the relation between North and

south areas (A_N,A_S) was:

$$\alpha = \frac{A_N}{A_S} = \frac{|I_{Nu} - I_{Nd}|}{|I_{Su} - I_{Sd}|}, \tag{33}$$

where, u and d subscripts denotes respectively upstream and downstream. Areas ratio then was found to be always in the range of $0.94 \div 1.14$.
The third kind of measure was a Langmuir probe characteristic, obtained varying from $-100V$ to $100V$ the probe polarization. Finally, thanks to a 4-parameters interpolation software available, Langmuir curves were analyzed to extract the plasma parameters of the plume. In fig.3.22 there is an example of a Langmuir acquisition along with anode current and voltage monitored. The probe polarization has been changed manually, keeping the thruster at the same running power. Sometimes arcs developed between anode and probes or anode and chamber, showing up like spikes in the anode voltage and probe current. To analyze data properly all the spikes were removed from raw data by the use of IDL software tools. Aside from those left into data, arcs were to avoid, but this was impossible where the HET worked at limit conditions, either stable or not. Whenever this implied a too low power, just one arc could switch off the thruster.
Another interesting example is the anode current scan, taken with fixed lowest probe polarization, in the ion saturation region. Note that plasma switched off when anode current dropped to zero even if anode voltage was still high. In fig.3.23 there are examples, for Ar and He, of Mach measures. Rotations make saturation current read, $I_{sat,i}$, decrease or increase depending on probe facing upward (less current) or downward (higher current). A typical Langmuir characteristic is shown in fig. 3.24.

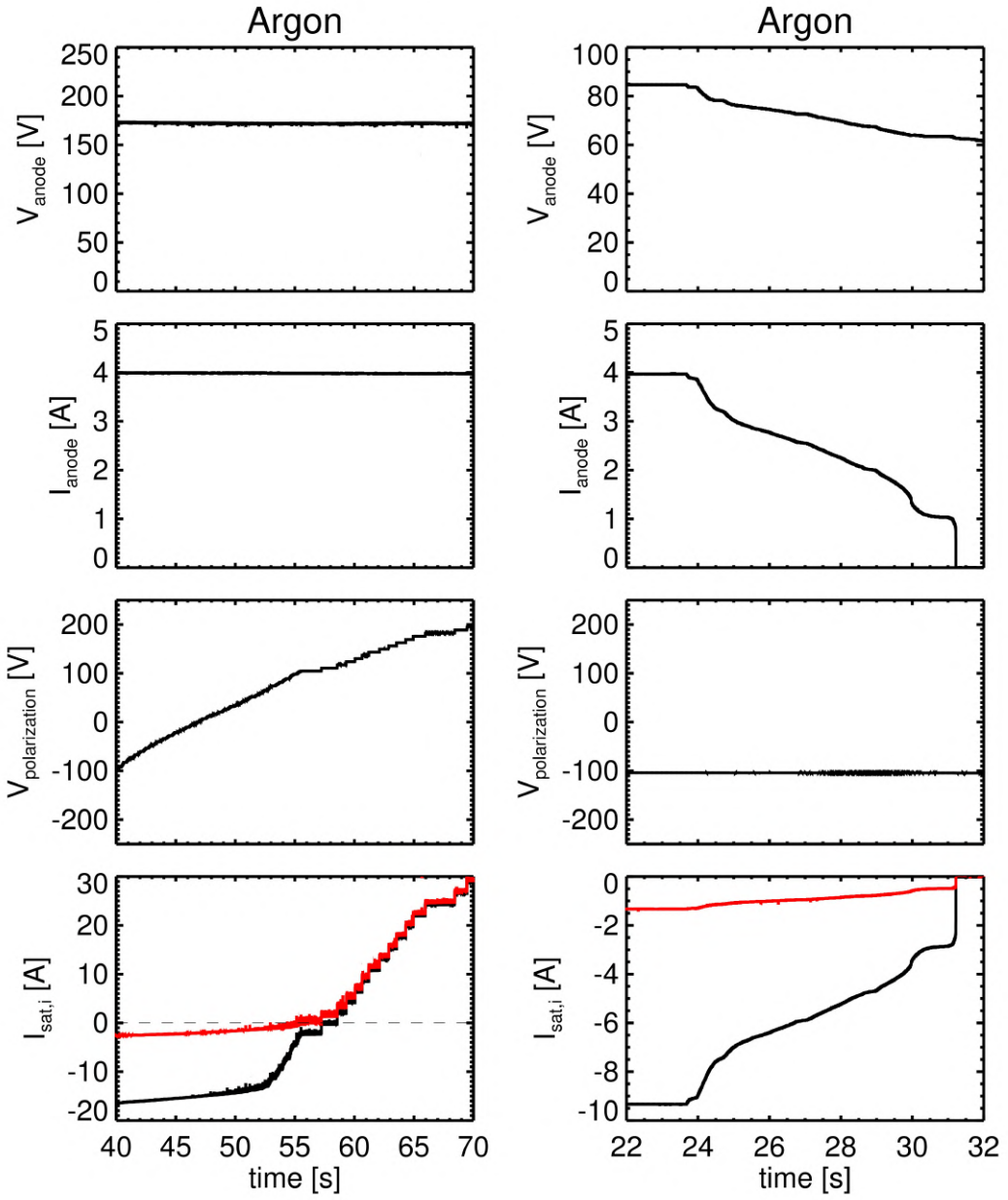

Figure 3.22: Examples of Langmuir scan and anode current scan. Ion saturation currents are both for the upstream probe (black line) and downstream probe (red line).

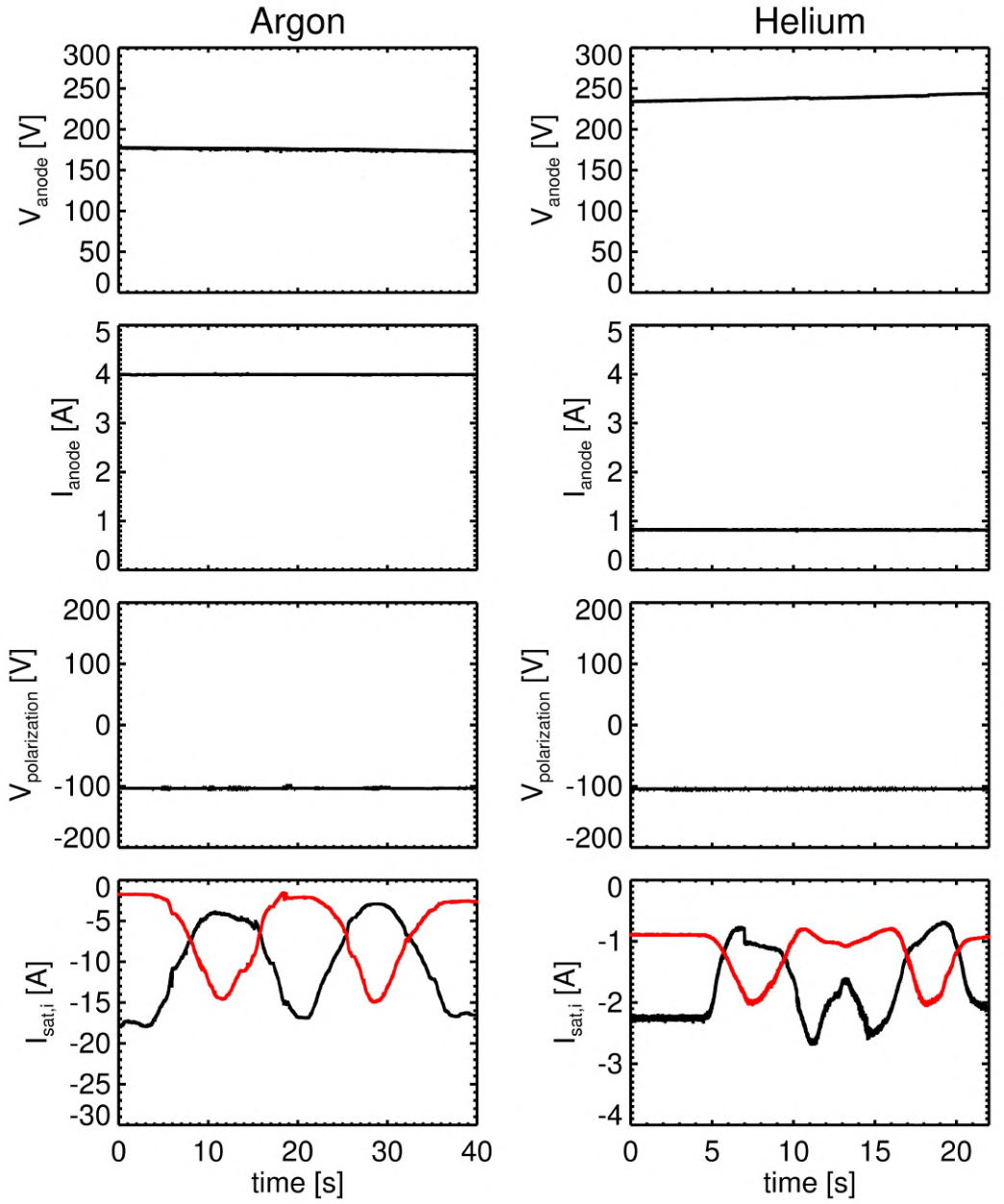

Figure 3.23: Example of Mach probe rotation, used to renormalize areas, both for Ar and He. Ion saturation currents are both for North probe (black line) and South probe (red line).

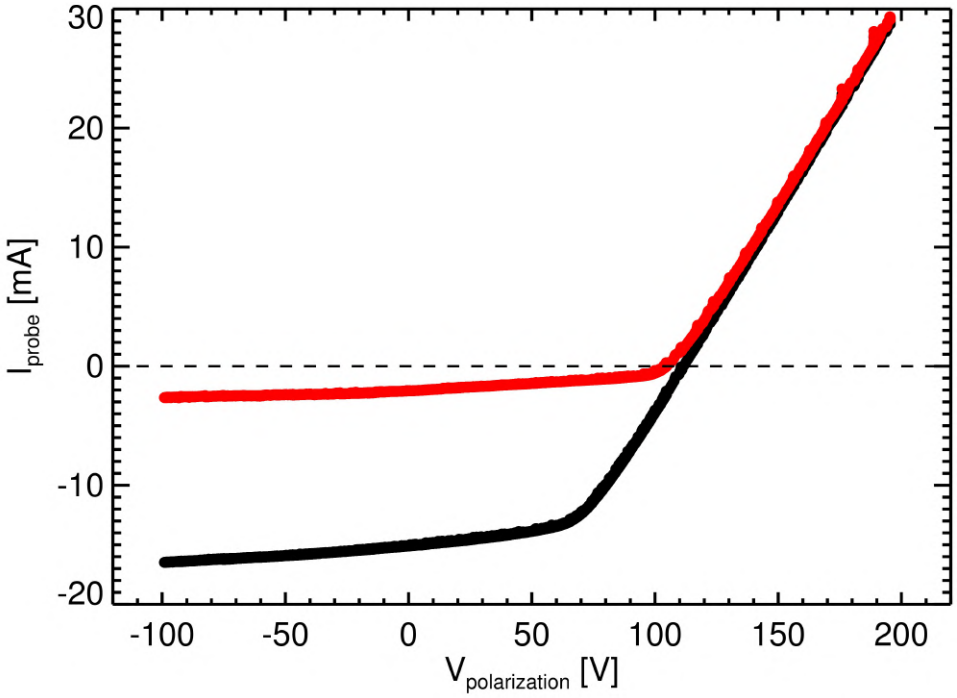

Figure 3.24: A typical Langmuir probe characteristic curve. Black curve is the upstream probe current, while red one is the downstream probe current. Note that the upstream probe collects more ions, since ion saturation current is higher.

3.4 ATHENIS plasma general properties

Mach probe has been used also as a Langmuir probe. It works by performing a scan, bringing the probe potential from -100 to 100. Fitting Langmuir characteristic curves was not so easy because of many reasons. Firstly, fit is on a sort of exponential around the floating potential. Choosing a too wide range or a too short range of points clearly affects the results in electron temperature. Because of this, it was often necessary to check fits with a logarithmic scale. Further on, especially at higher pressures, a second Maxwellian population of electrons showed up in Argon. It can be recognized easily in the purple curve of fig. 3.25: since $I \propto exp\left(\frac{eV}{T}\right)$, the higher is the temperature, the lower is the derivative on the curve, so the shoulder between 0 and 80V seems to be made of hotter particles (also fig. 3.28).

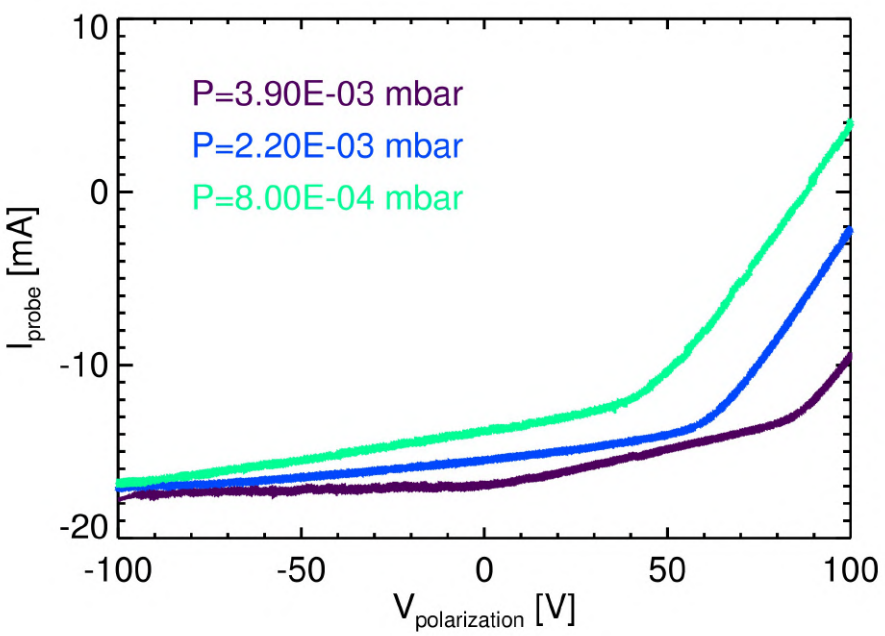

Figure 3.25: Langmuir characteristics at different pressures, same filament current of 6.4A

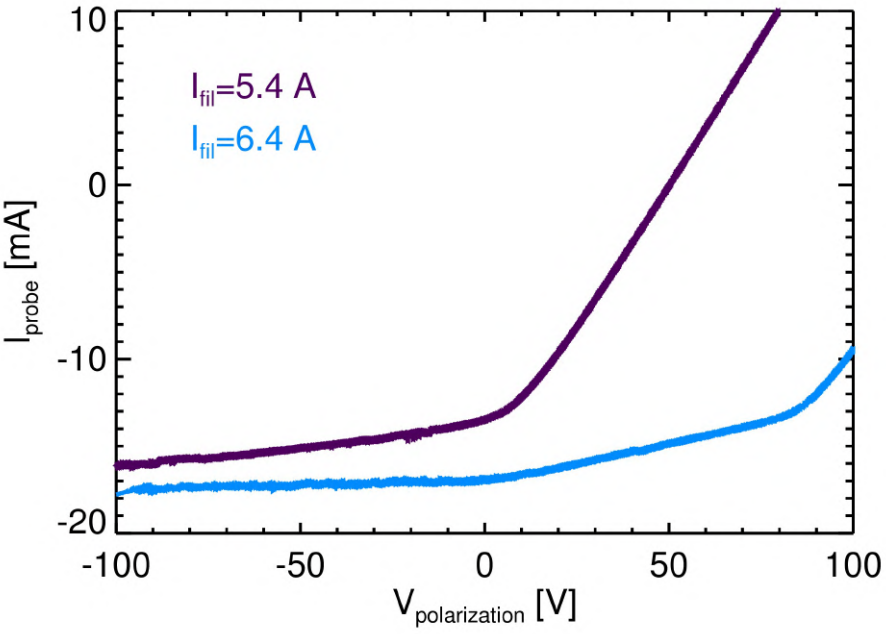

Figure 3.26: Langmuir characteristics at different filament currents, same pressure of $3.9 \cdot 10^{-3} mbar$.

This was never the case in Helium plasma, but the cause is not clear. It is maybe related to the different mass of the ions that, impinging on the cathode and the probe, cause sputtering and secondary electron emission. The highest zone of the electronic saturation region at positive voltage doesn't reach actually a saturation because of an increase of the Debye sheath around the probes that enlarges the actual collecting area. Because of the real difficulties in fitting, electron temperatures should not to be considered exact values.

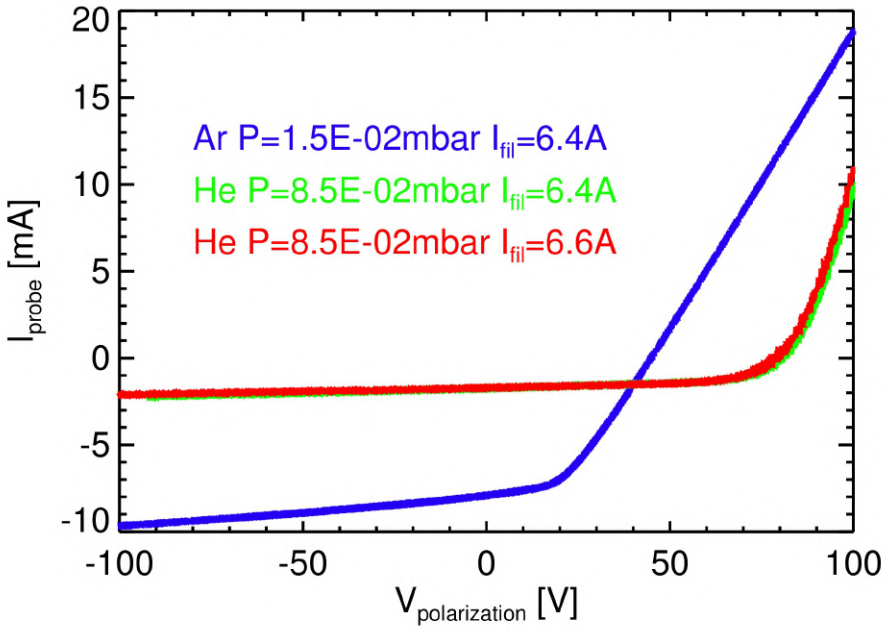

Figure 3.27: Langmuir characteristics comparing Ar and He.

Fig. 3.26 shows plasma characteristics at different filament currents, with fixed pressure of $3.9 \cdot 10^{-3} mbar$. Fig. 3.27 shows the comparison between Helium and Argon plasma, just to underline the two different regimes and the absence of hotter electrons.

Figures from 3.29 to 3.30 show plasma parameters obtained by Langmuir fit depending on pressure and power, with Argon and Helium gas as propellant. Helium data were obtained only with the $1.3A$ of anode current limit of the LI regime and they were both recorded at a pressure of $8.5 \cdot 10^{-2} mbar$. It is clear that filament current has no effects on these parameters since different current points lie very close to each other. As shown in fig. 3.33, zooming fig. 3.21, it is visible how emitted current is highly sensitive to filament current: a $1A$ step arises emitted current of one order of magnitude. Thus

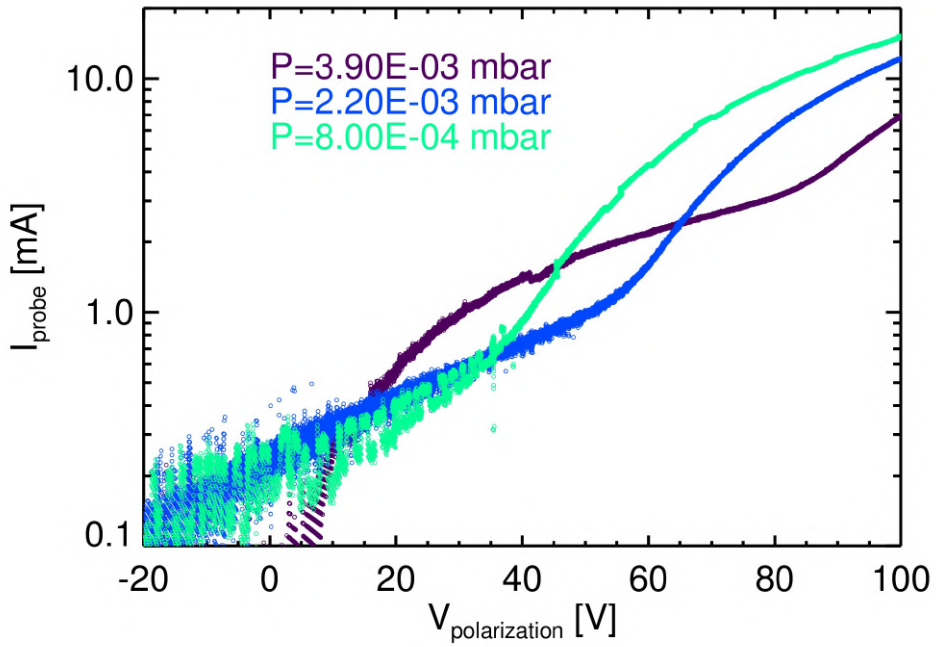

Figure 3.28: Electron populations with different temperature. They can be recognize by the slope of the curves. The flat region in the electronic saturation region at high positive voltage is due to an increase of the Debye sheath around the probes that increases the actual collecting area.

is confirmed that the greatest electron contribution, when the thruster is on, does not come directly from thermoionic emission of the cathode, which is also spatially limited by Child's law, but from spatial ionization. It must be kept in mind that ionization happens mainly in the ionization region, inside the hall thruster, where the magnetic field has its maximum and the axial electric field is boosted. The fact that the measures are taken in the plume suggests that the plume itself is sensitive to what happens in the ionization region inside the HET.

Electron temperature of Argon LI plasma plume falls between $7eV$ and $11eV$, while between $5.5eV$ and $7eV$ for HI. It seems that increasing working power directly arises electron temperature although temperatures are actually too close to be clearly distinguished, and it is the same when lowering the pressure. Apparently there is no significant difference between gases for what concerns electron temperatures and no trend can be explicitly recognized. Since the mach probe stood in the plume, electron temperatures are lower than those typical of electrons inside the channel $(20 \div 100eV)$ [2].

Argon plasma density, in ranges $1 \div 2 \cdot 10^{18} m^{-3}$ with HI regime and $3 \div 5 \cdot 10^{18} m^{-3}$ with LI regime, also shows a rise in power but it may have an optimum (fig. 3.30.b). In Argon data it is easy to recognize an optimum pressure also, even for both the two regimes that are neatly separated by a factor ~ 3 (fig. 3.30.a). The same behavior is obviously found in saturation current, since $I_{is} \propto n_0$ and $n_0 \sim n_e/2$. It is curious that electron densities are higher than expected from Hydrogen and Nitrogen previous study except for Helium which has electron density of $\sim 10^{17} m^{-3}$, and could be a topic to further investigate. It is clear that different gases work over completely different conditions considering electron densities on the gases used. Anyway this strictly depends on the fact that Helium, Hydrogen and Nitrogen need higher working pressure and higher voltage drop, in fact previous collected data were obtained running the HET with the same power supply attributable to our HI regime. Also, magnetic confinement may have a role, since Argon Larmor radius is 20 times greater than Helium radius. The role of magnetic confinement could be verified by measuring plume divergence.
Anode scan current has been done both versus pressure and filament current. Characteristic curves are shown in fig. 3.31 and 3.32. It is notable that plasma resistance, defined as

$$R_{plasma} = \frac{V_{anode}}{I_{anode}},$$

resembles a Paschen curves, when plotted versus pressure. Although plasma resistivity gives more information, because it is strictly related to physical quantities such as electron temperature, it is complicated to determine the exact plasma current section since the current closes its circuit over an unknown portion of the vacuum chamber, therefore I prefer to report only plasma resistance. Plasma resistance values lie between 100Ω and 800Ω.
Assuming a high degree of ionization, the electron-ion collisions (supposed the more relevant) have a frequency of about $\nu \sim 4 \cdot 10^8 s^{-1}$ [10]. Near the Mach probe, magnetic field is about $5mT$; consequently electron cyclotron frequency is estimated $\omega_{ce} \sim 3 \cdot 10^9 rad/s$, which means that in the plume, the hall parameter is $h = \frac{\omega_{ce}}{\nu} \sim 10$.

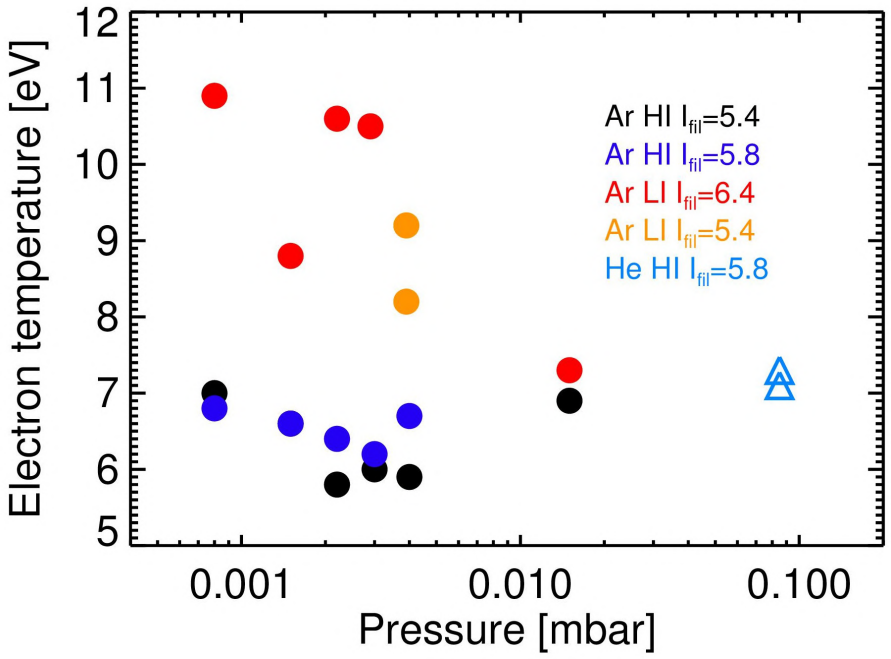

(a) .

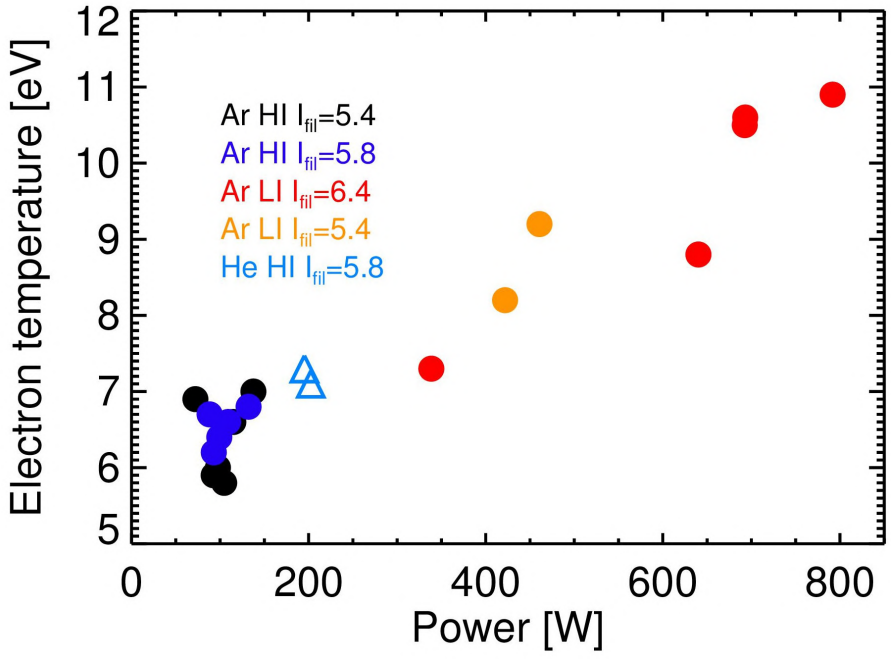

(b) .

Figure 3.29: Electron temperature depending on pressure (a) and power (b) for both Ar (dots) and He (triangles). Different filament currents do not affect significantly temperatures in the plume. Note that inside the channel, plasma is expected to be hotter, accordingly to literature about HETs. Different gases don't show great difference although operating in quite different conditions.

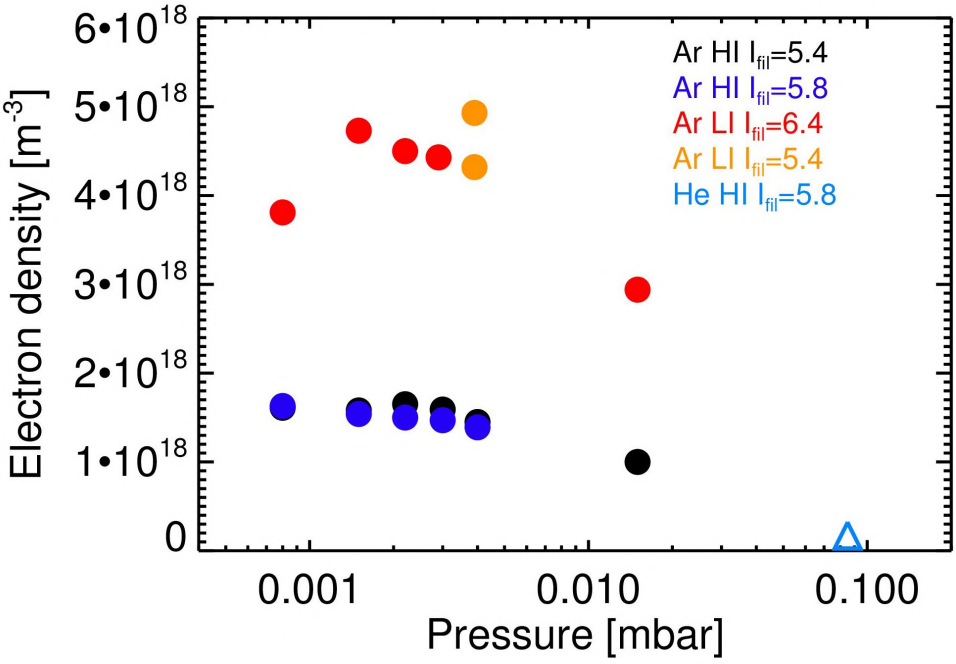

(a) .

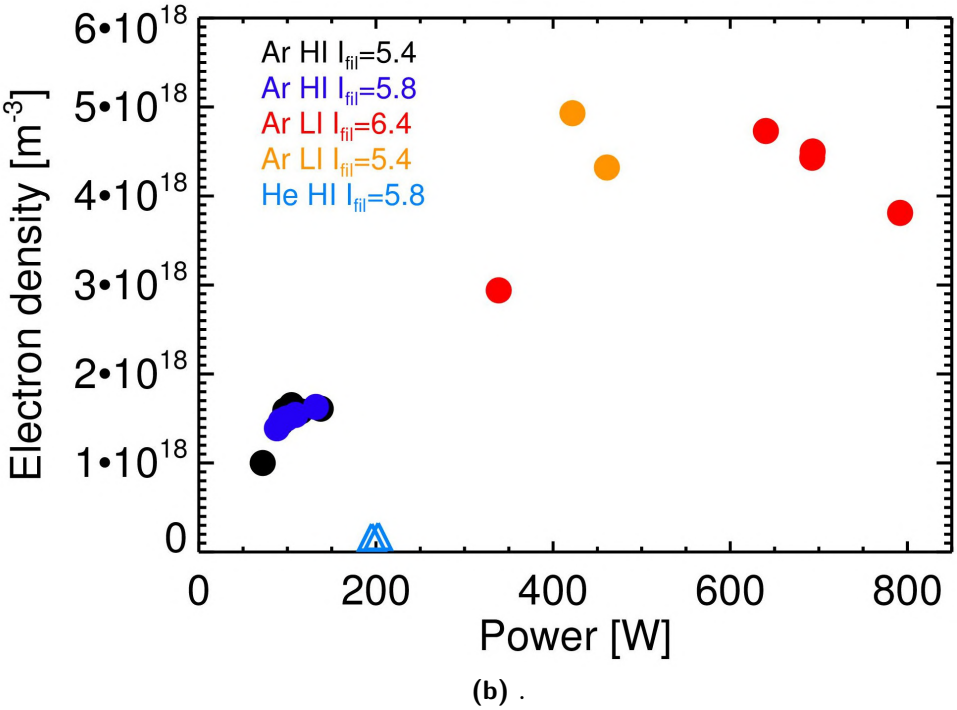

(b) .

Figure 3.30: Electron density depending on pressure (a) and power (b) for both Ar (dots) and He (triangles). Different filament currents do not affect significantly Ar densities in the plume as data lie on the same curve. Helium electron density is systematically lower than Argon.

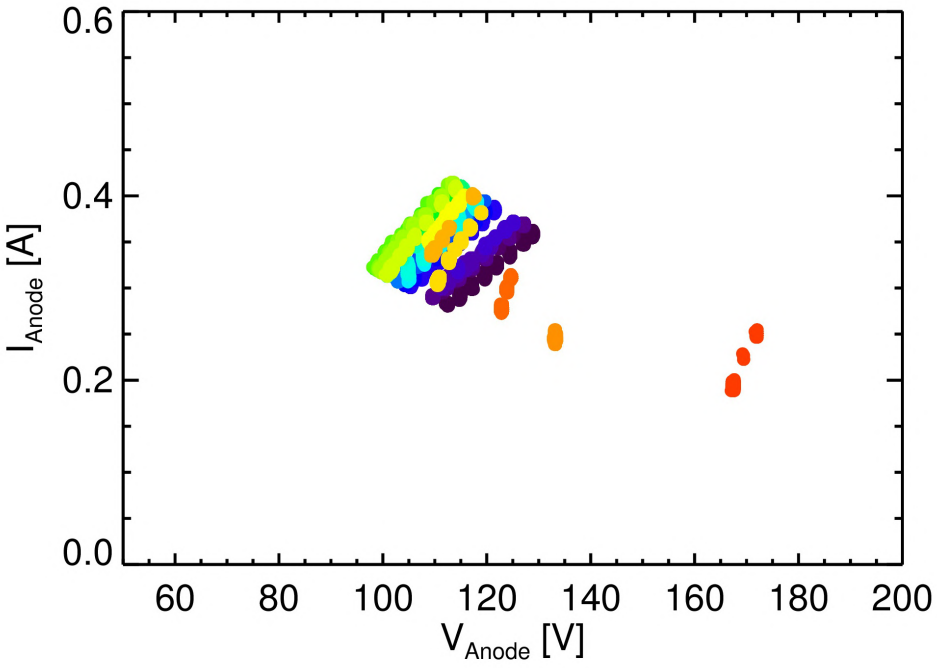

(a) .

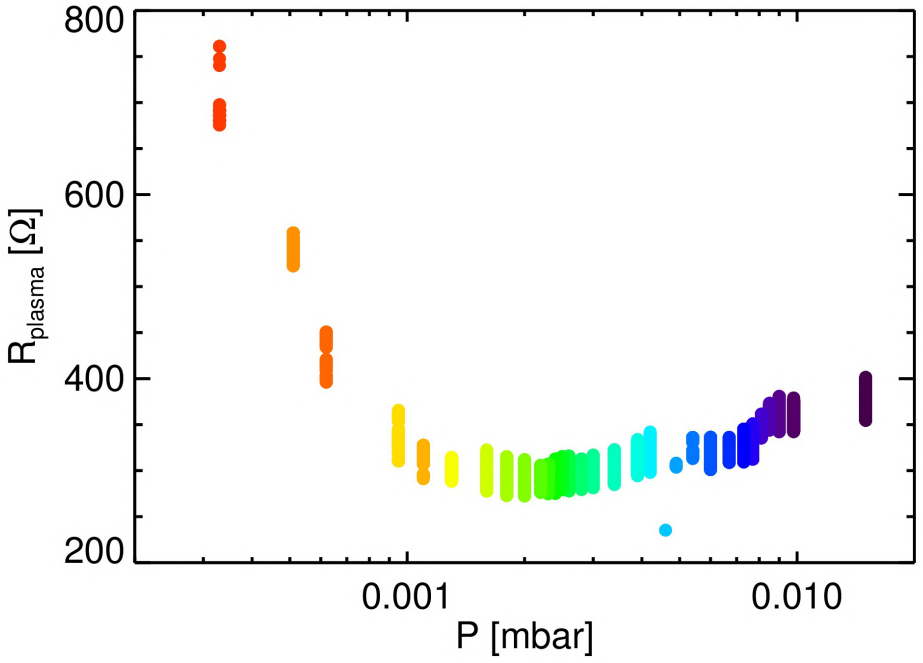

(b) .

Figure 3.31: Anode current scan and plasma resistance with power between 40 W and 60 W. Every color is a different pressure shot with same $I_{fil} = 6.6A$. Colors are the same for both figures.

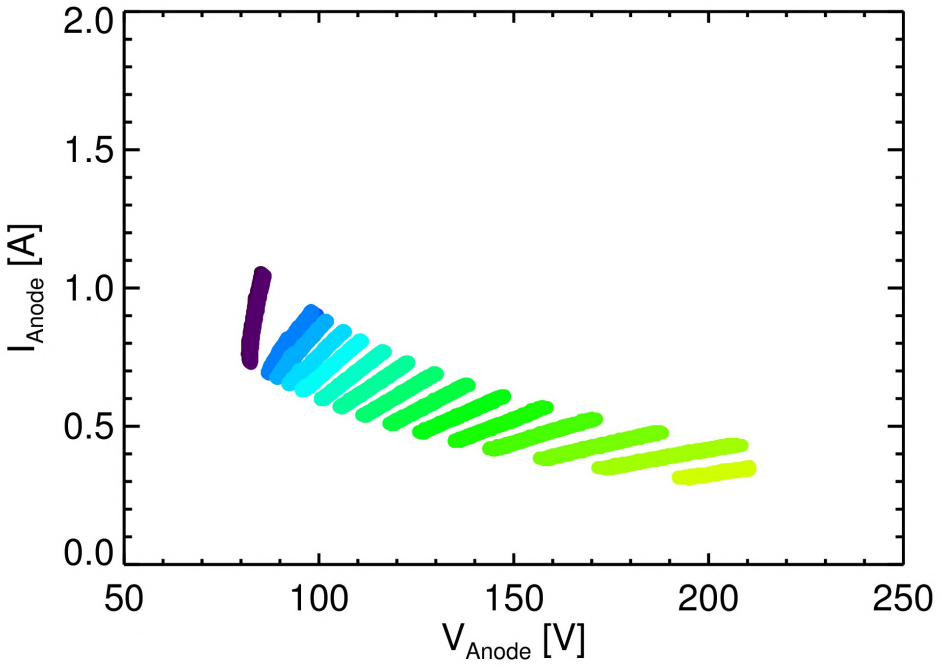

(a) .

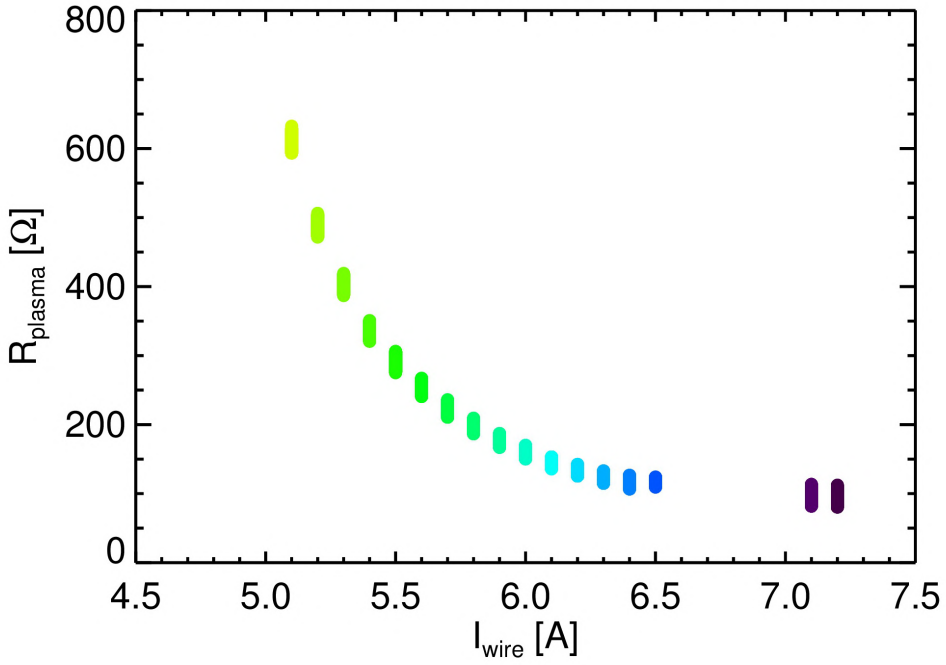

(b) .

Figure 3.32: Anode current scan and plasma resistance with power between 60 W and 90 W. Every color is a different pressure shot with same $P = 2.4 \cdot 10^{-3} mbar$. Colors are the same for both figures.

Talking about Mach measures, a single pressure scan at fixed filament current and a single filament current scan at fixed pressure have been performed. The choice of cross-scanning over parameters, without performing a complete map over the two parameters is due to the need of preserving the probe from sputtering and the lack of time to cover all the possible measures on this system.

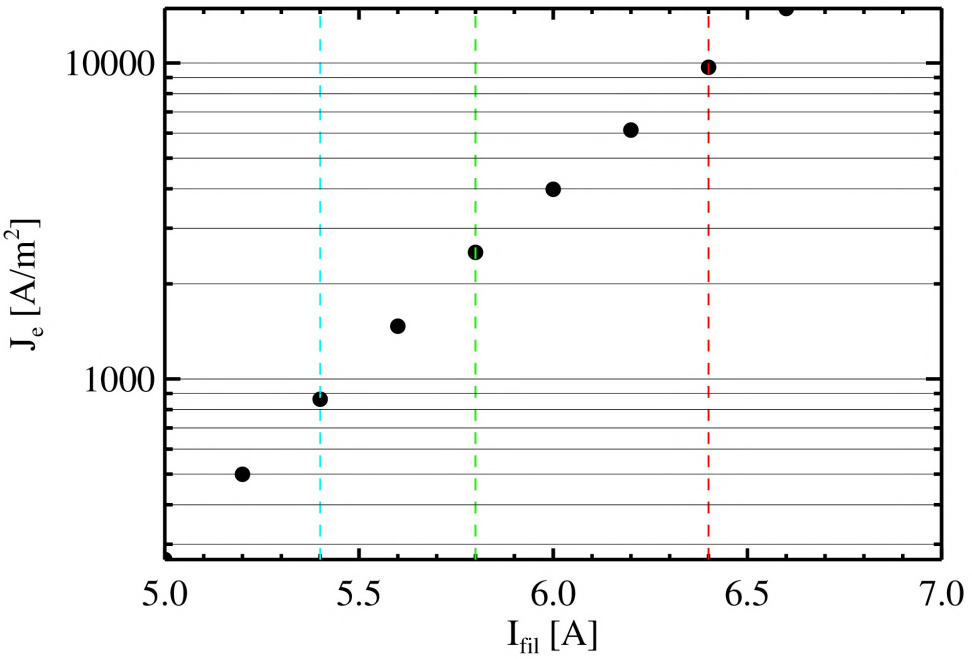

Figure 3.33: Zoom of emitted current density as function of filament current. Three of the most performed currents are shown by dotted lines: $5.4A$(cyan), $5.8A$(green), $6.4A$(red).

3.4.1 Mach number

Only working with Argon in LI regime data were clear enough to extract information about Mach numbers. Ion temperature has been assumed to be equal to electron temperature, since it was not possible to measure it. Therefore Mach numbers should be considered as estimates more than actual values. Assuming cold ions, let's say $T_i \sim 0.01T_e$, would just result in Mach numbers a factor 10 lower. Fig. 3.34 shows Mach numbers depending on pressure. A clear maximum is found at $\sim 3 \cdot 10^{-3} mbar$ which indicates that Ar ions are better accelerated at this pressure. Note that assuming equal ion and electron temperatures reduces Mach number results to the currents ratio and

the optimum pressure almost coincides with that found for electron density through independent measures. It is in fact natural to assume a stronger ionization in the plume where the thruster works better. Another interesting result is another optimum with $I_{fil} \sim 6.2A$. Note that while current scan has been done at fixed pressure of $2.4 \cdot 10^{-3} mbar$, which is very near to the maximum, the pressure scan has been done at $6.6A$, so that it was not the best condition. Assuming $T_e \sim 10eV$, then $c_s \sim 4.85km/s$. From formula (32) ion velocity is found to be $v_i = 3.89km/s$ at the $M = 0.8$ pressure maximum for $I_{fil} = 6.6A$ and $P = 2.8 \cdot 10^{-3} mbar$; or $v_i = 3.64km/s$ at the $M = 0.75$ current maximum for $I_{fil} = 6.2A$ and $P = 2.4 \cdot 10^{-3} mbar$. Note that these values are lower than typical HET ion velocities.

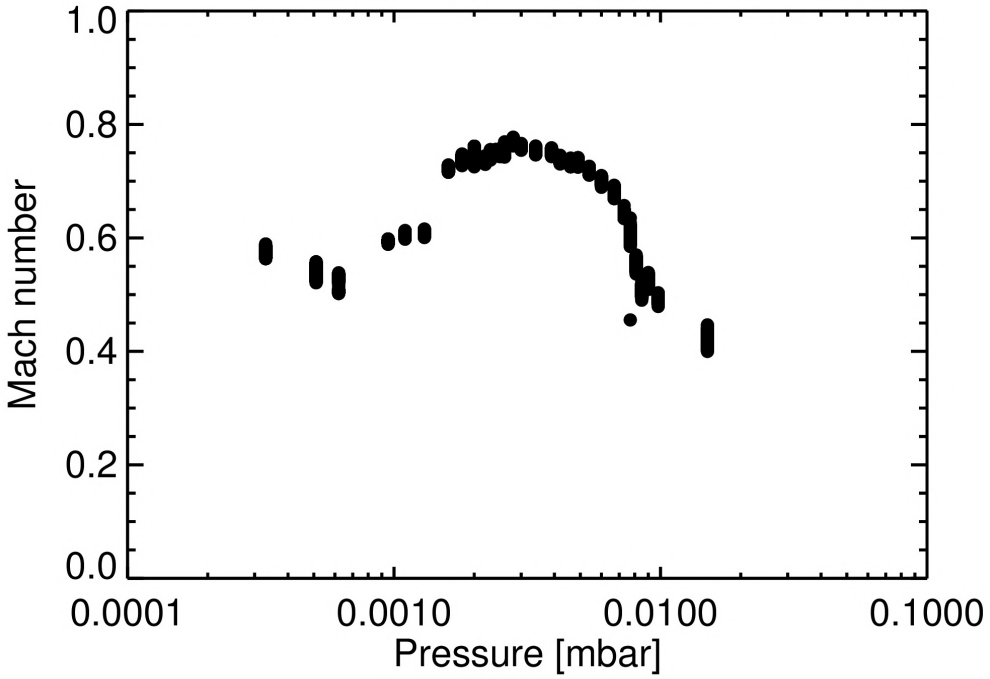

Figure 3.34: Mach number trend with pressure at $T_i \sim T_e$. It develops an optimum at about $3 \cdot 10^{-3} mbar$ of $3.2km/s$.

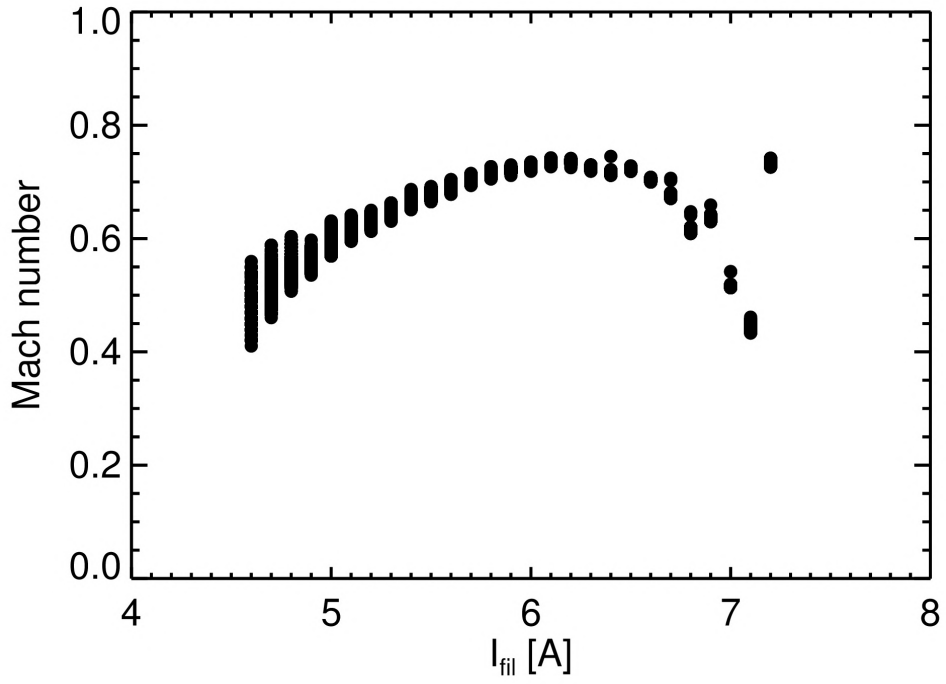

Figure 3.35: Mach number trend with filament current at $T_i \sim T_e$. It develops an optimum at about $I_{fil} \sim 6.2A$ of $3km/s$.

4 Electrostatic fluctuation

4.1 Fluctuations measuring method

Once the system was ready, a wave generator gave a single square wave pulse which triggered the acquisition. Modules trigger synchronization was set via software but the error introduced was negligible. The acquisition lasted 50 ms and stopped automatically. It recorded all 24 fluctuation signals on fast channels (WE7116, 20 Msps), anode current and voltage on slower isolated channels (WE7275, 1 Msps). Acquisition needed to be quick to preserve probes, but had to be long enough to observe low frequency modes. Fluctuations were, depending on pressure and current conditions, in the range of $1 \div 10V$ operating with Argon. Since fluctuations are small compared to the unperturbed floating potential (see fig. 4.44), probes were AC coupled to the oscilloscope, but also DC measures have been done to check ranges and noise reduction on power spectrum.

4.2 Fluctuation characterization

4.2.1 Argon fluctuations

Fig. 4.36 shows a few signals for different probes where an electrostatic perturbation is found operating with Argon. Oscillations came out in many operating conditions. Since different signals are not synchronized it is needed an analysis over multiple probes to understand whether these modes are stationary axial oscillations or azimuthal oscillations. In order to analyze oscillation frequency, a power spectrum has been obtained for each measure, by performing a Fourier analysis through IDL routines. A typical power spectrum is shown in fig. 4.37 for Ar at $4.4 \cdot 10^{-3} mbar$, $6.2A$ of filament current; AC signal is compared to DC signal to show noise reduction. Thanks to this tool, diverse frequencies are resolved and their relevance into the total oscillation pattern is made distinguishable. Noise from many sources add a background decreasing with frequency, while actual oscillations can be found in peaks centered at their characteristic frequency.

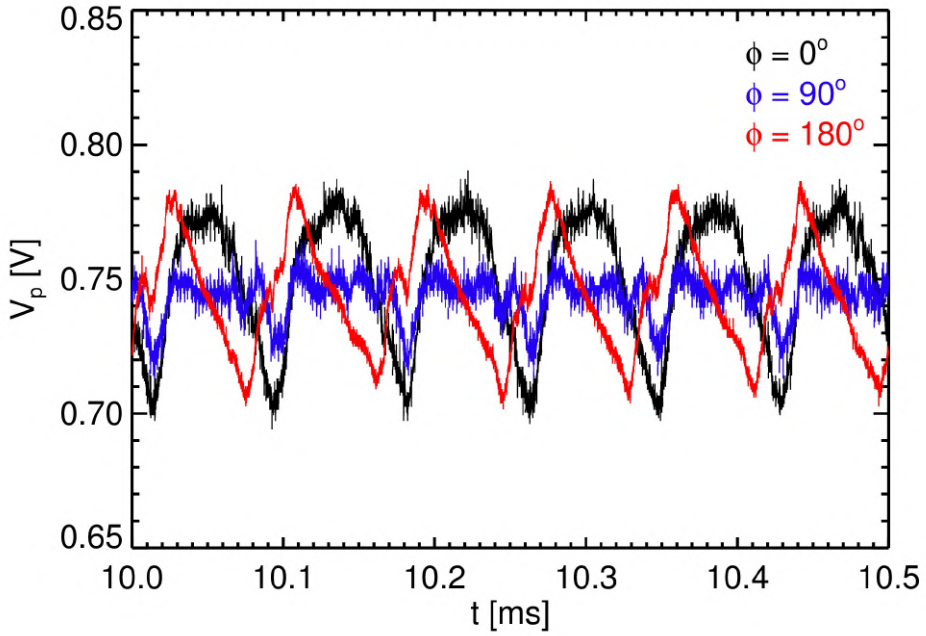

Figure 4.36: Fluctuations signals at different azimuthal positions at Argon pressure of $9.6 \cdot 10^{-3} mbar$ where a $12kHz$ oscillation is found. Signals are not in phase from one probe to another.

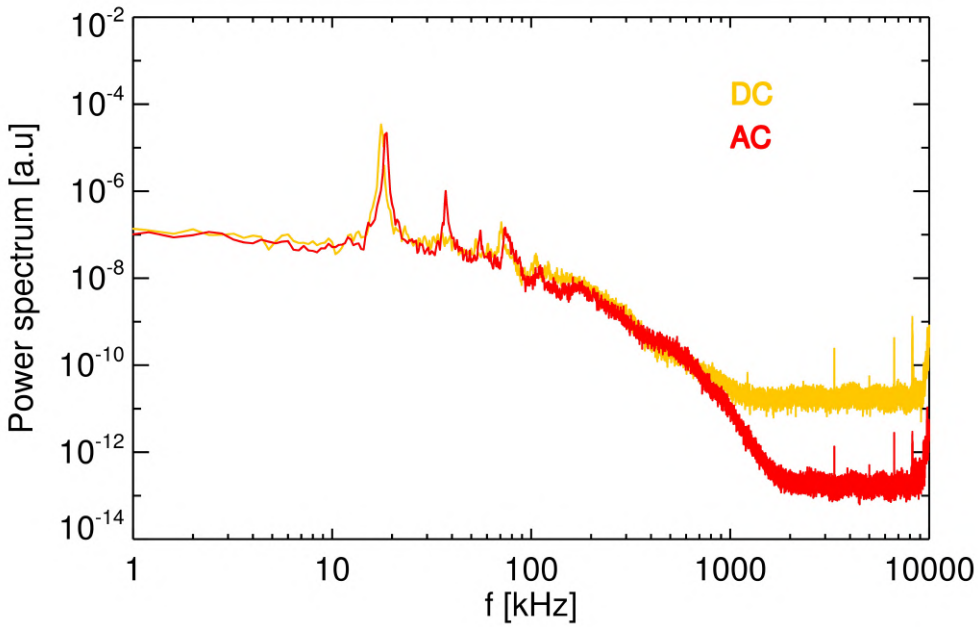

Figure 4.37: Comparison between AC coupled signals and DC coupled signals. High frequency noise is better recorder with AC coupling and consequently damped.

The frequency of the found oscillation lies always in the $10 \div 60kHz$ range, depending on pressure. For greater pressures, a narrower and lower frequency

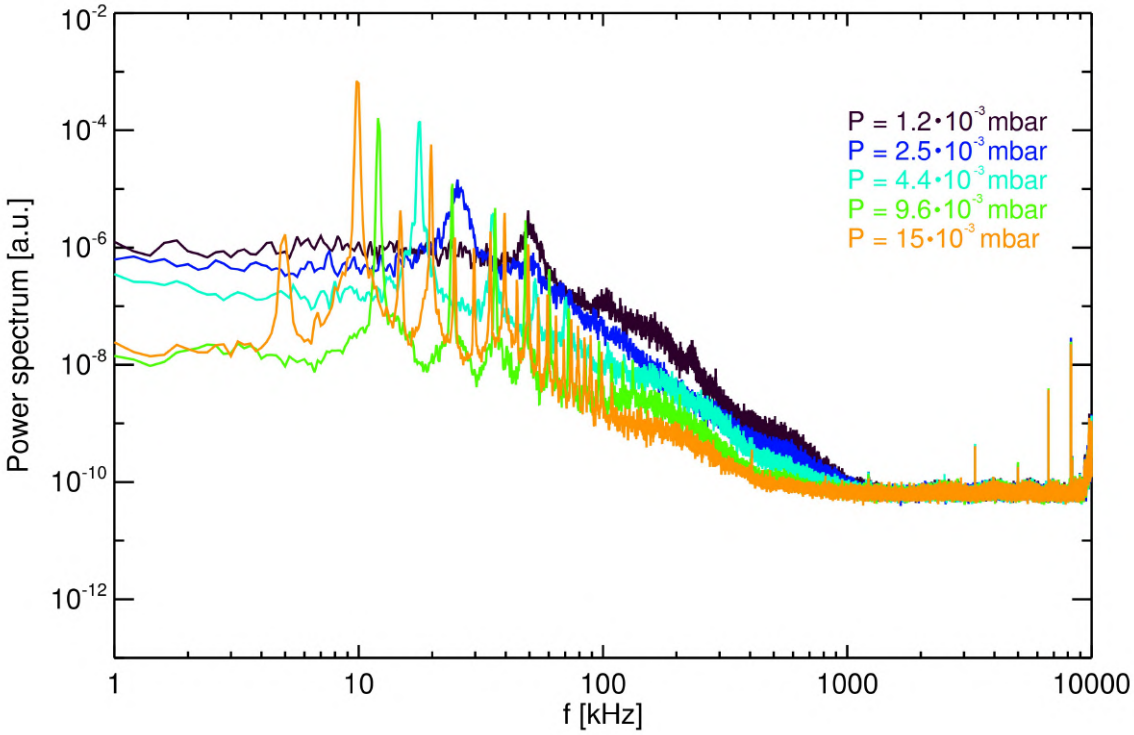

Figure 4.38: Argon power spectrum at different pressures. The greater the pressure the lower is oscillation frequency and the narrower is its peak. Higher pressure spectrum is enriched progressively with many higher harmonics.

peak is found in the power spectrum. A $50kHz$ peak starts developing at $10^{-3}mbar$ and it moves down to $10kHz$ at $1.5 \cdot 10^{-2}mbar$. This is the greatest pressure measured using Argon because higher pressures would have triggered easily arcs and damaged the turbo pump and the diagnostics. As the frequency lowers, many higher harmonics appear in the spectrum. All of this can be seen in fig. 4.38.

As shown in fig. 4.39 the perturbation moves along the channel in the azimuthal direction. Since the probes array is sorted clockwise looking from above, the perturbation is moving clockwise, opposite to $\mathbf{E} \times \mathbf{B}$. Because of its frequency range, at first glance we suppose it is a rotating spoke.

An analysis over its dispersion relation has been performed through IDL procedures. Although it is not a perfect tool to obtain accurate information, a clear result can be seen in fig.s 4.40, where the frequency spectrum of every couple of contiguous probes is summed and analyzed azimuthally, giving the power spectral density. The usual wave number, k, is not the proper quantity

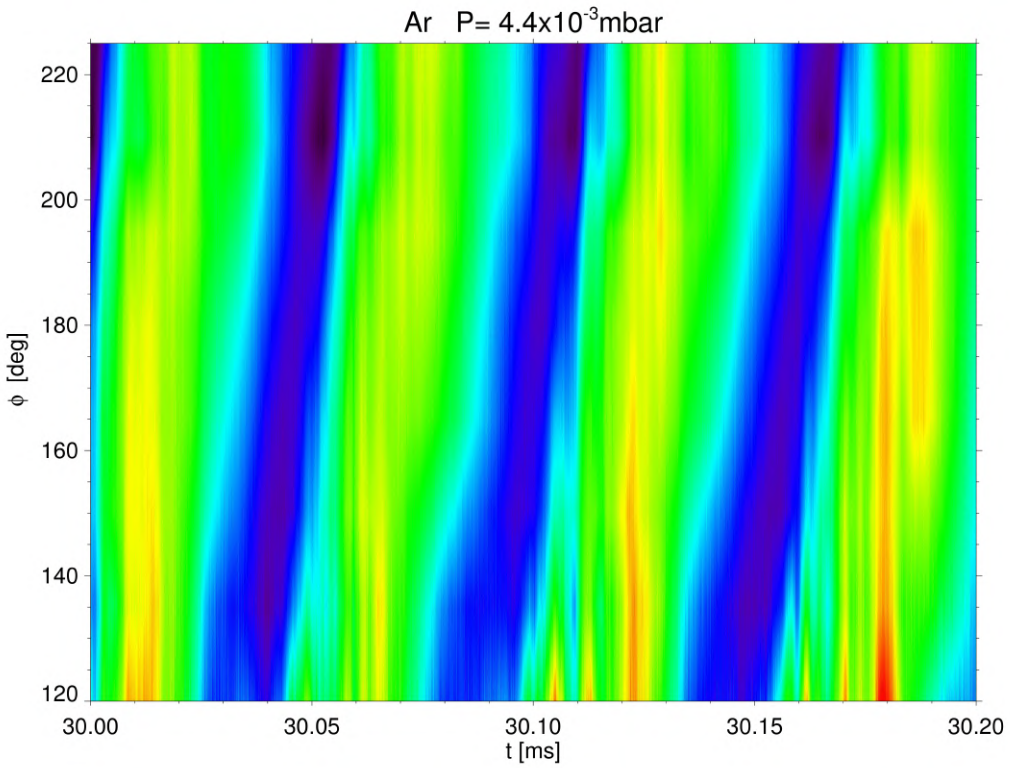

Figure 4.39: Argon fluctuation signals developing in time (x-axis) and showing a wave front moving azimuthally (y-axis). The oscillation moves clockwise looking the HET from the top, which means opposite to $E \times B$

to be used when dealing with azimuthal and periodic phenomena. Instead, we use the azimuthal mode number, defined as $m = kr$ with r the average radius of the channel. Over x axis it is shown m, the azimuthal mode number. Color scales are adapted to underline the peaks over the noise background. Note that non integer values of m comes from statistical uncertainties of k. From low to high pressure the peaks start with $m = 0$ then sharpen and move to $m = -1$. Is that actually what is going on? Why should it start axially then move azimuthally? Looking at coupled probes dispersion relation, apparently also $m = -2$ is touched, but the dynamics is not clear. The answer is simple, anyway: that perturbation which is moving in the channel is not a perfect wave. As discussed previously, rotating spokes are made of a single complex structure. Sampling frequencies and probe positions do not give a neat result because of the many harmonics that show up into a spoke structure.

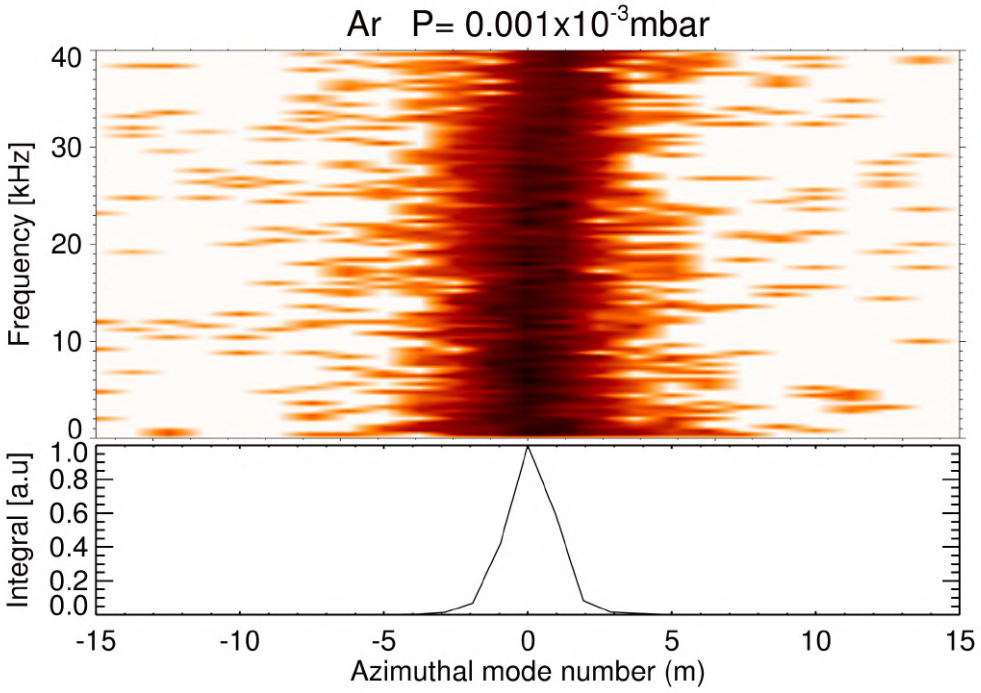
Ar P= 0.001x10-3mbar
Frequency [kHz]
40
30
20
10
0
Integral [a.u]
1.0
0.8
0.6
0.4
0.2
0.0
-15
-10
-5
0
5
10
15
Azimuthal mode number (m)

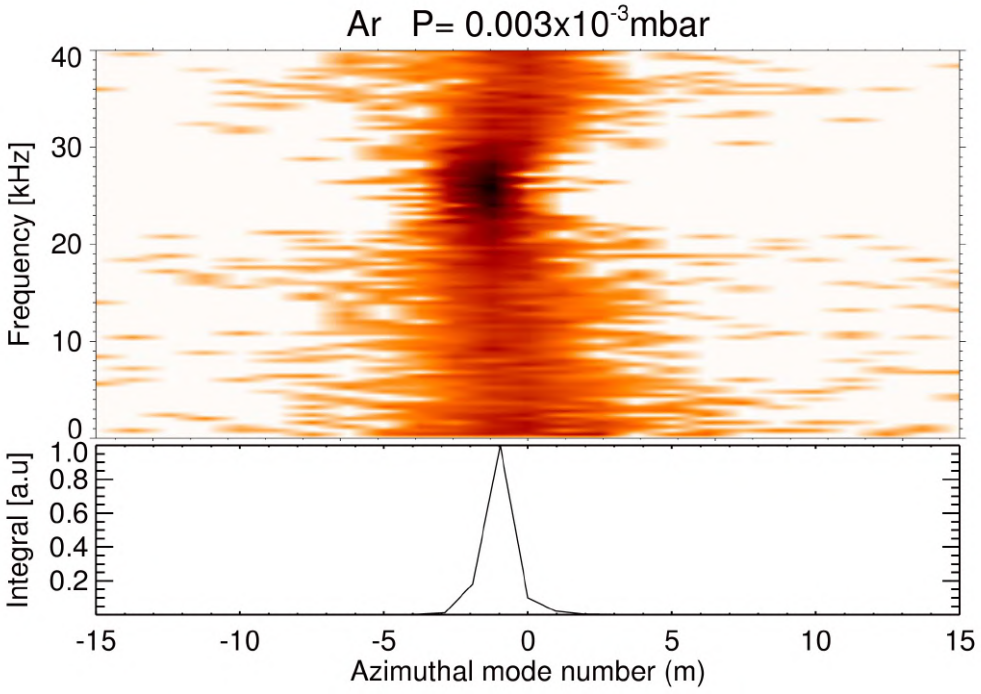
Ar P= 0.003x10-3mbar
Frequency [kHz]
40
30
20
10
0
Integral [a.u]
1.0
0.8
0.6
0.4
0.2
-15
-10
-5
0
5
10
15
Azimuthal mode number (m)

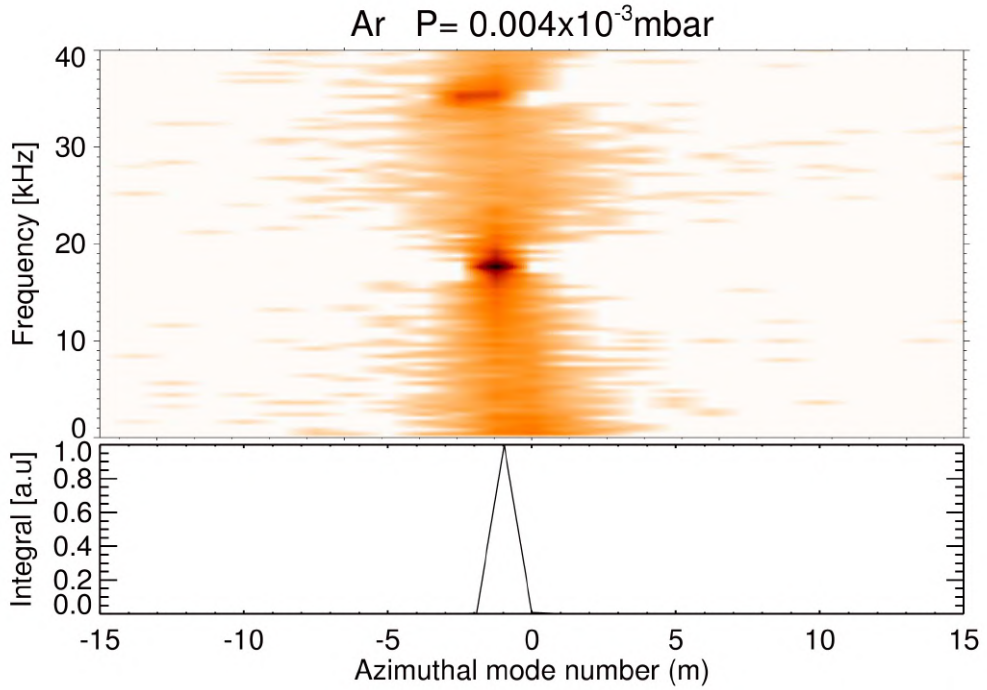
Ar P= 0.004x10-3mbar
Frequency [kHz]
40
30
20
10
0
Integral [a.u]
1.0
0.8
0.6
0.4
0.2
0.0
-15
-10
-5
0
5
10
15
Azimuthal mode number (m)

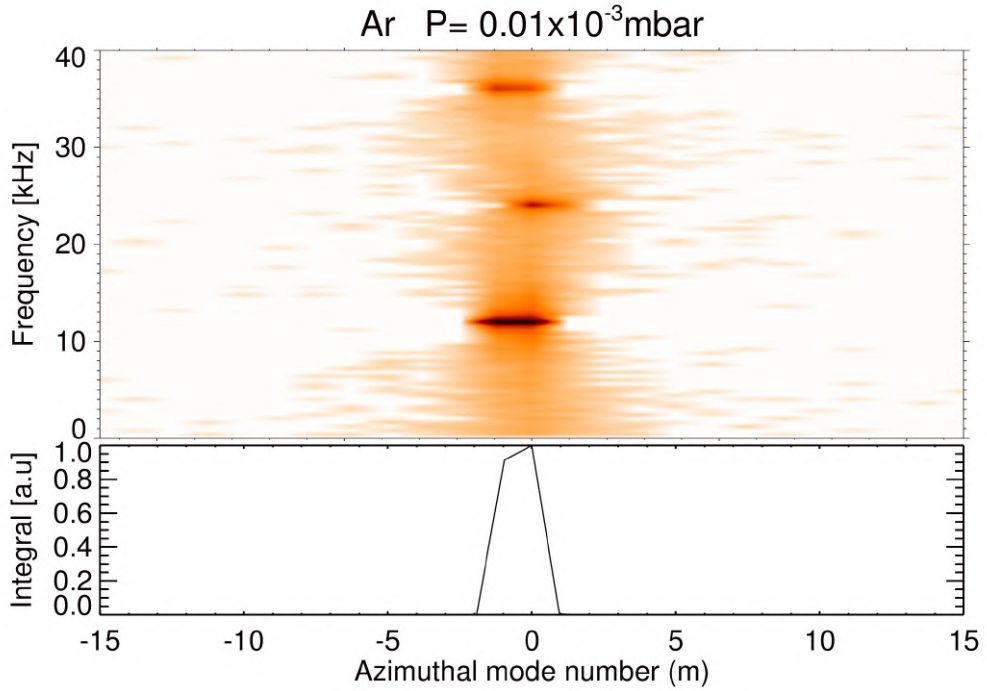
Ar P= 0.01x10-3mbar
Frequency [kHz]
40
30
20
10
0
Integral [a.u]
1.0
0.8
0.6
0.4
0.2
0.0
-15
-10
-5
0
5
10
15
Azimuthal mode number (m)

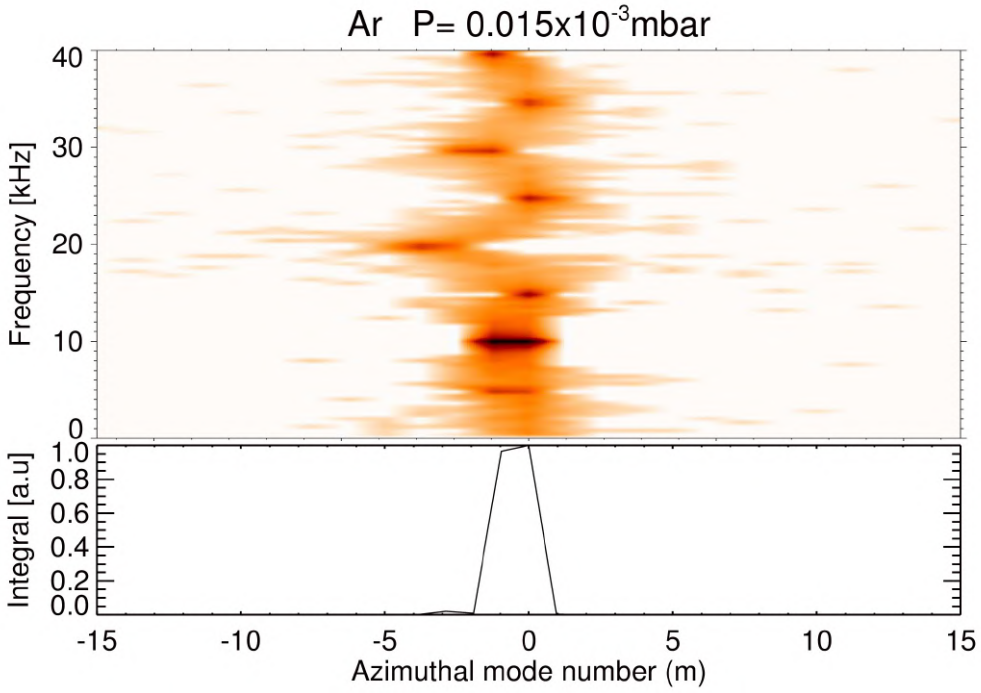

Figure 4.40: Argon power spectral density at different pressures. As the pressure increases, a m=-1 mode rises and its first harmonic peak frequency lowers. It is shown also its integral around the peak to underline at what azimuthal number the first peak is related. Working pressures are the same of fig. 4.38 although the titles are approximated.

Since it is a kind of delta-shaped wavefront, it is rich of many frequencies in Fourier components. this aspect can be seen in fig. 4.41 where the growing perturbation is clearly not a sine-like wave, but it resembles more a triangular wave, because of its complex structure. In the presented results, the average power mainly increases with pressure (looking at fig. 4.41, (a) $130W$, (b) $140W$, (c) $180W$, (d) $230W$ but for the last one (e) of $190W$). From the same figures another peculiarity can be found. Looking at fig. 4.38 the total power spectrum integral changes as the pressure increases. This might signify that while lower and higher frequency noise is reduced, the peaks are fed. The lowest pressure signals (fig. 4.41) do not display a clear coherent mode, but it is more likely to be turbulent. As the pressure is increased, the mode becomes more coherent and turbulence vanishes. This behaviour is completely opposite of what happens in higher frequency oscillations found in magnetron discharges [13].

To verify that a coherent mode is favored at higher pressures, we perform a study over the peaks by integrating and normalizing the peak integral over

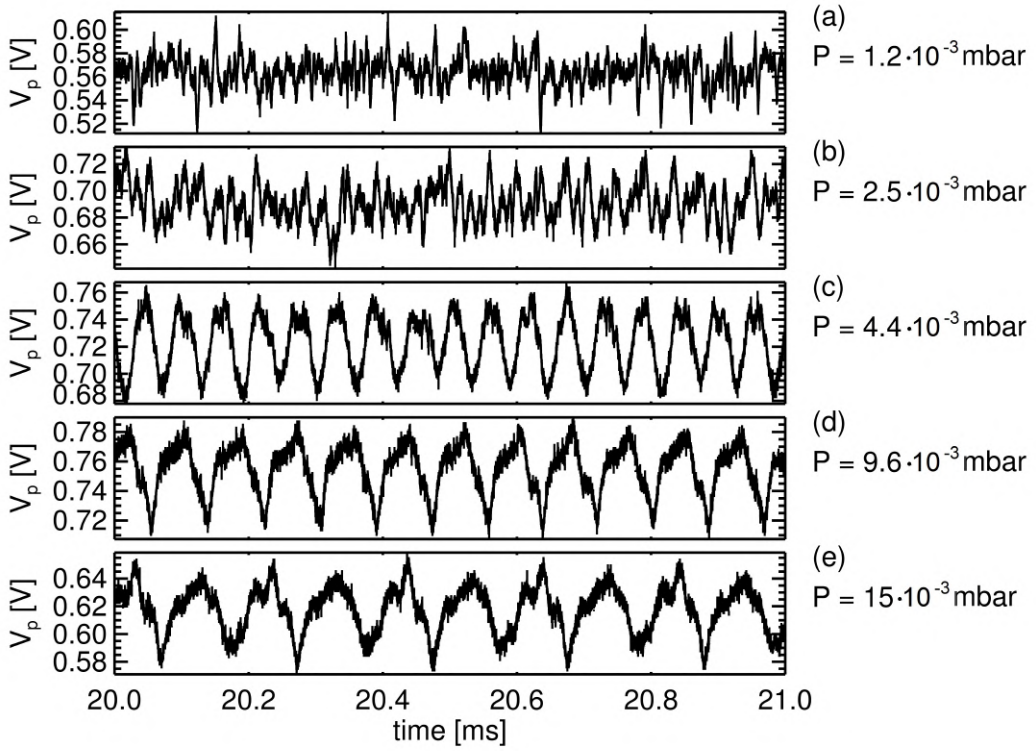

Figure 4.41: DC measured oscillations behaviour in time and pressure. Note that while at lower working pressures the mode is turbulent, as the pressure is increased, first a triangular wave rises then it shows a more complex but coherent structure.

the total integral of the spectrum. In this way it is possible to understand if the peaks actually grow over the background or not. As picture 4.42 shows, normalized peak integral grows logarithmically with pressure. Peak integrals are performed by applying a low-pass filter and a high-pass filter. Low-pass filter cutting frequency chosen as the highest point distinguishable from background; also high-pass filter has been chosen as the lowest distinguishable point from the background. Since their corresponding spectral values are enough smaller than peaks half maximum, a Gaussian-shaped peak is almost totally included. Errorbars are evaluated, in the same way, as the normalized peak integral varying high and low cutting frequencies by reasonable resolvable values. Since background decreases with frequency, low-pass filter should be affected by a greater error over the cutting frequency choice, but the decrease is completely covered by noise at least up to 50 kHz. Anyway, because of a higher background at low frequency, high-pass filter integral

error is absolutely comparable to the low-pass filter one.

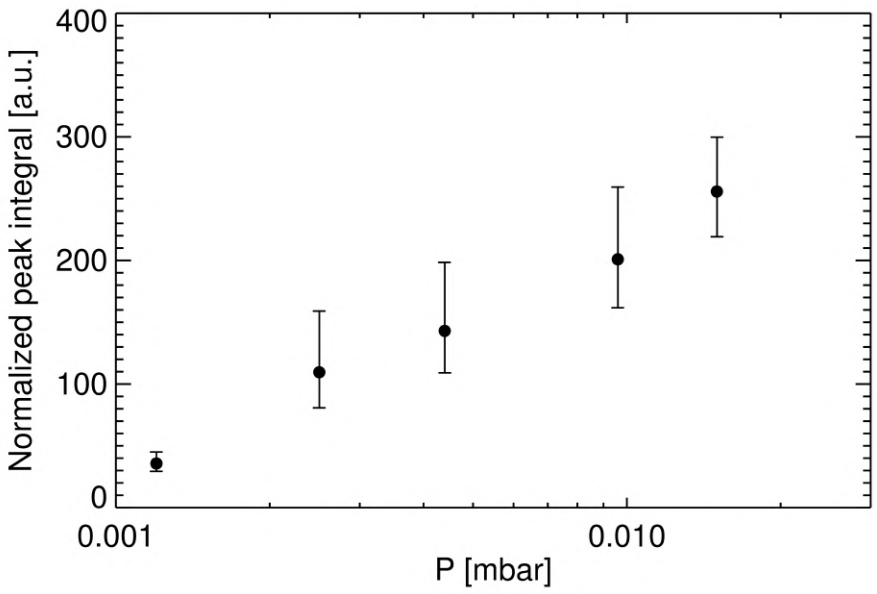

Figure 4.42: First harmonic peak integrals normalized by total integral and plotted as function of pressure. The growing confirms a feeding of coherent modes by the system, privileging them over turbulence.

Frequency trend with pressure is shown in fig. 4.43 along with the phase velocity trend. The phase velocity, v_{ph} is defined as

$$v_{ph} = \frac{\omega}{k}.$$

Adapted to our case it becomes

$$v_{ph} = \frac{\omega r}{m} = \frac{2\pi f r}{m}.$$

Having only a $|m| = 1$ mode together with the complex structure of the wavefront suggest strongly it is a rotating spoke, however its propagation is always opposite to $\mathbf{E} \times \mathbf{B}$, differently from other experimental results on it [11] [4]. Since the density and azimuthal electric field oscillations defined by Janes and Lowder lack of an explicit mechanism of feeding, it is not possible to know whether they should propagate in one or another direction.
It is curious to compare its velocity to other relevant velocities typical of the system. CIV, named to explain rotating spoke, is $\sim 8.69 \cdot 10^3 m/s$ for Argon. This value seems to be much too high, since estimated phase velocities

stand between $1km/s$ and $7km/s$. Ion sound speed, c_s, is more reasonable since, assuming ion and electron temperatures to be almost the same, it is in the range $4 \div 6 \cdot 10^3 m/s$. Unfortunately, the most coherent modes are lower than these values, as the high pressure tail shows. But we could not reject the hypothesis that c_s is related to spoke propagation because of two possible causes in wrong estimation. Firstly ion temperature should be accurately measured to calculate c_s and might be reasonably less than electron temperature.

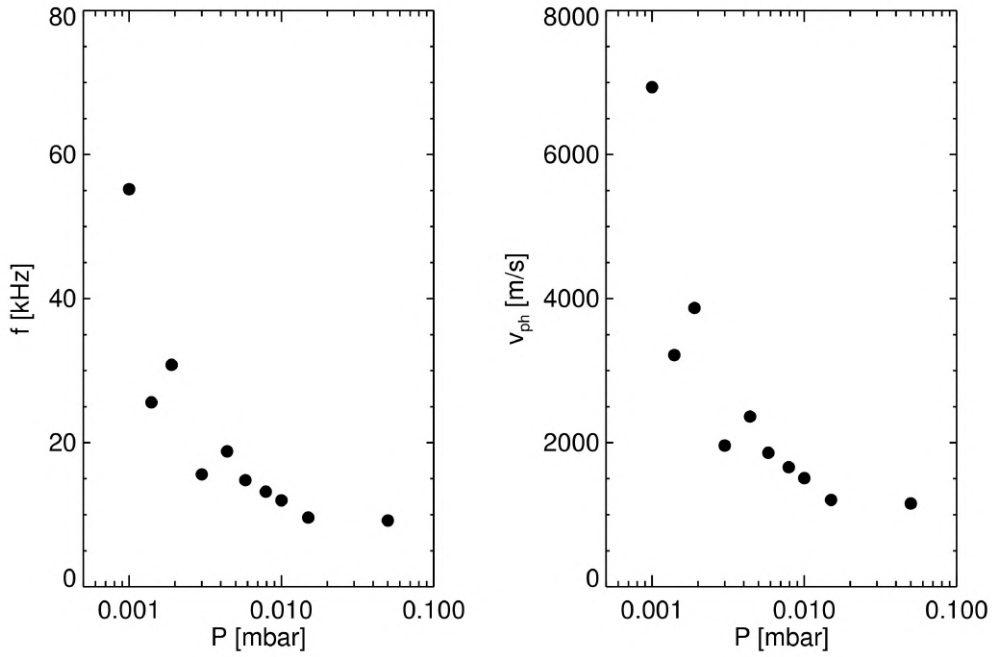

Figure 4.43: Frequency and phase velocity as functions of pressure. Ar critical ionization velocity is about $8.69 \cdot 10^3 m/s$ while ion sound velocity is $4 \div 6 \cdot 10^3 m/s$.

Hardly we can expect a higher temperature, because of the very great inertia of Argon ions. Secondly: the rotating spoke is said to develop mainly in the bottom of the thruster, so that the region where our measures have been done is at the very end of the measurable perturbation. There is no theory developed yet that ensure wave fronts to be in-phase all over the axial dimension. On the contrary, it is said rotating spoke is tilted about 15° and develops in a helical fashion. Since PIC simulations rely on uniform magnetic field, it is possible that more complex dynamic set in which slow down the spoke proportionally to **B** or increasing axial electric field E_x. The said, ion acoustic velocity, is further justified in Sekerak et al. works [15] [16].

Finally, to know exactly if $E \times B$ velocity is related to this kind of oscillation, the exact electric field profile should be measured inside the thruster. Since it was beyond the scope and the tools for this thesis, it is not possible to give a precise estimate.
Total fluctuations intensities never exceeded 6% of the DC signal, i.e. the discharge voltage, when using Argon gas, while they reached 50% of the discharge voltage in He (fig. 4.44). No trends emerged clearly but a light decreasing with pressure. If a trend was to be found, it would be related to performances, so similar or specular to Mach number chart 3.34. This absence confirms results from other experiments which suggest rotating spoke has no effect on performance.

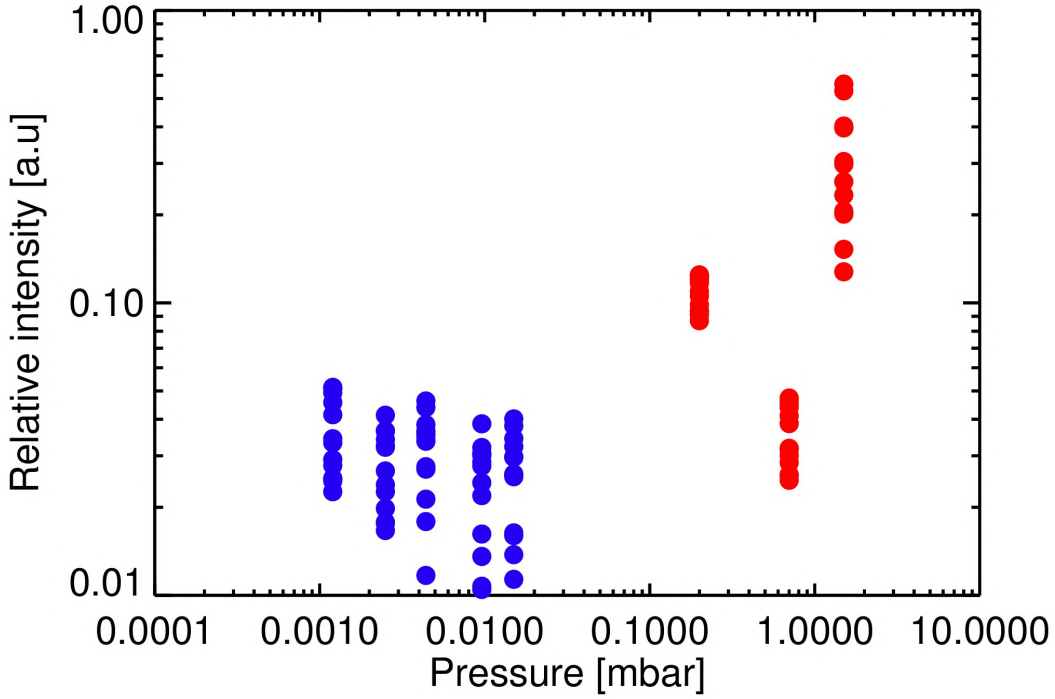

Figure 4.44: Fluctuations normalized intensity. Every dot is a probe signal. Blue dots refer to Ar data, while red ones refer to He data.

Frequency dependence with filament current is not robust because of the small number of trials. In fig. 4.45 it can be seen three power spectrum at three different filament current. Their respective power density spectrum is shown in fig. 4.46. Similarly to the pressure analysis, it is shown the integral around the peak frequency. The first peak has a lower frequency at $I_{fil} \sim 5.8A$. It might have a meaning since Mach maximum is around $6.2A$. However, since the Mach number maximum is related to a better ionization, if the drop

in frequency should be strictly related to a higher ionization also a frequency minimum would have been found in pressure.
What actually changes is the average input power, P_i, for the three measures at $5.2A$, $5.8A$ and $6.6A$, respectively $133W$, $114W$ and $305W$. As power trend seems to follow the frequency drop, it might have a role in determine the spoke frequency and velocity. Not to speculate over this topic, I suggest a better statistics to analyze the possible relation between working power and spoke frequency.

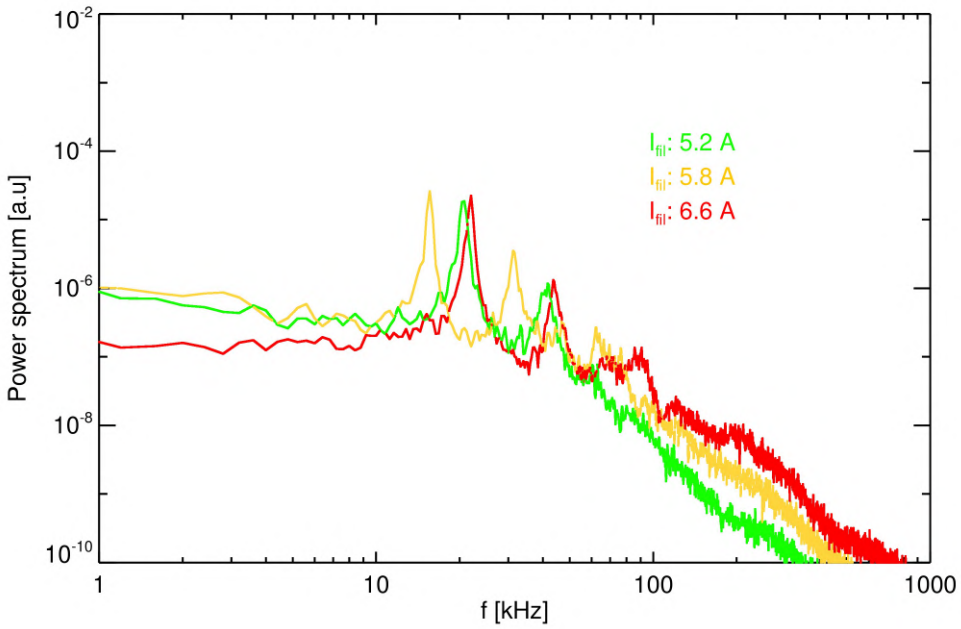

Figure 4.45: Argon fluctuations power spectrum for different filament current: $I_{fil} = 5.2A$ and $P_i = 133W$ (green), $I_{fil} = 5.8A$ and $P_i = 114W$ (yellow) and $I_{fil} = 6.6A$ and $P_i = 305W$ (red). It is notable a decreasing for the first peak around Mach optimum filament current.

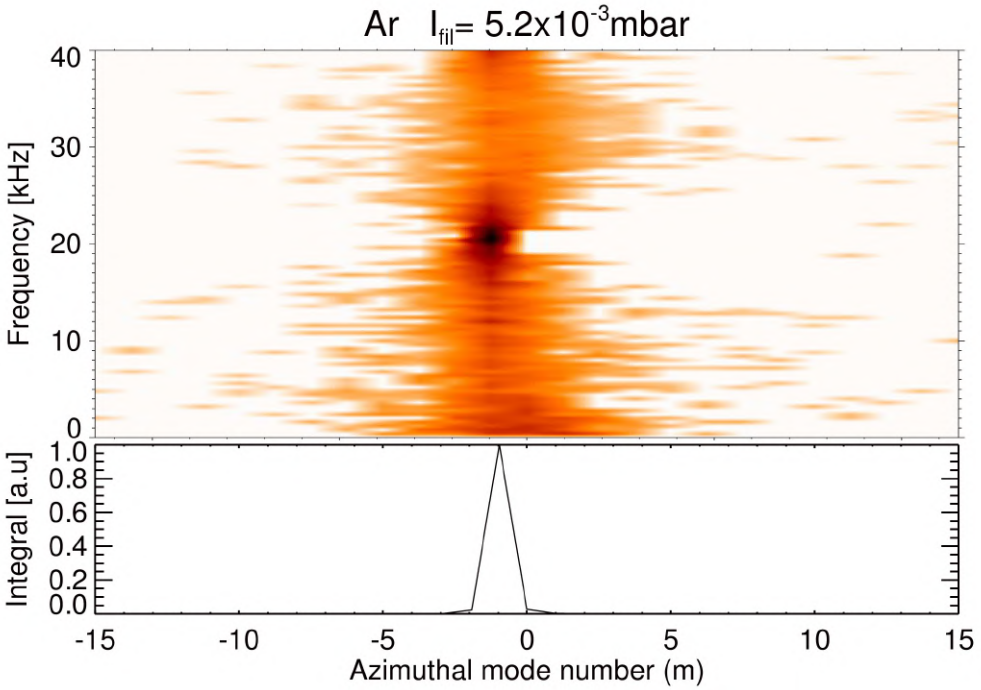
Ar I_fil= 5.2x10^-3mbar
Frequency [kHz]
40
30
20
10
0
Integral [a.u]
1.0
0.8
0.6
0.4
0.2
0.0
-15
-10
-5
0
5
10
15
Azimuthal mode number (m)

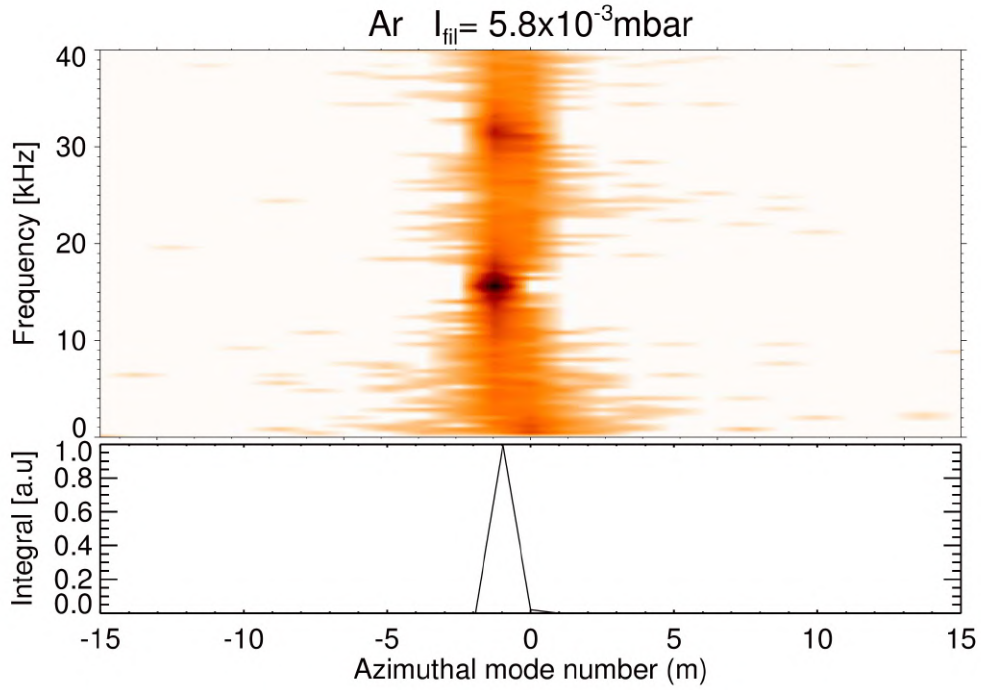
Ar I_fil= 5.8x10^-3mbar
Frequency [kHz]
40
30
20
10
0
Integral [a.u]
1.0
0.8
0.6
0.4
0.2
0.0
-15
-10
-5
0
5
10
15
Azimuthal mode number (m)

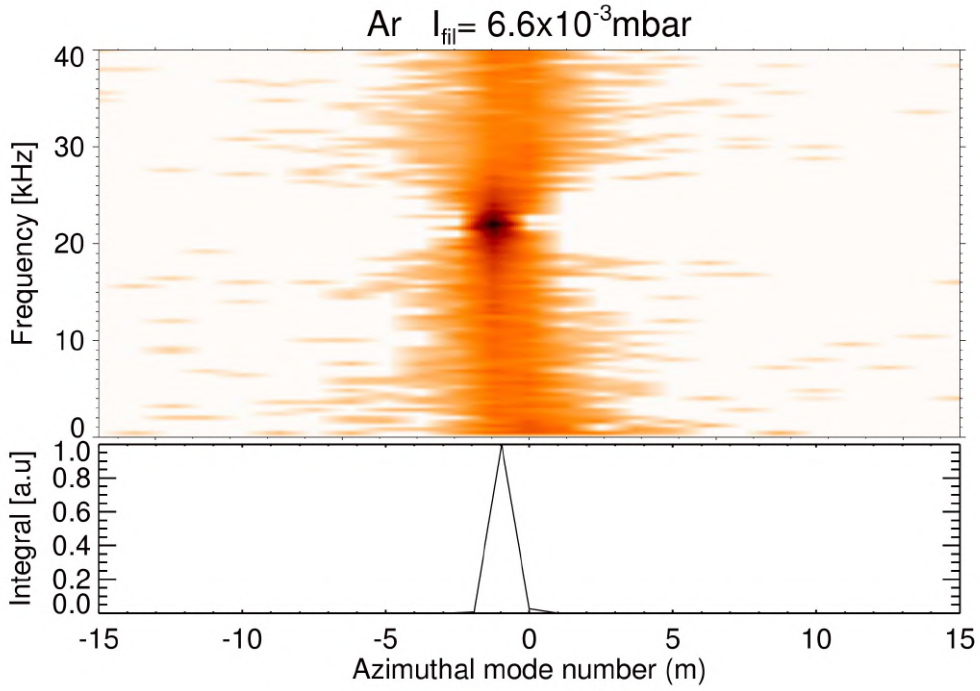

Figure 4.46: Power density spectrum at different filament current. Similar to fig.4.40 an integral over the same frequencies is performed and shown under the spectrum.

4.2.2 Helium and Hydrogen fluctuations

Comparing different gases is possible for Argon, Helium and Hydrogen. No measures have been done with other gases. A power spectrum comparison can be found in fig. 4.47, done at the most similar pressures available. Completely different from Argon spectrum Helium and Hydrogen spectra present a $\sim 100kHz$ peak which is more likely to be transient-time oscillations since they appear to be essentially axial perturbations. Oscillations in Helium, which are shown in fig. 4.48, are perfectly axial. In fig. 4.49 also dispersion relation confirms to be transient-time kind of oscillations. Hydrogen oscillation, instead, moved clockwise and its propagation can be found in fig. 4.50. It has a $m = -1$ mode as it can be understood from fig. 4.51 . Since transit-time has a small azimuthal component and Helium and Hydrogen have a similar mass, it is reasonable that both oscillations belong to the same classification. Helium shows also a peculiar peak between $500kHz$ and $900kHz$. A closer analysis of this peak has been done, extracting it from the background thanks to high-pass and low-pass filters, similarly to integral analysis. This frequency range suggests it is an oscillation of the type presented in sec. 1.5.3 [7].

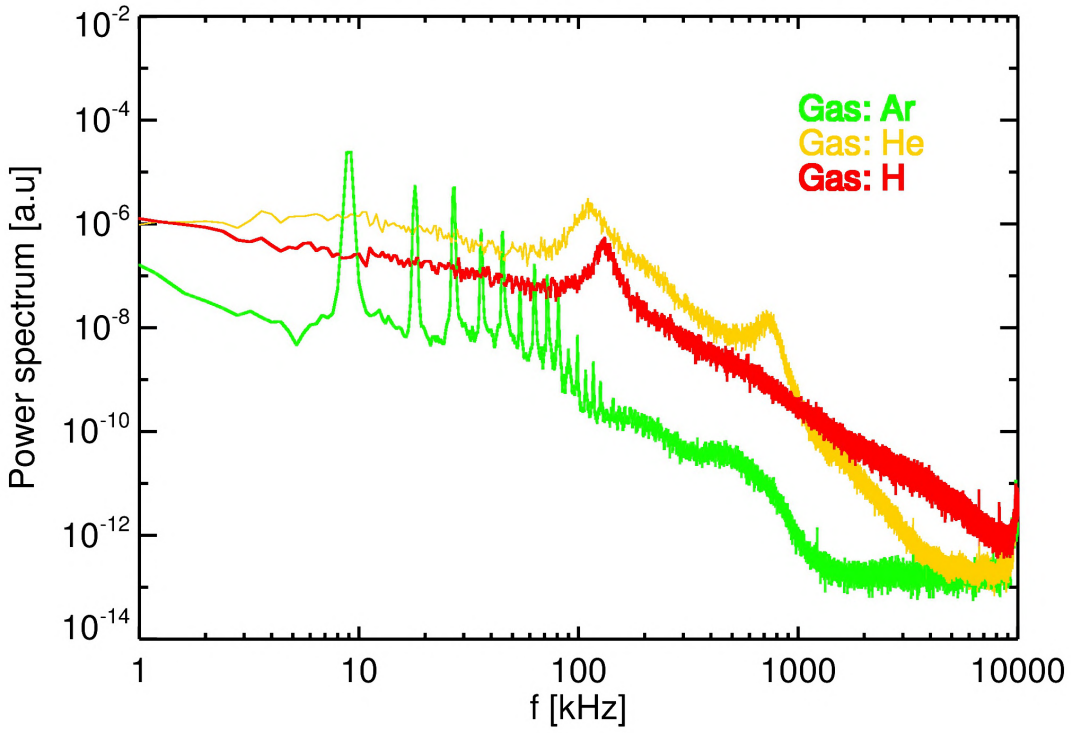

Figure 4.47: Different gases spectra compared at their most similar pressure. Both Hydrogen and Helium show a $100 \div 150 kHz$ axial perturbation, completely absent for Argon.

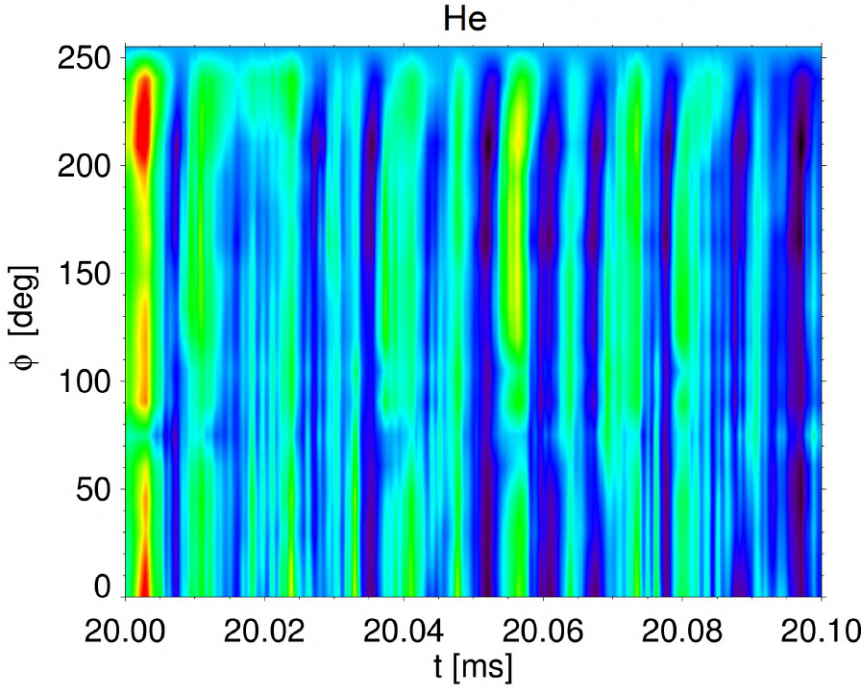

Figure 4.48: Helium fluctuation signals developing in time (x-axis) and moving axially.

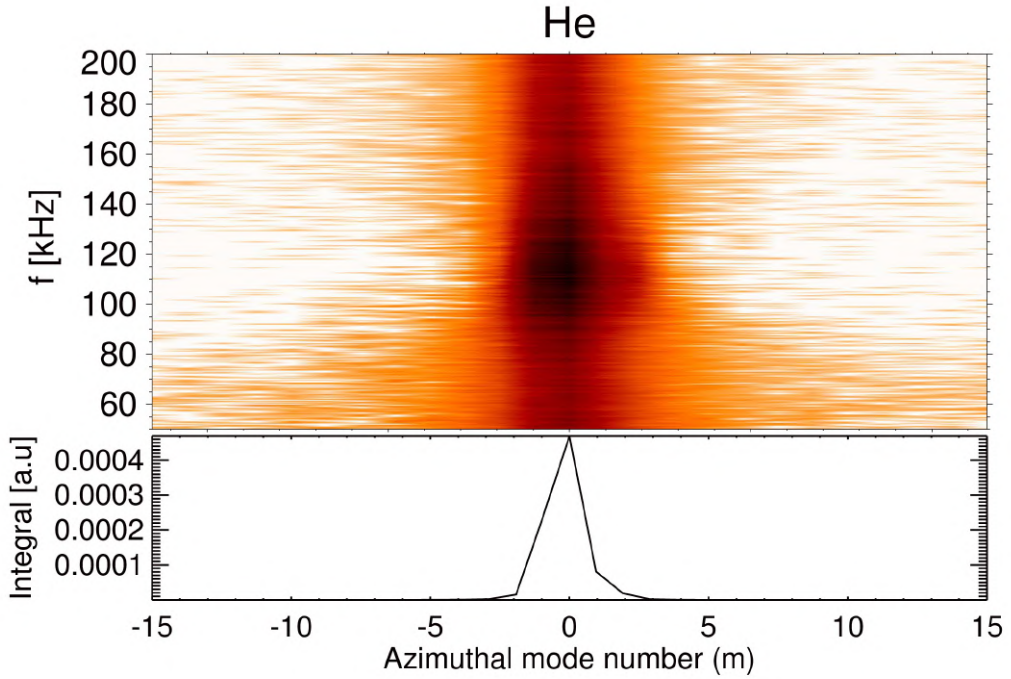

Figure 4.49: Helium power density spectrum at different filament current. An integral over the same frequencies is performed and shown under the spectrum.

The completely different nature respect to the other oscillations found in this work is justified immediately looking at fig. 4.52 where frequencies grow with a neat pressure dependence. Also, just looking at the spectrum in 4.47, it cannot simply be a transit-time oscillation higher harmonic. It is important to underline that this oscillation is definitely axial, since no mode number emerges from the dispersion relation analysis in the power density spectrum, so that flute solutions of the system studied by Simon [17] are completely useless. Since Hydrogen present the same transient-time oscillations but not a higher frequency of this sort, the difference between the two gases might hide in the fact that Hydrogen is not a noble gas, but neutrals fed from the bottom of the HET are mainly bond in H_2 molecules. The eventuality of atomic bonds between propellant gas neutrals could result in quite different oscillations after all.

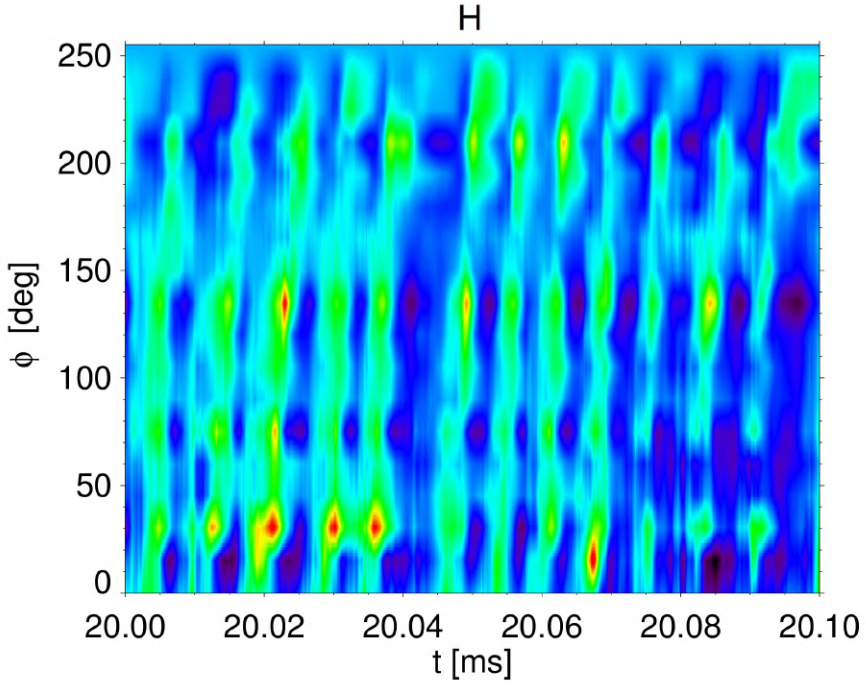

Figure 4.50: Hydrogen fluctuation signals developing in time (x-axis) and moving quasi-axially. The small tilt reveals an azimuthal propagation in th clockwise direction.

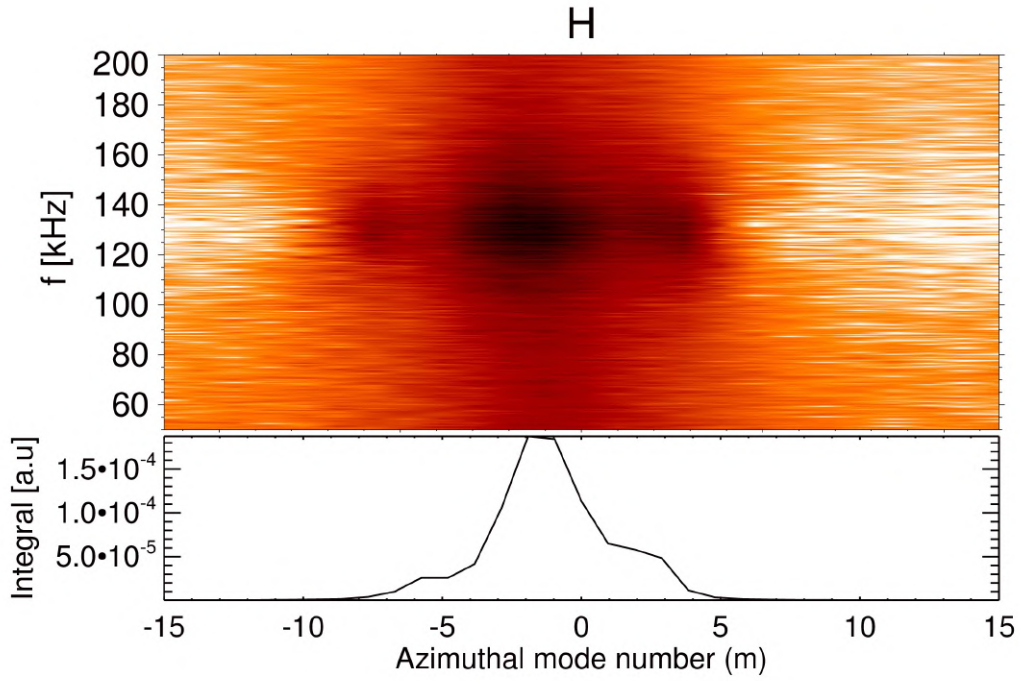

Figure 4.51: Hydrogen power density spectrum at different filament current. An integral over the same frequencies is performed and shown under the spectrum.

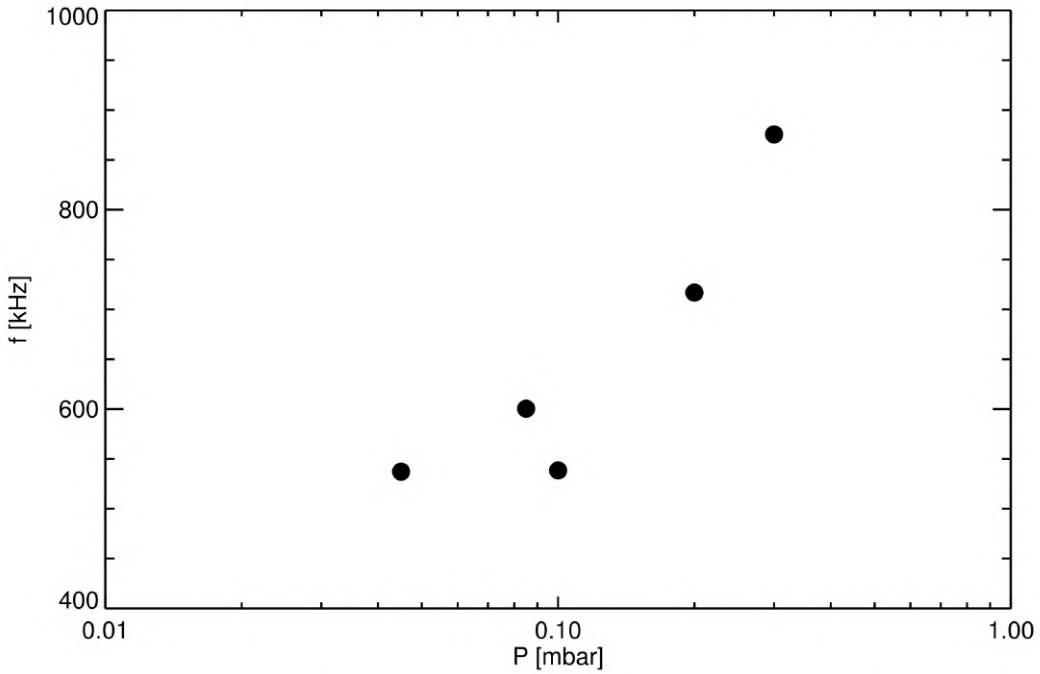

Figure 4.52: He MHz peak frequencies dependence with pressure. As the pressure is raised, also frequency grows touching MHz

5 Conclusions

ATHENIS is a Hall Effect Thruster used as a Hydrogen ion source for studying the production of H^- ions, needed in fusion experiments for heating Tokamak plasmas. Thanks to a permanent magnetic field, ions are accelerated toward a Tungsten filament cathode, while electrons are confined into the thruster channel. A study on ATHENIS plasma properties and oscillations has been performed through a pressure scan, a filament current scan and changing the propellant gas used. It was done with the use of a Mach probe and a multiple electrostatic probe expressly built and it revealed many notable features of its working conditions, especially for Argon propellant, for which it was possible to obtain a great number of measures. It was possible to adopt two working regimes thanks to intrinsic current limits of the power supplies. The two regimes differed in power thanks to different limits on the circuit current. High voltage $(300 \div 600V)$ and low current $(< 1.3A)$ regime (HI) was characterized by lower average power $(< 200W)$, lower electron density $(1 \div 2 \cdot 10^{18} m^{-3})$ and slightly lower electron temperature $(5 \div 7eV)$. Instead low voltage $(50 \div 200V)$ and high current $(< 4A)$ regime (LI) had higher power $(300 \div 800W)$, higher electron density $(3 \div 5 \cdot 10^{18} m^{-3})$ and higher electron temperature $(7 \div 11eV)$. The overall difference is strictly caused by the current limit. Anyway, since Langmuir characteristics were hard to fit because of a double electron population, it would be wrong to suppose a dependence in T_e. In the Argon LI regime it has been possible to estimate Mach numbers. It resulted in the presence of a maximum both varying pressure and filament current. An optimum at the same optimum pressure is possibly found in electron density and it could be a point to investigate. It would be good to measure ion temperatures in the adopted measuring conditions to estimate more precisely and, possibly, construct a model of the calibration parameter, K, for what concerns Mach number measures. Finding the actual ion velocities, especially for Hydrogen, would be very useful to select ion energy in order to extract H^- ions in the best way from cesiated surfaces. Doing it by a Mach number estimate would avoid calorimetric measures. Less invasive would else rely on doppler effect.

Fluctuation analysis brought to light three kinds of oscillations. Firstly a rotating spoke of which frequency drop with increasing pressure. It is re-

markable that a coherent mode emerges from turbolence as the pressure is raised and, moreover, that the mode is gradually fed, damping down other sources of perturbation in the remaining band. The feeding of rotating spoke over stochastic perturbations might become a useful tool to avoid the said oscillation or to select between competitive modes, since rotating spoke has no evident effect on HET performances as confirmed by the results. Also frequency might have a minimum related to the optimum Mach filament current, but certainties on the role of filament current need a deeper and finer study. The fact that input power shows a minimum together with the minimum frequency at $5.8A$ may be a sign of a correlation between frequency and power, but, again, recorded data on this topic are too little to have a statistical relevance.

A second kind of oscillation observed developed both in Hydrogen and Helium. It is the well known transit-time oscillation which is a quasi-axial oscillation as described in the introduction. Helium oscillations were perfectly axially oriented, while Hydrogen shown an $m = -1$ mode moving, once more, clockwise.

The third found oscillation appears only when using Helium and its located in the MHz region of the spectrum. Its presence is referable to oscillations described by Simon and Esipchuck et al. Unfortunately, showing that it is actually an oscillation due to a density fluctuation and an anisotropic coupling with the magnetic field of that kind is not possible unless the density profile is measured or estimated in a precise way. This would lead moreover to a further theoretical discussion of the model solutions. Because of the concurrent axial transit-time oscillation, the effect of the higher frequency oscillation over ATHENIS plasma is screened and it is not possible to deduce how heavy is it role in HET performances. It is anyway clear that also its frequency is related to neutral gas pressure.

Every fluctuation found can be eventually studied deeper by measuring magnetic field fluctuations. If any relevant fluctuation is found, magnetic field will have an active role in driving oscillations. A better understanding of magnetic field role, especially its gradient, would permit to avoid or select certain modes when needed. Magnetic fluctuations could be measured making a similar probe array used to electrostatic fluctuations but with inductive sensors such as small coils.

In the end, the whole analysis permitted to understand in what conditions ATHENIS works with different gases, what kinds of electrostatic oscillations are present and how they depend on adjustable parameters. Further studies should be performed about cathode role and, most of all, about alternatives to Tungsten filament, that has a relatively short life even if screened with a cage. Few alternatives even to hollow cathode are remarkable, such as field effect cathode and pulsed arcs. Still a great work is needed to deduce more useful pieces of information but a general trace is already marked for the most accessible and interesting gases.

References

[1] Lecture 17 notes: Hall thruster efficiency. https://ocw.mit.edu/courses/aeronautics-and-astronautics/16-522-space-propulsion-spring-2015/lecture-notes/MIT16_522S15_Lecture17.pdf, 2015.

[2] J. P. Beouf. Tutorial: physics and modelling of hall thrusters. *Journal of applied physics*, 121, 2017.

[3] F. F. Chen. *Introduction to plasmas physics and controlled fusion*. Plenum Press, second edition edition, 1974.

[4] E. Chesta, C. M. Lam, N. B. Meezan, D. P. Schmidt, and M. A. Cappelli. A characterization of plasma fluctuations within a hall discharge. *IEEE Trans. Plasma Sci.*, 29, 2001.

[5] A. R. Chouduri. *The physics of fluids and plasmas*. Cambridge University Press, 1998.

[6] E. Choueiri. An overview of plasma oscillations in hall thrusters. *European Space Agency SP*, 465, 2000.

[7] Y. B. Esipchuck and G. N. Tilinin. Drift instability in a hall-current plasma accelerator. *Soviet Physics*, 21, 1976.

[8] M. Fadone, V. Antoni, D. Aprile, G. Chitarin, A. Fassina, E. Martines, G. Serianni, E. Sartori, F. Taccogna, and M. Zuin. Plasma characterization of a hall effect thruster for a negative ion source concept. AIP Conference Proceedings, 2018.

[9] J. M. Fife, M. Martinez-Sanchez, and J. Szabo. A numerical study if low-frequency discharge oscillations in hall thrusters. 33rd Joint Propulsion Conference, 1997.

[10] R. J. Goldston and P. H. Rutherford. *Introduction to plasma physics*. Institute of Physics Publishing Bristol and Philadelphia, 1995.

[11] G. S. Janes and R. S. Lowder. Anomalous electron diffusion and ion acceleration in a low-density plasma. *The Physics of Fluids*, 9, 1966.

[12] J.P.Beouf and L. Garrigues. Low frequency oscillations in a stationary plasma thruster. *Journal of applied physics*, 121, 2017.

[13] E. Martines, R. Cavazzana, G. Serianni, M. Spolaore, L. Tramintin, M. Zuin, and V. Antoni. Electrostatic fluctuations in a direct current magnetron sputtering plasma. *Physics of plasmas*, 8, 2001.

[14] E. Martines, M. Zuin, V. Antoni, R. Cavazzana, G. Serianni, M. Spolaore, and C. Nakashima. Experimental investigation of low-frequency waves propagating in a direct current planar magnetron plasma. *Physics of plasmas*, 11, 2004.

[15] M. J. Sekerak. Ph.d. *Michigan State University*, 2014.

[16] M. J. Sekerak, B. W. Longmier, A. D. Gallimore, D. L. Brown, R. R. Hofer, and J. E. Polk. Azimuthal spoke propagation in hall effect thrusters. *IEEE Trans. Plasma Sci.*, 43, 2015.

[17] A. Simon. Instability of a partially ionized plasma in crossed electric and magnetic fields. *Physics of Fluids*, 6, 1963.

[18] B. M. Smirnov. Phyics of weakly ionized gases. Mir Publishers, 1981.

[19] A. I. Smolyakov, W. Frias, Y. Raitses, and I. D. Kaganovich. Gradient instabilities in hall thruster plasmas. 32nd International Electric Propulsion Conference, 2011.

[20] X. Zhang, D. Dandurand, T. Gray, M. R. Brown, and V. S. Lukin. Calibrated cylindrical mach probe in a plasma wind tunnel. *Review of Scientific Instruments*, 82, 2011.

6 Acknowledgments

The efforts I made in these years is concluded in this work. The University of Padua enriched my knowledge and my mathematical approach to the smallest as to the greatest problems in nature. It gave me, during the Master Degree, many tools to understand what actually happens in life that we cannot directly see and that most of the people cannot even imagine.
My thesis enriched my laboratory experience as never before and it is a pleasure for me to bound theory with manual skills, above all dealing with the most fascinating topic for me. Being able to create, manipulate and test what extends the beauty of the fire, an element that served mankind across the ages, has been a great experience for me and I shall thank many people for that.
A great thank goes to **Professor Matteo Zuin**, my supervisor during the practical work, who gave me countless advice as for my Bachelor so for my Master Degree. He renewed that interest in physics which intense study sometimes weakens. Also I must thank **Professor Emilio Martines** who taught me many things on laboratory plasmas and gave me the opportunity to undertake this work. Thank to **Professor Leonardo Giudicotti** for his patience in waiting the results.
Thank to **Darion Barison** who shared with me the experience across many practical difficulties and whose humor was a pleasant support.
Thank to **my parents**, who supported me in studying a few more years and stood the times I could not cover my homely role to study and go through exams.
A great thank goes to **Agata**, who boosted my effort in the last studies and took care about me more than I could.
Finally, I shall thank **my friends all** that accompanied me through the whole University way sharing sometimes hard and sometimes funny experiences.
But the greatest gratitude goes to every little event happened in my life that drove me exactly where I am, along a road that could not ever be different for, even if we cannot overwhelm natural quantum limits and we hide our huge ignorance behind the statistical mechanics, the Law of Physics is unavoidable and exquisitely astonishing in moving the Universe we observe and experience, from the subtle to the manifest.